Proteoid Biodynamers and Cell-Penetrating Peptide Conjugates as Tools to Overcome the Gram-negative Bacterial Cell Envelope

Dissertation

zur Erlangung des Grades

des Doktors der Naturwissenschaften

der Naturwissenschaftlich-Technischen Fakultät

der Universität des Saarlandes

von

Mohamed Ashraf Mostafa Kamal

Saarbrücken

2025

Tag des Kolloquiums	04.09.2025
Dekan:	Prof. Dr.-Ing. Dirk Bähre
Berichterstatter:	Prof. Dr. Claus-Michael Lehr
	Prof. Dr. Anna K. H. Hirsch
Vorsitz:	Prof. Dr. Marc Schneider
Akademischer Mitarbeiter	Priv.-Doz. Dr. Jessica Hoppstädter

Die vorliegende Arbeit wurde von Januar 2022 bis February 2025 unter der Leitung von Herrn Prof. Dr. Claus-Michael Lehr, Frau Jun-Prof. Sangeun Lee, und Frau Dr. Brigitta Loretz am Helmholtz-Institut für Pharmazeutische Forschung Saarland (HIPS) in der Abteilung für Wirkstoff-Transport angefertigt.

“He grants wisdom to whoever He wills.

And whoever is granted wisdom is certainly blessed with a great privilege.

But none will be mindful ˹of this˺ except people of reason.”

Surah Al-Baqarah 2:269

Table of Contents

Summary

The Bacterial cell envelope, especially for Gram-negatives, serves as a major defense mechanism against antibiotics. It is composed of lipopolysaccharides, lipid bilayer, periplasm, and another lipid bilayer, which combine to restrict most molecules to reach their intracellular targets by diffusion. Such restriction represents a bottleneck for the antibiotics pipeline.

Cationic dynamic polymers allow interactions with the LPS layer. My studies reveal that ArgBD, an arginine-based biopolymer, interacts specifically with the lipid A component of the LPS, creating gaps in the existing LPS barrier. Resultingly, ArgBD can potentiate colistin 32-fold by accessibility to the lipid bilayer in a novel mechanism.

In order to further improve this effect of ArgBD alone, it was conjugated to the cell-penetrating peptide HIV-1 TAT to additionally interact with the lipid bilayers of the bacterial envelope. This covalent conjugate, TAT-ArgBD, could indeed improve bacterial killing with a membranolytic index of >64 and less hemolytic toxicity than colistin at the same xMIC. When combing TAT-ArgBD with various antibiotics, namely novobiocin, chloramphenicol, and imipenem, an up to 256-fold synergy was observed. Interestingly enough, the activity of novobiocin, which is notoriously restricted to Gram-positive bacteria, could also be expanded to include Gram-negatives.

Zusammenfassung

Die bakterielle Zellhülle, insbesondere bei Gram-negativen Bakterien, dient als wichtiger Abwehrmechanismus gegen Antibiotika. Sie besteht aus Lipopolysacchariden, einer Lipiddoppelschicht, dem Periplasma und einer weiteren Lipiddoppelschicht, die zusammen verhindern, dass die meisten Moleküle per Diffusion ihre intrazellulären Zielstrukturen erreichen. Diese Barriere stellt einen Flaschenhals für die Entwicklung neuer Antibiotika dar.

Kationische, dynamische Polymere ermöglichen Interaktionen mit der LPS-Schicht. Meine Studien zeigen, dass ArgBD, ein argininbasiertes Biopolymer, spezifisch mit der Lipid-A-Komponente der LPS interagiert und dabei Lücken in der bestehenden LPS-Barriere erzeugt. Folglich kann ArgBD Colistin durch einen neuartigen Mechanismus um den Faktor 32 verstärken, indem es den Zugang zur Lipiddoppelschicht ermöglicht.

Um diesen Effekt von ArgBD weiter zu verbessern, wurde es an das zellpenetrierende Peptid HIV-1 TAT konjugiert, um zusätzlich mit den Lipiddoppelschichten der bakteriellen Hülle zu interagieren. Dieses kovalente Konjugat, TAT-ArgBD, verbesserte tatsächlich die bakterizide Wirkung mit einem membranolytischen Index von > 64 und geringeren hämolytischen Toxizitäten als Colistin bei gleichem Vielfachen der minimalen Hemmkonzentration. Bei Kombination von TAT-ArgBD mit verschiedenen Antibiotika—namentlich Novobiocin, Chloramphenicol und Imipenem—wurde eine Synergie von bis zu 256-fach beobachtet. Interessanterweise konnte durch diese Kombination auch die Aktivität von Novobiocin, das üblicherweise nur gegen Gram-positive Bakterien wirkt, auf Gram-negative ausgeweitet werden.

Abbreviations

AMP	Antimicrobial Peptide
AMR	Antimicrobial Resistance
ArgBD	Arginine Biodynamer
asPNA	Anti-sense Peptide Nucleic Acid
asRNA	Anti-sense-Ribose Nucleic Acid
ASOs	Anti-sense Oligonucleotides
ATP	Adenosine Triphosphate
CD	Circular Dichroism
CFU	Colony Forming Unit
CPP	Cell-Penetrating Peptide
CuAAC	Copper-Catalysed Azide–Alkyne Cycloaddition
DDEL	Wirkstofftransport über biologische Barrieren
DNA	Deoxyribose Nucleic Acid
eNTRy	ionizable **N**itrogen, **T**hree-dimensionality, **R**igid
FDA	Food and Drug Administration
GARDP	Global Antibiotic Research and Development Partnership
GSK	GlaxoSmithKline
HIV-1	Human Immunodeficiency Virus 1
LPS	Lipopolysaccharide
MBC	Minimum Bactericidal Concentration
MDR	Multiple Drug Resistance
MIC	Minimum Inhibitory Concentration
NDA	New Drug Application
NHS	National Health Service
OD_{600}	Optical Density at 600 nm
PBS	Phosphate-Buffered Saline
PEIL	PolyEthyleneImine, Linear
PK	Pharmacokinetics

PLA	Poly-L-Arginine
PLL	Poly-L-Lysine
PNA	Peptide Nucleic Acid
POPG	1-**P**almitoyl-2-**O**leoyl-sn-glycero-3-(**P**hospho-rac-(1-**G**lycerol))
RNA	Ribose Nucleic Acid
SAXS	Small-Angle X-ray Scattering
SEM	Scanning Electron Microscopy
TAT	GRKKRRQRRRPQ
UK	United Kingdom
WHO	World Health Organization

1. Background and Significance

1.1 The Bacterial Cell Envelope as a Biological Barrier

Before diving into antimicrobial resistance (AMR), it is essential to outline the fundamental structural differences in bacterial cell envelopes, which determine how molecules can be taken up or excluded. In case of comparing gram-negative bacterial cell envelope to the Gram-positive one, as shown in Figure 1, the relative complexity of Gram-negatives cell envelope can be noticed as it consists of (from inside to outside): a lipid bilayer (inner membrane), a thin periplasm consisting of peptidoglycan, another lipid bilayer (inner leaflet of the outer membrane), then a unique LPS layer (outer leaflet of the outer membrane) consisting of lipid A and sugar moieties. Therefore, it is a complex barrier with alternating hydrophilic and hydrophobic elements, leading to the prevention of passive unfacilitated uptake of most molecules into the intracellular compartment of the bacteria, except for very small molecules like gas molecules, waters, salts. On the other hand, Gram-positives have a thick peptidoglycan layer with embedded Teichoic and Lipoteichoic acids on top of a lipid bilayer. While the Gram-positive cell envelope is less complex and resistant than the Gram-negative one, it is still a major hurdle for the passive uptake of many molecules.

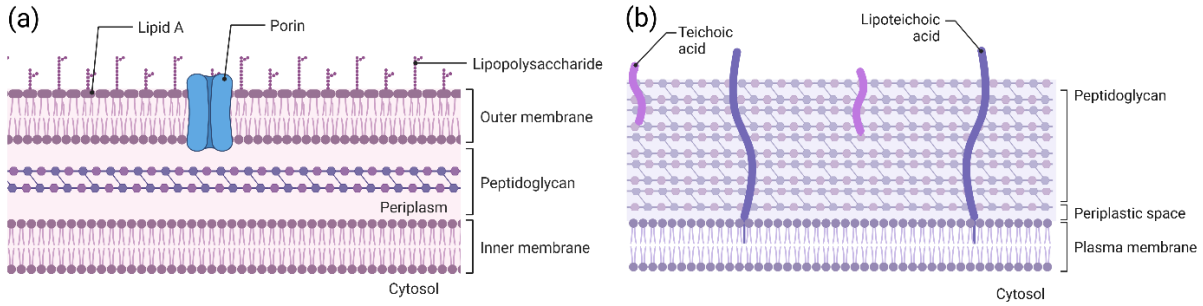

Figure 1: Bacterial cell envelope of (a) Gram-negative bacteria, and (b) Gram-positive bacteria. Figure created with Biorender ®

Taking *P. aeruginosa* as an example, only four classes out of many antibiotic classes can go into the intracellular compartments or periplasm and reach their targets, namely Aminoglycosides, Fluoroquinolones, carbapenems, and ß-lactams. Given enough time and antibiotics misuse, bacteria can indeed turn off its uptake machineries which constitutes a non-sustainable solution. [1] On the other hand, an older class of antibiotics, namely polymyxin, can target the bacterial membrane itself so it does not have the prerequisite of penetrating the bacterial cell envelope to reach its target and become active. However, some steric hinderance can happen due to the LPS sugar moieties. This could be taken as an advantage, but it is challenging to keep a molecule 100% selective towards bacterial membranes and not mammalian membranes, hence, resulting in some toxicity as evidenced in the case of Polymyxins.[2] Hence, the highly organized bacterial cell envelope, especially in Gram-negatives, forms a key barrier restricting antibiotic uptake.

1.2 Antimicrobial Resistance

Antimicrobial Resistance (AMR) is one of the major challenges for human health and will form a threat to the global health system, if not addressed sufficiently. AMR is represented in the form of the ability of an organism to a certain treatment which aims to eliminate the infection. Bacteria are among the most adept organisms at developing resistance to antibiotics. AMR is foreseen to increase the number of deaths from ~700,000 per year to ~10 million by 2050, which would bring AMR to the become the leading cause of death, if no action was taken beforehand to prevent this scenario. [3]

Definition and Mechanisms

As there is bioavailability of drugs in humans, the concept of bacterial bioavailability has been raised in bacteria, where three processes take place in parallel (uptake, efflux, and bacterial metabolism). [4] The resultant of the three processes gives the so-called bacterial accumulation. Resistance of the administered drugs, regardless of the processes of the human body, can be caused by limited uptake, increase of efflux, or increase of bacterial drug metabolism. On the molecular level, there are numerous ways by which a bacterium can become resistant to antibiotics, as depicted in Figure 2. The amount of uptake is limited by the continuous evaluation of bacteria, as a rapidly evolving prokaryote, towards having an excellent and advanced cell envelope barrier, especially for Gram-negative bacteria, or down-regulation of porins. An increase in efflux can be seen by the overexpression of efflux pumps. While intracellularly taken up, antibiotics can be metabolized. Another possibility is that the antibiotic target can be modified by the bacteria, protected by another molecule, or bypassed by a new protein. [5]

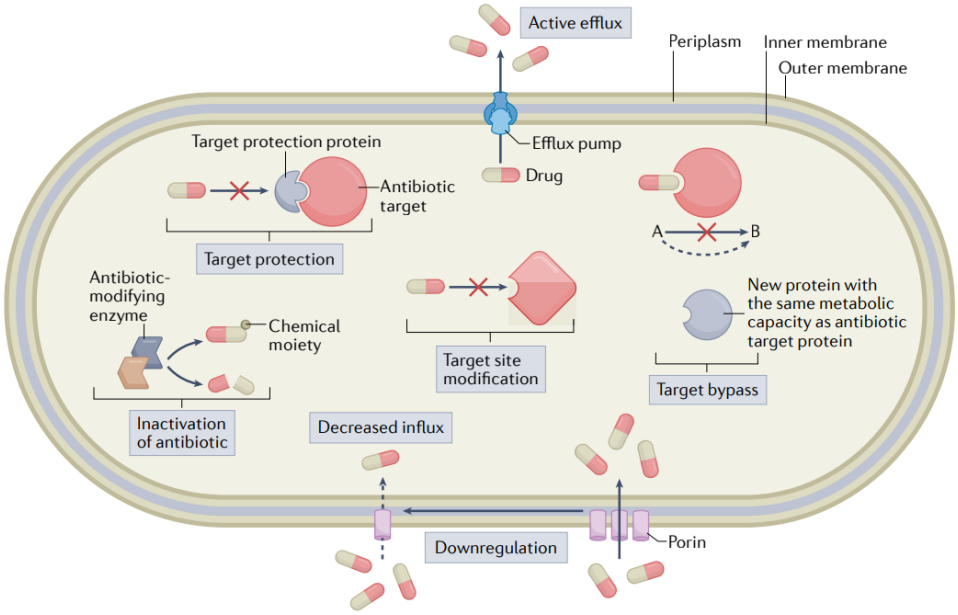

Figure 2: Various resistance mechanism of bacteria including intracellular mechanism as well as uptake and efflux mechanism. Figure reprinted with permission.[5]

History of Occurrence and Inherent Problem

In the beginning of the last century, the discovery of antibiotics was booming. Thanks to serendipity, the age of antibiotics started, which was later pushed by rational drug design so that the pace of antibiotics discovery was picking up with the new challenge of microbes. Unfortunately, as shown in Figure 3, it was not long until AMR hit every single new antibiotic discovered only in the matter of a few years. Novel classes of antibiotics against critical priority pathogens have been slowing in the past 30 years leading to an innovation gap and MDR infections. Rate limiting steps of discovery of novel class of antibiotics can be summarized as the limitation of the chemical scaffolds which can overcome bacterial barriers and the choice of targets which are not easily mutating and hence resistance can easily arise in community settings later. [1]

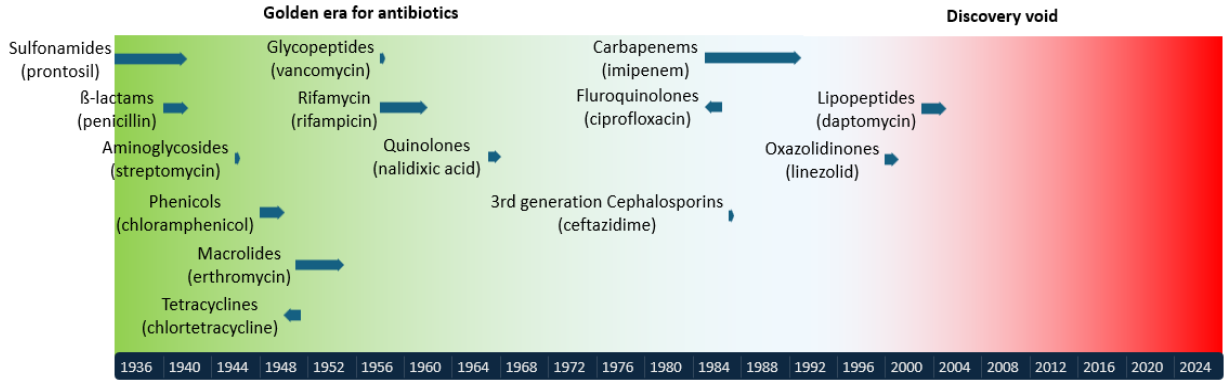

Figure 3: Example durations from the start of the commercialization to the first report of resistance against this class of antibiotics. Left pointing arrows means that resistance report was before commercialization and vice versa. [17,61]

In a frankly depressing example, GSK initiated a screening initiative to target 67 essential genes with a huge compounds' library comprising of up to 530,000 compounds, only to have 16 hits. Out of these 16 hits, 5 leads could be achieved, while no chemical modifications could generate proper leads for the remaining 11 hits, where the selectivity towards bacterial enzymes was 10x those of the mammalian ones. To our knowledge, this program led nowhere later on, and the project was dropped accordingly. Hence, one can conclude that it is extremely difficult to find targets in bacteria which can be targeted away from their mammalian versions. [6]

Current Situation in terms of Drug Development

There is a long list of reasons for the propagation of AMR. One of the top reasons is that large pharmaceutical companies have widely abandoned antibiotic research in favor of other therapeutic areas. A typical infection takes an antibiotic course for 3–5 days, while in case of cardiology pathologies, for example, one gets a life-time treatment course. Even in the infection case, the patient gets started on the first-line option which is usually an older drug with expired IP and generic alternatives, not the recently approved drug this year or a few years ago. This discourages big pharma to refrain from engaging extensively in research for novel antibiotics due to economic

reasons.[7] While some charitable initiatives are ongoing towards a more sustainable development of antibiotics, this funding might not itself be sustainable or enough as a sole solution. Some suggestions arise calling for the so-called Netflix model. In a Netflix model, companies are getting paid a subscription by health providers for the supply of antibiotics regardless of whether the novel antibiotics were to be used or the conventional ones. Such a model has been adapted by the NHS in UK.[8,9] Additionally, government-academia-industry partnerships have raised like GARDP allowing for facilitated communication and funding securing for early development of lead compounds. Additionally, the absence of antibiotics stewardship in some regions, natural occurrence as well as cattle exposure to antibiotics also plays a role to propagate the antimicrobial resistance.[1]

According to the 2024 WHO priority pathogens list, it is clear that Gram-negative bacteria are dominating the list of the most resistant bacteria, not necessarily due to limited uptake of the antibiotics into the bacteria, but due to the extreme difficulty of finding novel antibiotics which fulfill both human drugs criteria like Lipinski's rule of five and bacterial uptake criteria like eNTRy rules for Gram-negatives, while still keeping the correct SAR of the molecule to bind to and act on its target. [10,11]

The difference between a class derivative and a novel class of antibiotics has to be drawn before moving to the next part. Unfortunately, a moiety change of the scaffold aiming to better PK profile or improvement of the efficacy does not imply that the new molecule will overcome the existing resistance against the former molecule, which both probably use the very same uptake mechanisms and target. Hence, a huge importance is given to novel chemical scaffolds representing novel class against new targets in bacteria, in contrast to the widespread “me-too” marketing approach by companies to have a share in the market.[12]

Special emphasis should be given to products which represent a novel class of antibiotics due to cross-resistance among the same class. The WHO antibacterial observatory, which tracks ongoing trials in the antibiotics field, shows interesting state-of-the-art nowadays, as shown in Figure 5. [13] In total, there are 97 antibacterial products which are in clinical trials or pre-registration phase, with 16 products in phase III and 4 in the pre-registration phase, which looks for the first glance as promising. Out of these 97 products, only 26 products happen to be a novel class with some innovation. Then the number of products falls to a mere 3 products in phase III and one in pre-registration. Going further, out of these 26 products, only 6 products are active against *A. baumannii, P. aeruginosa*, or carbapenem-resistant Enterobacterales, which are the really stubborn pathogens. These 6 products have only one representative in phase II and only one in pre-registration. [13] Depressing enough, FDA has rejected the NDA for the pre-registration product. [14] This leaves only one phase II product as the best promising option against these pathogens, namely inhaled Murepavadin, developed by Spexisbio. Murepavadin is a peptidomimetic antibacterial targeting the outer membrane cell envelope of Gram-negatives, which is relevant to the research presented in this thesis as well as bypasses the prerequisite of bacterial uptake into the bacteria. [15]

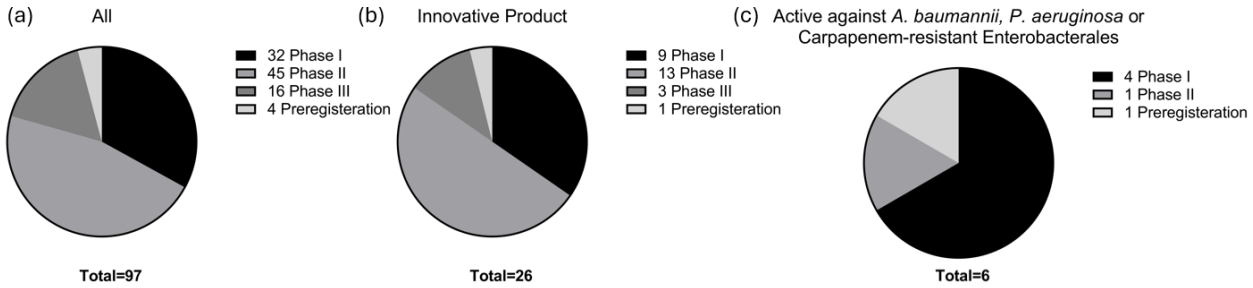

Figure 4: Portion of antibacterial products in different clinical phases, where in (a) all products are displayed, while in (b) only innovative products having no cross resistance to existing antibiotics, new scaffold, new target, and new mode of action are displayed, finally in (c) only innovative products which have antibacterial activity against A. baumannii, P. aeruginosa, or Carbapenem-resistant Enterobacterales. [13]

The current antibiotics pipeline looks quite pessimistic, if combined with the clinical trials success rates fact figures. As shown in Figure 6, the chance that antibiotic proceeds from one phase to the next one is quite low, which threatens companies by the loss of revenue and investments in this case, lowering their appetite for antibiotics research. A combined chance of a drug to proceed from phase I to approval is around 11.8%. Given the fact that only four products in phase I and one product in phase II exist for hard-to-treat pathogens and represent novel class, there is a near 50% chance that no new antibiotic will ever exist from the current pipeline in clinical trials and that the world will have to wait for at least ten years until a new product is developed and proceeds through all clinical trials and get approved. By that time, it could have been already too late for the global healthcare system, especially due to the increasing rate of MDR case reports. [16]

Forecast and Next Steps

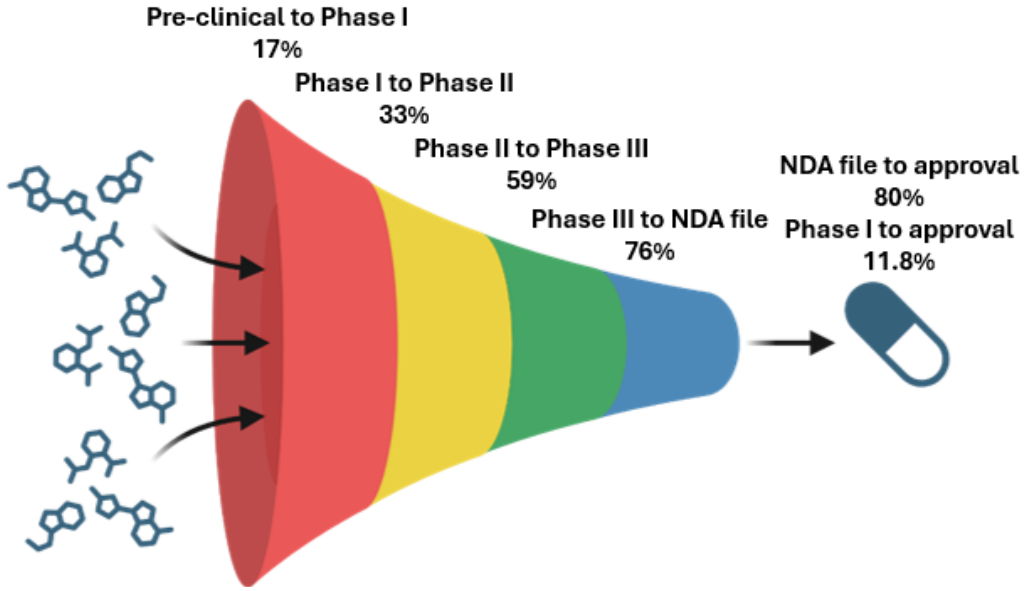

Figure 5: Chance of a potential drug to proceed to the next clinical trial phase. [16] Created with Biorender ®

It is noticeable that new antibacterial agents face a high failure rate in clinical trials. The reasons for this failure could be summarized, as shown in Figure 4. The top reason for the clinical trials failure is toxicity and inferiority to existing treatments, accounting for around half of the failures for a known reason. While this is also probable in other drugs, not related to infectious diseases, two other reasons are much more evident in especially infectious diseases treatments. These two reasons, as shown in the exploded portions in Figure 4, are resistance and commercial reasons. In the context discussed earlier, these two over-represented reasons are justifiable and understandable. In the case of resistance, bacteria can develop resistance against treatments in many ways as discussed already. As for the commercial reasons, they are due to the special short-term nature of infections and the existence of good, but not for long, treatment options. Special efforts have to be made to address these two reasons which are over-represented in infectious diseases. The rest of the reasons are normal and exist in other pathologies as well and can be addressed in an overall drug discovery improvement process by big pharma. [17]

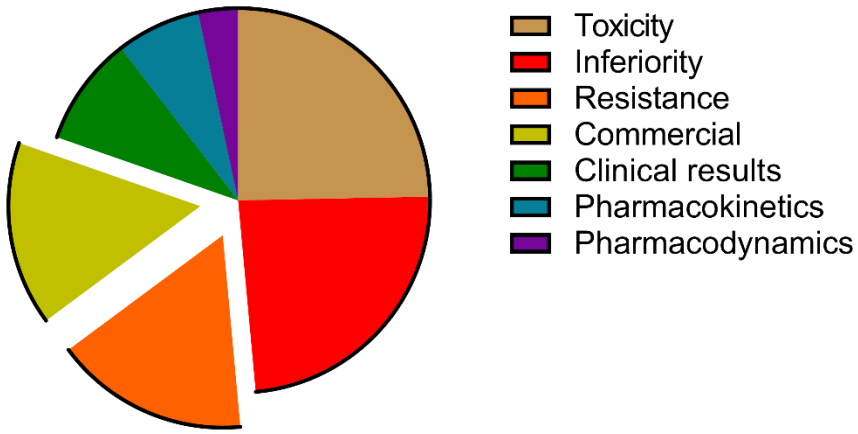

Figure 6: Reasons for termination of antibiotics development (31 March 2017). [16]. Terminations due to an unknown reason were excluded. Exploded portions represent reasons over-represented in antibiotics drug development. [62]

At the end of this chapter, we see that Gram-negative bacteria are especially problematic, both intrinsically (due to their complex outer membrane) and in the context of limited new antibiotics that fulfill all the required criteria. Hence, the envelope itself can be considered a possible target or barrier to overcome, which leads directly into the next chapter that discusses strategies to cope with the bacterial cell envelope as a biological barrier.

1.2 Strategies to Cope with the Bacterial Cell Envelope for Anti-Infective Drug Delivery

Parts of this chapter have been adapted from a previously published paper.[4] *Reprinted in section 9.1 of this thesis.*

Naturally Occurring Options for Transport

The problem with the bacterial cell envelope is that it prevents many potentially antimicrobial agents from reaching their intracellular targets. However, embedded proteins in the membrane can help regulate the transport of molecules to achieve intracellular delivery of antibacterials. Unfortunately, these channel proteins require meeting very specific physiochemical criteria.[18,19]

The simplest way to get through the bacterial cell envelope is by simple passive diffusion where only small neutral molecules, such as water, amino acids, and gases, can diffuse through the LPS layer, lipids, and peptidoglycan freely. For larger and more complex molecules, this route is nearly impossible due to the layered and chemically distinct composition of the Gram-negative bacteria. [19]

Some bacterial outer-membrane proteins form channels which can enable the passage of molecules without the need for ATP. This facilitated passive diffusion relies on the concentration gradient. Yet, mutations or downregulation of these channels are frequently observed in *P. aeruginosa, A. baumannii*, and *K. pneumoniae* as a resistance mechanism. [20] Some examples of these channels include porins, LamB, Tsx, FadL, and CymA, which respectively facilitate hydrophilic molecules, maltose, nucleotides, fatty acids, and cyclodextrin. These molecules are key substrates for bacterial growth, but not all antibiotics meet these narrow requirements. [21–24]

On the other hand, ATP- or proton gradient-dependent channels exist in bacteria as well. One prominent example is the TonB-dependent transporter, which can move siderophores into the bacteria. The process starts by the binding of a ligand to a receptor, such as ferrichrome binding to FhuA), then TonB utilizes cellular energy to mediate transport across both lipid membranes and the periplasm to reach the cytoplasm of the bacteria. These active channels have the advantages of being able to transport exceptionally large molecules as well as exhibiting high affinity to the ligand enabling transport against the concentration gradient. This makes TonB-dependent transporters a good target for "Torjan Horse" drug strategies. [25]

Ultimately, only molecules with suitable physiochemical and structural properties can reliably exploit these natural pathways. Many potential antibiotics simply do not meet these stringent requirements. Therefore, additional measures are needed to enhance uptake or circumvent the outer membrane barrier.

Transport-Enabling Strategies

The "Trojan Horse" strategy aims to conjugate a drug to a carrier which can be actively imported into the bacteria, where the drug may then be cleaved intracellularly and released inside the bacteria acting on its target at higher intracellular concentrations. Consequently, antibiotic-siderophores conjugates, such as cefiderocol, have been highlighted recently. [26,27] Nevertheless, bacterial adaptation or downregulation of the targeted transporters may still occur.

A contrasting approach, however, is to attack the bacterial membrane itself. The distinction must be made here between the demolishment strategy and the permeabilization strategy. In the demolishment, antibacterial agents work by demolishing the bacterial cell envelope leading to the leakage of intracellular contents and bacterial killing. While in the permeabilization, the bacterial cell envelope is mildly disrupted leading to the free diffusion of some agents in the extracellular space into the bacteria, acting on their targets leading to bacterial killing. The former can be fast and highly bactericidal but risks toxicity; the latter can synergize with otherwise membrane-impermeable antibiotics.[11,28,29] Membrane-disrupting agents can act on the bacterial cell envelope by a variety of mechanism, which include detergent-like effect, forming α-helical conformations in the lipid layer, production of reactive oxygen species, metal complexation in the bacterial membrane.[29–32] However, maintaining specificity towards bacterial membranes is an ongoing challenge, causing toxicity towards mammalian cells as well. [33,34]

Permeabilizing agents can open transient pores in the bacterial cell envelope, where such pores were shown lower antibiotics MIC by up to 128 folds. This can potentially transform antibiotics against Gram-positives into broad spectrum antibiotics, in case that the bacterial cell envelope is the limiting factor for their activity in Gram-negatives.[35] Permeabilization thus preserves synergy with existing agents but requires precise bacterial selectivity to avoid side effects.

Another strategy is triggered drug delivery due to the infection itself, such as acidic pH or bacteria-secreted enzymes. The acidic pH in the infection environment can affect the pH-responsive materials leading to them acquiring a positive charge, which leads to instability and release of the loaded antibiotic into the vicinity of the infection.[36] Another example is the siderophore-drug conjugate with esterase-sensitive linker. The linker is liable to the esterase secreted in infections, leading to the release of the drug only in the infections as well as siderophore selectively carrying the molecule into the bacteria.[37]

In many cases, the most successful formulations combine several of these strategies to achieve high selectivity toward the infected site while minimizing systemic exposure. Moreover, formerly ineffective or abandoned antibiotics may be repurposed when paired with an appropriate transport-enhancing or membrane-perturbing approach.

1.3 Polymers and their Peptide Conjugates to Potentiate Antimicrobial Activity

Some polymers have intrinsic antibacterial activity which can be utilized as coatings to materials for implants, for example, or in-solution antibacterials against several pathogens. Most of the antibacterial polymers used have cationic character, mainly made of amines. The cationic character can then interact with the anionic character of the bacterial cell envelope leading to bacterial killing. This cationic character can also be utilized in the coating process of some materials which are anionic in nature by ionic attraction or by covalent binding them. Coating these materials will then protect them from bacterial growth and biofilm formation. [38]

Applying a simple modification to a polymer (poly(isobutylene-alt-N-(N^1,N^1-dimethylaminopropyl)maleimide)) by conjugating one amino acid yield interesting results in literature. The best antimicrobial activity was achieved with valine, leucine, and isoleucine, which

happen to be all hydrophobic. The addition of some hydrophobicity had the best activity, while anionic amino acids had the worst activity, probably due to the repulsion with the bacterial cell envelope. This highlights the potential of antimicrobial polymers in engineering, medicine, and the food industry upon simple modification and blending with other materials to avoid microbial growth. [39]

Moving to AMPs, they are also active partially due to their cationic charge, which interacts with the anionic bacterial cell envelope. Other than the charge, there is more available modifications and properties which can influence their antibacterial activity. One of the major reasons for that is the secondary structure. On one hand, ß-sheet forming peptides were found to be more resistant to proteolysis, especially when stabilized by a disulfide bridge. It was also noticed with ß-sheet forming peptides that the increased amphiphilicity has increased potency against bacteria, probably to the better interaction with the bacterial interface with the extracellular aqueous environment. On the other hand, having α-helical structures can actually have better binding and interactions to the bacterial membrane by comparing two peptides with the same sequence but scrambled in a different order, specifically α-helix ($(KIAGKIA)_3$-NH_2) vs β-sheet ($(KIGAKI)_3$-NH_2). As α-helical almost always needs some hydrophobic residues in their structure to be potent, it is thought that some embedding of the peptide into the lipids is likely. [40]

As a strategy to ruin the helicity of peptides, some L-amino acids residues can be replaced with the D-amino acids leading to decreased helicity, thus, less potency against bacteria. However, interestingly enough, also the hemolysis character also decreased, leading to an overall better membranolytic selectivity index, which is the ratio between the concentration which can lyse RBCs and the concentration which can destroy bacterial membrane. As a learnt lesson from the cited example, it is always important to keep an eye on the selectivity index whilst trying to improve the antibacterial potency. [41]

To solve this riddle, a study developed peptoids which have varying flexibility and helicity. In this study, peptoids 1 had the more helicity in aqueous solution and good helicity in bacterial envelope mimicking environment, while peptoid 16 showed decreased helicity in aqueous solution and bacterial envelope mimicking environment, and peptoid 17 showed decreased helicity in aqueous solution and increased bacterial envelope mimicking environment. Peptoid 1 had the best potency against bacteria, followed by peptoid 17, then peptoid 16. Most importantly, peptoid 17 had the best membranolytic selectivity towards bacteria. What can be concluded in this regard, the solution for the riddle of selectivity towards bacteria is having pronounced helicity structure only with the bacterial membrane, but not aqueous solutions. This reflects that peptides or peptoids need to be thermodynamically preferring to change their shape into a more suitable one with the bacterial envelope. [42]

Hydrophobicity was also observed to have some effect on the antibacterial activity. Due to the necessity of some hydrophobic interactions with the lipids of the bacterial cell envelope, the choice of hydrophobic residues in a peptide is important. For instance, the aromatic phenylalanine was found to improve the activity against bacteria whilst other non-aromatic residues leucine, valine, and isoleucine were found to be inferior. [43] Meanwhile amphiphilicity has influence on antibacterial activity, however, it is not a consistent influence towards better or worse antibacterial

activity, but rather a very certain arrangement of the hydrophobic residues is needed and not just viewing amphiphilicity as a molecular descriptor that needs to be increased or decreased. [44]

Two of the biggest challenges for peptides are the high salts and protein content *in vivo*, leading to loss of activity. In work by Tam et al, AMP linear constructs were synthesized with different multimericities ranging from 1 to 8. For the monomer and the dimer, activity was observed in low salt conditions, but it was not late until this activity was lost in high salt conditions. However, only the tetramer and octamer were able to preserve their activity in low as well as high salt conditions, in addition to having better activity than the monomer and the dimer. Also, the tetramer could retain 80% of its activity even after 24 hours, while the linear repeats (not connected to a common backbone or core) of the same peptides could only retain 20% of its activity. [45]

So, to conclude what features are needed for a successful membrane-active antibacterial peptide, it needs to be cationic, less α-helical in water, more α-helical in bacterial environments, having some aromatic residues, and have a certain arrangement of the hydrophobic residues within the chain of the peptide, and having 17–19 residues.

A recent focus has been drawn to peptides conjugated to polymers. Peptides in this case are antimicrobial peptides, and sometimes referred to as cell-penetrating peptides, are conjugated in a multivalent manner. This allows each peptide moiety to interact independently with the bacterial cell envelope simultaneously in the same proximity on the bacterial cell envelope as they are connected to the same backbone, as well as displaying more resistance to proteolysis. These multimeric interactions are then combined, so their potency is exponentially elevated. [44]

As one example to multimeric peptide conjugates to a natural polymer, the AMP, anoplin, which is a decapeptide isolated from the venom of wasps, was conjugated to chitosan. To get got conjugation rate close to 100%, Copper(I)-catalyzed azide-alkyne cycloaddition (CuAAC) chemistry was used through the 2-azidoacetyl groups on chitosan. The chitosan was modified to yield an azide-containing chitosan was a range of conversion of 5%, 15%, and 24%. The CuAAC was then conducted with anoplin peptide to yield 12–40 repeats of the peptide per chitosan chain and a conversion rate close to 100%. The best MIC achieved was 18 μg/mL worth of peptide in *P. aeruginosa* conjugated to chitosan, compared to 512 μg/mL in the case of free anoplin peptide, representing a 28.4-fold improvement in the case of 12 peptide repeats per chitosan chain. In terms of membranolytic selectivity index (Bacteria to RBCs), the selectivity was improved from 8 to >100 leading to a safe product in terms of hemolysis. [46] It can be concluded that CuAAC is a very good option for conjugating peptides to backbones with high efficiencies and multimeric peptide polymer conjugates represent a viable option to improve AMP activity and selectivity.

Looking at the benefits of multimeric peptide polymer conjugates in terms of antimicrobial potency as well as selectivity, another aspect which is the choice of a peptide, which has a secondary structure. Combining these aspects together yielded even better results. Chan et al utilized dextran as a backbone and conjugated it to many peptides. The MIC of the free peptide was compared to the conjugated construct yielding fold increase of potency in the following order WLBU2, Lactoferrin, LL-37, Pexiganan, PR-26, $S4_{13}$-PV, Buforin 2, 4D-K_5L_7. Accordingly, it was noted that WLBU2, being a naturally α-helical cationic peptide, could benefit the most in

terms of potency from multimericity. Another aspect is the utilization of such conjugate as antibiotics potentiator. Normal, poorly soluble, as well as Gram-positives' antibiotics could be potentiated by up to 4096 folds in the presence of 0.5 xMIC of WLBU2-dextran conjugate, namely WD40 with PA14 strain. Additionally, WD40 could re-sensitize MDR strains as well as broaden the spectrum of some Gram-positive antibiotics to include Gram-negatives as well. [47]

1.4 Biodynamers as Dynamically Bio-responsive Polymers and their Potential to Interact with Biological Membranes

Polymers may consist of irreversible bonds or may as well consist of reversible bonds between their monomeric entities. Reversible bonds can be responsive due to a number of factors depending on the nature of the dynamic polymers (dynamers) and external conditions, such as pH. These mild conditions which can influence covalent bonds fall under the umbrella of constitutional dynamic chemistry, where conditions can influence the polymer on the supramolecular level to impact non-covalent interactions. On the other hand, the reversible covalent bonds of the dynamers can as well be impacted by the very same conditions in parallel, leading to the emergence of a species known as doubly dynamic polymers. Since dynamers have the ability to assemble and disassemble, depending on the thermodynamically favorable path, they are seen as adaptive materials, which can be extended to microenvironments, which can influence such polymers allowing for adapting its structure depending on the new microenvironment. [48,49]

A common type of dynamers are the acylhydrazone and imine bounded polymers. As shown in Figure 7, a condensation reaction can be conducted by the elimination of water via an acid affording an acylhydrazone or imine.[50]

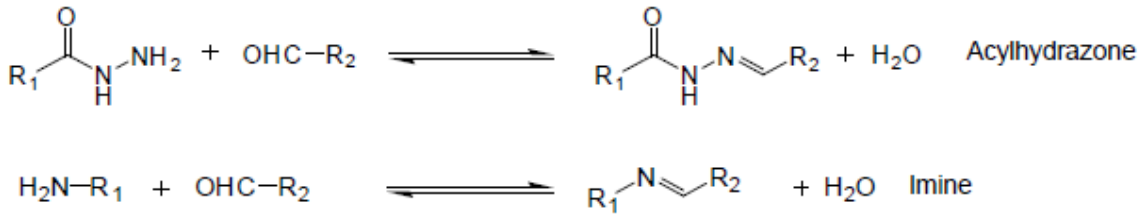

Figure 7: Reaction scheme of the formation of acylhydrazone and imine bond-based polymers. Figure reprinted with permission.[50]

An introduction of a bi-functional monomer containing both hydrazide and amine moieties leads to a polymer formation where both imine and hydrazones exist. The nice thing about these dynamers is that it is possible to dope or integrate some different monomers within this polymer leading to delivery of these monomers in the field of drug delivery. This also allows for fine-tuning of many physiochemical properties of the whole construct, for example, solubility and thermal conductivity, or even more complex properties like the 3D self-assembled structure of the dynamers. [50]

Going further with this, the class of dynamers, known as biodynamers, was developed. Upon incorporating biological moieties, such as amino acids, polysaccharides or DNA, the dynamers are, therefore, based on biological materials as well. This can afford biological activity, good biocompatibility, and good elimination from the biological setting upon degradation. Such biodynamers can self-organize and polymerize forming imine and arylhydrazone bonds, yielding reversible polymers, which are pH responsive. To maximize their biocompatibility, they are designed in a way that mimics proteins, where hydrophobic interactions influence their folding, amide-similar hydrazone bonds exist, and amino acids can be incorporated into the sequence of the polymer. [51]

To aid in hydrophobic interactions, carbazole-based biodynamers were developed and showed good polydispersity with a molecular weight of tens of thousands of daltons, in possibly a nanorods structure. The achieved molecular weight is a result of the so-called nucleation-elongation, where the dimer is formed and then due to the thermodynamically favorable folding leading to the incorporation of the next monomer into the polymer chain and so on, until the aldehyde groups are totally consumed into imine and hydrazone bonds. [52]

Incorporating arginine-bearing monomers into biodynamers marries the polymers' constitutional adaptability with the guanidinium group's extraordinary affinity for anionic interfaces. In bulk solution the cationic side chains keep the chain in an extended, highly hydrated state, but when the polymer approaches a negatively charged membrane the guanidinium units form bidentate ion pairs with surface phosphates or carboxylates. This local charge-neutralization triggers the chain to collapse into a compact, amphipathic secondary structure that can nestle into the interface, transiently loosening or sealing nanoscale pores. Because the biodynamer backbone itself is held together by reversible covalent links, the membrane-induced rearrangement is fully reversible: once the electrostatic field dissipates, bond exchange restores the original conformation and the barrier reseals. Arginine-decorated biodynamers have already been shown to assemble into charge-sensitive nanorods that ferry proteins and nucleic acids across cellular membranes without harming mammalian cells—behavior that closely parallels arginine-rich cell-penetrating peptides and confirms the value of guanidinium/proton coupling as a molecular switch for adaptive membrane engineering. [53,54]

2. Aim of the Thesis

AMR represents a growing global health crisis, which necessitates the development of innovative materials to act as novel antibiotics, to enhance the efficacy of existing antibiotics, or to broaden the spectrum of existing narrow spectrum antibiotics. Despite recent advancements in drug discovery, particularly in novel functional materials, the complex architecture of the Gram-negative bacterial cell envelope remains a formidable barrier, and no definitive solution has yet been achieved to surmount it. In Gram-negative bacteria, the LPS-rich outer membrane severely restricts antibiotic entry, limiting intracellular accumulation and preventing many drugs from effectively reaching their targets, thus diminishing therapeutic outcomes. Resultingly, this thesis aims to address these challenges by leveraging material design strategies to make new or potentiate existing antibiotics for overcoming the bacterial cell envelope. The thesis focuses on the exploration of multivalent macromolecules (polymeric and peptide-based constructs) to enhance antibiotic delivery across the bacterial cell envelope, especially against stubborn pathogens, such as Gram-negative bacteria.

2.1 General Objective

The overarching objective of this thesis is to design, synthesize, and evaluate innovative materials that achieve targeted perturbation of the Gram-negative bacterial cell envelope. To meet this goal, these materials focus on abundant bacterial components, not typically present in mammalian membranes, such as the cationic lipid membrane and lipopolysaccharides (LPS). This specificity aims to address the urgent need for novel classes of antimicrobials and to extend the lifespan of existing antibiotic families, particularly in combating multidrug-resistant (MDR) bacterial strains.

2.2 Specific Aims

1. Development of LPS-targeting Materials
    a. Design and synthesis of dynamic polymers which are capable of interacting with the LPS layer.
    b. Design of such materials, which are capable of interactions with the LPS layer, to facilitate passive diffusion of antibiotics into the intracellular compartment of the bacteria.
    c. Investigate the antibacterial potency or to potentiate other antibiotics against a variety of strains and compare this to the mammalian toxicity concentration range.
    d. Evaluate and validate the detailed mechanism of such antibiotic potentiation.
2. Exploration of Biodynamers for Antibacterial Applications
    a. Explore arginine biodynamers (ArgBD) as antibiotic potentiator to improve antibiotics uptake across bacterial membranes.
    b. Explore and pinpoint the interactions between ArgBD with LPS and lipid A, including the secondary structure change in the case of interactions.
3. Synthesis and Evaluation of Multivalent Conjugates
    a. Conjugate CPPs, such as HIV-1 TAT, with ArgBD to create multivalent constructs that can target LPS via the ArgBD backbone and can target lipid bilayers via the CPP.

b. Investigate the impact of multivalency in enhancing antibacterial activity and reducing mammalian cytotoxicity
c. Determine the *in vitro* therapeutic window to explore the applicability of further *in vivo* studies.

4. Mechanistic Insights into Membrane Interactions
    a. Employ state-of-the-art analytical, biological, and imaging techniques, such as circular dichroism (CD) spectropolarimetry, scanning electron microscopy (SEM), small-angle X-ray scattering (SAXS), and bacterial knockout strains, to elucidate mechanism of potentiation and action on the bacterial membranes.
    b. Investigate the secondary structure change of polymers and peptide-polymer conjugates upon exposure to bacterial microenvironment.
5. Expanding the Spectrum of Antibiotic Activity
    a. Evaluate the ability of developed materials to broaden the spectrum of antibiotics from Gram-positives to conclude Gram-negatives as well.
    b. Quantify the exact synergy between the developed materials and antibiotics, especially in clinically relevant strains such as *P. aeruginosa*, *A. baumannii*, and *S. aureus*.
    c. Explore developed materials as enablers for anti-sense oligonucleotides to act as antibacterials.
    d. Explore the potential for clinical translation using the achieved antibacterial potency, hemolytic potential, and mammalian toxicity.

2.3 Broader Impact

Addressing the permeability barriers of Gram-negatives and designing novel materials contributes to the aim of the thesis by providing a foundation for next-generation macromolecule-based antibiotic therapies. The outcome of this thesis can have potential in the future to:

- Enhance the efficacy of existing antibiotics against resistant clinical strains.
- Reduce the adverse side effects of some antibiotics by reducing the required dose.
- Inspire the development of novel drug delivery materials which can act as a potentiator and carrier simultaneously.
- Find new therapeutic modalities for better treatment of infectious diseases.

Ultimately, this research contributes to the efforts exerted globally to combat AMR and expand the available arsenal of therapeutics available to treat MDR infections.

3. Major Outcomes of the Thesis

Across my studies, the overarching goal was to address a key challenge in treating Gram-negative bacterial infections as provided by their most restrictive outer membrane that severely limits antibiotic delivery. By engineering dynamic, arginine-rich polymers (biodynamers) and further conjugating them with a cell-penetrating peptide (TAT), I sought both to create potent stand-alone antibacterial agents and to boost the performance of conventional antibiotics.

3.1 "Arg-biodynamers as antibiotic potentiator through interacting with Gram-negative outer membrane lipopolysaccharides"

In the first project (cf. section 9.2), the focus centered on Arg-biodynamers (ArgBD) themselves—without TAT conjugation—and their role as antibiotic adjuvants to permeabilize the Gram-negative outer membrane. Although ArgBD alone exhibited modest antibacterial effects, it showed a dramatically improved safety profile compared to conventional cationic polymers like poly-L-arginine. Arginine biodynamers targeted the LPS layer of Gram-negative bacteria—namely Escherichia coli and P. aeruginosa—and were capable of folding into β-sheet–rich structures upon interacting with LPS. This structural rearrangement facilitated localized membrane disruption without causing significant harm to mammalian cells. Most notably, ArgBD, when paired with antibiotics such as colistin, enhanced their bactericidal efficiency by up to 32-fold. Using spectroscopic methods (circular dichroism) and microscopy (SEM, confocal imaging), we demonstrated how ArgBD assembled on the bacterial surface. Through partial pore formation and mild destabilization of the outer membrane, ArgBD improved antibiotic penetration and coverage, particularly for those agents usually restricted by bacterial membrane impermeability. The study's comparative approach—highlighting ArgBD against non-dynamic polymers—reveals the unique advantage of biodynamers in selectively binding LPS while minimizing toxicity.

3.2 "A Multivalent TAT-Arginine-Biodynamer Conjugate to Overcome the Bacterial Cell Envelope barrier by Bacteria-Specific Membrane Interactions"

In the second project (cf. section 9.3), a TAT–Arginine-Biodynamer (TAT–ArgBD) conjugate was designed and evaluated. Unlike free TAT peptides, the conjugate displayed pronounced antibacterial effects against *P. aeruginosa, A. baumannii,* and *S. aureus*, with MICs in the range of 2–8 μg/mL, as well as showing rapid and efficient bactericidal activity, with an MBC of 32 μg/mL. Mechanistic analyses revealed that TAT–ArgBD interacts strongly with bacterial membrane lipids, particularly POPG and cardiolipin, forming pores and adopting an α-helical structure in this lipid environment. At sub-lethal concentrations, it caused visible membrane disruption in scanning electron microscopy experiments, and at higher doses, it accelerated bacterial killing much faster than colistin, a last-resort antibiotic. Notably, the TAT–ArgBD construct retained good selectivity for bacterial cells: it induced minimal hemolysis in red blood cells and caused limited toxicity in mammalian fibroblasts and macrophages at therapeutically relevant doses. Beyond its direct antimicrobial action, TAT–ArgBD functioned synergistically

with conventional antibiotics—such as novobiocin, chloramphenicol, and imipenem—lowering their required inhibitory concentrations by up to 256-fold in certain strains. This synergy was attributed to TAT–ArgBD's pore-forming ability, which enhanced antibiotic penetration of bacterial envelopes.

Taken together, these papers underscore the versatility of biodynamers as both potent membrane disruptors and antibiotic potentiators. Whether conjugated to TAT or used alone, arginine-based biodynamers can selectively breach Gram-negative bacterial envelopes, amplify the effectiveness of existing antibiotics, and maintain a favorable safety margin toward host cells, opening new avenues for combating multidrug-resistant infections.

3.3 Exploratory Study to combine Polymeric Constructs with ASOs as Anti-Infective Therapy

Abstract: Having shown that ArgBD and its TAT-conjugate can breach the Gram-negative outer membrane and turbo-charge conventional antibiotics, we next explored whether the same permeabilizing polymers could ferry antisense oligonucleotides (ASOs) into bacteria. Section 3.3 presents this pilot work: ASOs targeting essential genes co-applied with free TAT, ArgBD, TAT-ArgBD, or other polymers can be intracellularly taken up to inhibit the growth. The study tests whether membrane-active biodynamers can extend their utility from antibiotic potentiation to sequence-specific gene silencing.

Introduction: Among the promising alternatives for antibiotics are antisense oligonucleotides (ASOs), such as anti-sense Ribose Nucleic Acid (asRNA) and anti-sense Peptide Nucleic Acid (asPNA). ASOs can leverage sequence-specific gene silencing to inhibit essential microbial functions. To our knowledge, there is no solution to get the ASOs to permeate into bacteria in their free form in normal bacteria. Researchers have been able to conjugate asPNA to CPPs to facilitate their accumulation intracellularly within the bacteria. However, the most prominent current challenge is the off-target activity in mammalian cells as well because the length of the asPNA which can be internalized into bacteria via the CPP conjugation is around 9 nucleotides.[55] For successful specific targeting and having limited off-targets, one need to design ASOs in the range of 20 nucleotides, meaning that CPP-ASO conjugates will low specificity to bacteria and tend to have off-targets caused toxicity in humans. [56]

Methods: To directly assess the needed endpoint which the functionality of ASOs, ASOs were incubated with bacteria in combination with free peptides, biodynamer, or peptide-polymer conjugates as permeabilizers to internalize the ASOs into the bacteria to exert its silencing function. 10^5 CFU/mL of *E. coli* MG1655 was inoculated in M9 medium with a known concentration of the ASOs with a co-treatment, then they were incubated for 24 hours, then OD_{600} was measured to assess the bacterial growth. Alternatively, after the 24 hours combination, the bacteria were washed twice with PBS to remove any excess free treatment, then the bacteria was lysed with a dry sonication probe (20% power for 10 seconds twice) leading to release of intracellular components and internalized treatment, then it was measured at the respective wavelength on a plate reader and the background was subtracted.

Results and Discussion:

As a pilot first experiment, 10 µg/mL non-functional Alexa Fluor™ 568-labeled RNA was combined with 3 µg/mL of free TAT peptide, 3 µg/mL of ArgBD, or 3 µg/mL of TAT-ArgBD. The bacteria were then lysed, and the fluorescence was measured with excitation of 580 nm and emission at 604 nm. Bacterial growth was noticed in all of the samples. As shown in Figure 8, no significant uptake was noticed in any of the sample except for TAT-ArgBD which showed around 11% uptake of the added amount of the RNA. There is the possibility that the RNA is taken up by the bacteria, however, there is also the possibility that bacteria break down RNA to small chunks and the labelling dye made it inside the bacteria.

This gave the encouragement to try asPNA in combination with TAT-ArgBD or other permeabilizers as a potential combination therapy. Accordingly, two asPNA were designed. The first (anti-acpP, CTCATACTCTT) should silence acpP essential gene and the second (anti-rpsH, CTCATCTGTCT) should silence the rpsH essential gene in addition to a scrambled anti-rpsH (TTCACTATCTC), and labelled cy5-scrambled anti-acpP (cy5-TTCACTATCTC).

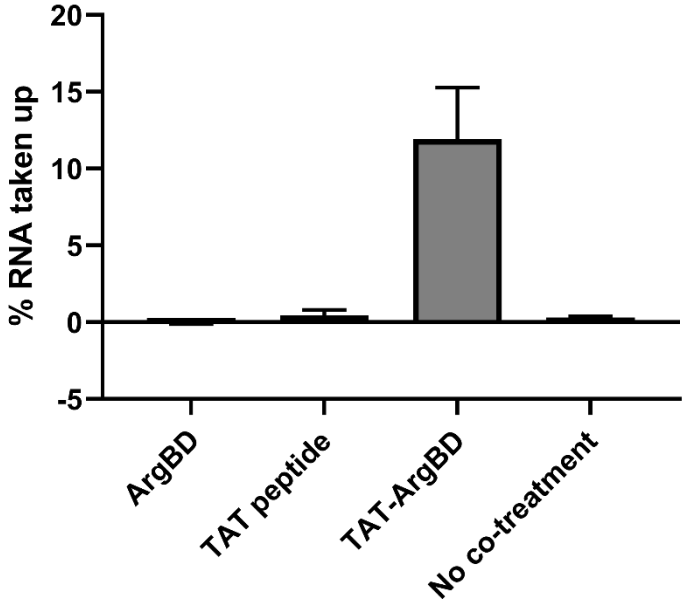

Figure 8: Fluorescence signal from lysed *E. coli* after treatment with 10 µg/mL of labelled siRNA combined with different materials. Three replicates were performed.

The uptake experiment was repeated using the same method in combination with 0.25% TritonX, or 3 µg/mL of TAT-ArgBD in combination with 10 µg/mL of cy5-scr-anti-acpP to confirm the uptake. Then the fluorescence was measured at the cy5 excitation (600 nm) and emission (669 nm). As shown in Figure 9, TritonX showed uptake lower uptake than the control indicating some inhibition to the number of grown bacteria after the incubation time. As for TAT-ArgBD, it showed a slight non-significant increase than the control. Comparing Figures 8 and 9 shows that RNA indeed gets internalized due to its degradation and not in its intact form, with some hope that the small amount of functional asPNA can really inhibit the bacterial growth.

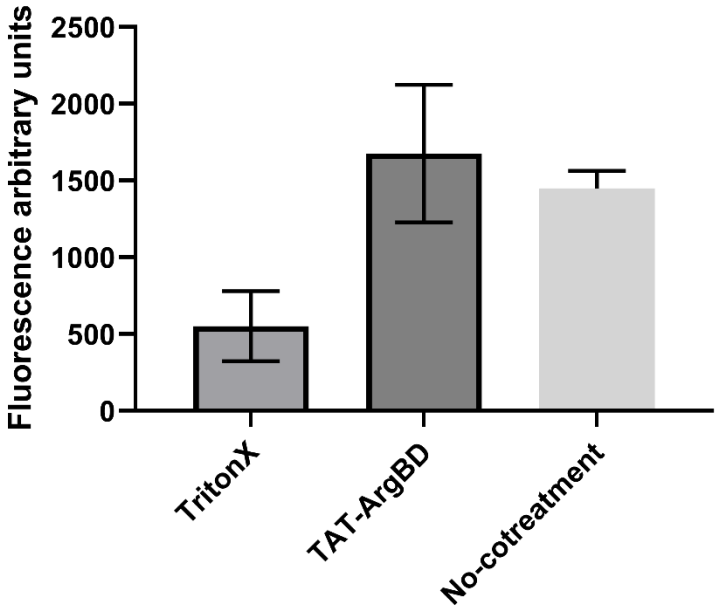

Figure 9: Fluorescence signal from lysed *E. coli* after treatment with 10 µg/mL of cy5-scr-anti-acpP combined with different materials. Two replicates were performed.

The following polymers were screened for their MICs against *E. coli* linear polyethylenimine (PEIL), 70kDa poly-l-arginine (PLA70), 70kDa poly-l-lysine (PLL70), TAT-peptide, TAT-ArgBD yielding MICs of 256, 8, 16, 8, 8 µg/mL, respectively. Afterwards, 0.25 xMIC of each of these polymers were combined with 50 µM of anti-acpP or 50 µM of anti-rpsH in M9 medium against *E. coli*. As shown in Table 1, most of the polymers showed increased bacterial growth relatives to normal control, with OD_{600} reaching 2x the normal control. Although asPNA would be expected to inhibit bacterial growth, it actually did the exact opposite indicating that bacteria could compensate for the silenced genes somehow and overcoming this in a very effective way leading to overgrowth due to sensing that something is wrong. Only PLA70, should a promising result in one of the replicates by inhibiting bacterial growth.

Table 1: *E. coli* bacterial growth in co-treatment of different macromolecules with asPNA. ++ indicates bacterial growth above 100% of the control, + indicates bacterial growth around 100% of the control, while +/- indicates one replicate inhibited and one at 100% of the control. Two replicates were conducted.

	PEIL	PLA70	PLL70	TAT	TAT-ArgBD
No asPNA	+	+	+	+	+
Anti-acpP	+	+/-	++	++	++
Anti-rpsH	+	++	++	++	++

As bacteria are known to compensate for the silencing of essential genes like acpP, it was concluded to use two asPNA against two different essential genes simultaneously to block as much

as possible of the bacterial growth cycle.[57,58] Additionally, a checkerboard assay was conducted using different concentrations of 1:1 mix of anti-acpP and anti-rpsH with different concentrations of PLA70 to reveal if there is any chance a certain mixture ratio was needed to inhibit the bacteria and not cause it to overgrow.

PLA70 (µg/mL) \ 1:1 mix of anti-acpP and anti-rpsH (µM)	50	25	12.5	6.25	3.125	1.5625	0.78125	0.390625	0.195313	0.097656	0.048828
8	0.44%	-0.14%	-0.30%	-0.38%	-0.87%	-0.71%	0.03%	-0.14%	0.93%	1.34%	0.93%
4	187.44%	150.74%	139.85%	86.12%	71.54%	43.85%	26.81%	38.36%	28.37%	29.11%	26.81%
2	199.56%	182.28%	144.35%	128.30%	112.49%	85.54%	77.19%	61.79%	61.71%	56.22%	64.25%
1	207.75%	190.31%	173.19%	137.72%	122.24%	104.30%	101.43%	87.43%	75.30%	78.91%	75.47%
0.5	172.04%	166.23%	142.47%	131.25%	120.76%	95.62%	92.18%	86.44%	89.64%	84.48%	65.88%
0.25	161.72%	178.68%	135.34%	119.70%	109.87%	107.49%	97.67%	88.00%	84.56%	91.52%	65.31%

Figure 10: OD_{600} of checkerboard assay of asPNA mix and PLA70 after subtracting background absorbance and normalizing to a control well (only bacteria, no treatment) as 100%.

As shown in Figure 10, it was found that the higher concentration of asPNA, the more the bacteria can counteract this and overgrow with the PLA concentration being not detrimental for the degree of this compensatory mechanism extent. On the other hand, 781–49 nM of PNA combined with 4 µg/mL of PLA70 (0.5 xMIC) was found to partially inhibit the bacterial growth beyond 75% of the control, indicating the ability of the bacteria to ultimately overcome this strategy of essential genes silencing.

As a conclusion, asPNA is likely to really inhibit some of the essential genes of bacteria, but with the bacteria able to overcome this, even two genes at a time. We propose that a large cocktail of asPNA targeting >2 genes at a time, could potentially outsmart the bacteria sensing mechanism. However, huge resources would be necessary due to the number of possible combinations of asPNA targeting different genes as well as the cost to synthesize custom-made PNAs.

To our knowledge, no research was able to achieve bacterial inhibition *in vitro* beyond 75% using free asPNA in any Gram-negative seriously pathogenic bacteria. In one similar study, MIC_{50} (inhibition of 50% of bacterial growth) was used to determine the potency instead of the usual MIC_{80}, indicating that the researchers likely observed only partial inhibition and not complete inhibition.[59] In the case of our study, we would have reported a MIC_{50} of less than 1.5 µM as seen in Figure 10, which is more potent than CPP-asPNA conjugates.[55] This indicates that the challenges faced by the selection of CPP and the increased molecular weight upon conjugating (limiting its internalization) can indeed be potentially overcame by simply co-treating with PLA at 4 µg/mL.

Additionally, there is no research paper reporting negative with free asPNA, like the data observed here, likely due to the bias to report only positive results in literature. Furthermore, to our knowledge, there is likely not a single paper (except for the one mentioned above) reported what MIC criteria they used to report an MIC.[60] This indicates a huge concerning literature gap in methods reporting and probable bias towards reporting only positive results.

4. Conclusion and Future Perspective

This thesis sets out to address the global problem of AMR, especially by Gram-negatives, by exploring novel bioresponsive polymers which can selectively target the bacterial cell envelope. Collectively, the two studies presented in this thesis mainly introduce ArgBD and their derived conjugate TAT-ArgBD as powerful strategies to (i) act as an antibiotic, (ii) permeabilize the notorious Gram-negative outer membrane, (iii) potentiate the activity of existing antibiotics.

In the first project on ArgBD as a potentiator, ArgBD themselves were studied as antibiotic adjuvants. These dynamic polymers could bind to the LPS of the Gram-negative membranes, leading to a remodeling of the local membrane architecture without causing mammalian cell toxicity. ArgBD could show mild intrinsic antibacterial activity but rather excel as antibiotic potentiators. Most notably, ArgBD could reduce the MIC of colistin by up to 32 folds in E. coli. Detailed spectropolarimetry analysis showed that ArgBD can adopt a predominantly majorly ß-sheet conformation in the microenvironment of LPS, in contrast to adopting random coil in aqueous environment, eventually break the LPS-LPS tight barrier, hence, permeabilizing the bacterial cell envelope. Interestingly, linear cationic polymers, such as poly-L-arginine, exhibited much inferior selectivity indices and is cytotoxic to mammalian cells, underscoring the advantages of dynamic polymers.

In the second project on TAT-ArgBD as antibacterial and potentiators, the concept of multimeric peptide constructs in which multiple TAT peptide repeating units are covalently linked to a ArgBD backbone with around 12 repeating units per polymer chain. TAT-ArgBD construct displays potent antibacterial action against P. aeruginosa, A. baumannii, and S. aureus, but not E. coli. The antibacterial activity was also found to be very fast in less than one hour. Mechanistic studies revealed a strong affinity to anionic bacterial membrane lipids, namely POPG and cardiolipin, leading to pore formation and leakage of intracellular components, thereby bypassing the usual prerequisite for antibiotics for intracellular uptake to have activity. Beyond the direct antimicrobial activity, TAT-ArgBD showed very good synergy with many antibiotics, such as novobiocin, chloramphenicol, imipenem, potentiating the activity for some and broadening the spectrum of some of these antibiotics from narrow spectrum, active only on Gram-positives, to include Gram-negatives even below the known breakpoint of these antibiotics, hinting towards a great potential to use them as treatments to Gram-negative bacterial infections.

Collectively, these findings emphasize the potential of dynamic biopolymer, especially arginine biodynamers, for addressing the gap of membrane-targeting strategies and antibiotics activity. ArgBD and TAT-ArgBD show great promise to combat stubborn Gram-negative bacterial infections due to maintaining bacterial selectivity over mammalian one, acceptable *in vitro* therapeutic window, and proven bacterial membrane permeabilization. Referring back to the core objectives, ArgBD-based systems indeed demonstrated selective LPS targeting, enhanced antibacterial efficacy, and a favorable safety margin—a critical trifecta against MDR Gram-negative strains.

Additionally, the attempted ASO-based approach showed partial, inconsistent bacterial inhibition, suggesting that multi-gene targeting or improved carrier design may be necessary to overcome bacterial compensatory mechanisms.

In the future, these biodynamers could be further optimized by (i) fine-tuning their polymeric backbone for even greater bacterial specificity, (ii) exploring synergy with additional antibiotic classes, and (iii) developing advanced formulations for co-delivery of nucleic acids. Such efforts will help push these platform technologies toward practical applications in the ongoing fight against AMR, offering hope for improved therapeutic outcomes even against the most resistant pathogens.

5. References

[1] Silver LL. Challenges of antibacterial discovery. Clin Microbiol Rev 2011;24:71–109. https://doi.org/10.1128/cmr.00030-10.

[2] Moubareck CA. Polymyxins and bacterial membranes: A review of antibacterial activity and mechanisms of resistance. Membranes (Basel) 2020;10:181. https://doi.org/10.3390/membranes10080181.

[3] Naghavi M, Vollset SE, Ikuta KS, Swetschinski LR, Gray AP, Wool EE, et al. Global burden of bacterial antimicrobial resistance 1990–2021: a systematic analysis with forecasts to 2050. Lancet 2024;404:1199–226. https://doi.org/10.1016/s0140-6736(24)01867-1.

[4] Bali A, Kamal MAM, Mulla G, Loretz B, Lehr CM. Functional materials to overcome bacterial barriers and models to advance their development. Adv Funct Mater 2023;33:2304370. https://doi.org/10.1002/adfm.202304370.

[5] Darby EM, Trampari E, Siasat P, Gaya MS, Alav I, Webber MA, et al. Molecular mechanisms of antibiotic resistance revisited. Nat Rev Microbiol 2022;21:280–95. https://doi.org/10.1038/s41579-022-00820-y.

[6] Payne DJ, Gwynn MN, Holmes DJ, Pompliano DL. Drugs for bad bugs: confronting the challenges of antibacterial discovery. Nat Rev Drug Discov 2006;6:29–40. https://doi.org/10.1038/nrd2201.

[7] Van Der Gronde T, Uyl-De Groot CA, Pieters T. Addressing the challenge of high-priced prescription drugs in the era of precision medicine: a systematic review of drug life cycles, therapeutic drug markets and regulatory frameworks. PLoS One 2017;12:e0182613. https://doi.org/10.1371/journal.pone.0182613.

[8] Plackett B. Why big pharma has abandoned antibiotics. Nature 2020;586:S50–2. https://doi.org/10.1038/d41586-020-02884-3.

[9] Duddy C. Netflix for antimicrobials: The antimicrobial products subscription model. House of Commons Library (UK Parliament) 2024. https://commonslibrary.parliament.uk/netflix-for-antimicrobials-the-antimicrobial-products-subscription-model/ (accessed January 22, 2025).

[10] Chagas CM, Moss S, Alisaraie L. Drug metabolites and their effects on the development of adverse reactions: Revisiting Lipinski's rule of five. Int J Pharm 2018;549:133–49. https://doi.org/10.1016/j.ijpharm.2018.07.046.

[11] Richter MF, Hergenrother PJ. The challenge of converting Gram-positive-only compounds into broad-spectrum antibiotics. Ann N Y Acad Sci 2019;1435:18–38. https://doi.org/10.1111/nyas.13598.

[12] Aronson JK, Green AR. Me-too pharmaceutical products: History, definitions, examples, and relevance to drug shortages and essential medicines lists. Br J Clin Pharmacol 2020;86:2114–22. https://doi.org/10.1111/bcp.14327.

[13] Antibacterial products in clinical development for priority pathogens. World Health Organization 2024. https://www.who.int/observatories/global-observatory-on-health-research-and-development/monitoring/antibacterial-products-in-clinical-development-for-priority-pathogens (accessed January 22, 2025).

[14] Dall C. FDA rejects new drug application for cefepime-taniborbactam. Center for Infectious Disease Research & Policy 2024. https://www.cidrap.umn.edu/antimicrobial-stewardship/fda-rejects-new-drug-application-cefepime-taniborbactam (accessed January 22, 2025).

[15] Díez-Aguilar M, Hernández-García M, Morosini MI, Fluit A, Tunney MM, Huertas N, et al. Murepavadin antimicrobial activity against and resistance development in cystic fibrosis Pseudomonas aeruginosa isolates. J Antimicrob Chemother 2021;76:984–92. https://doi.org/10.1093/jac/dkaa529.

[16] Farrell LJ, Lo R, Wanford JJ, Jenkins A, Maxwell A, Piddock LJV. Revitalizing the drug pipeline: AntibioticDB, an open access database to aid antibacterial research and development. Journal of Antimicrobial Chemotherapy 2018;73:2284–97. https://doi.org/10.1093/JAC/DKY208.

[17] Stephens LJ, Werrett M V., Sedgwick AC, Bull SD, Andrews PC. Antimicrobial Innovation: a Current Update and Perspective on the Antibiotic Drug Development Pipeline. Future Med Chem 2020;12:2035–65. https://doi.org/10.4155/FMC-2020-0225.

[18] Sleytr UB, Schuster B, Egelseer EM, Pum D. S-layers: Principles and applications. FEMS Microbiol Rev 2014;38:823–64. https://doi.org/10.1111/1574-6976.12063.

[19] Demchick P, Koch AL. The permeability of the wall fabric of Escherichia coli and Bacillus subtilis. J Bacteriol 1996;178:768–73. https://doi.org/10.1128/JB.178.3.768-773.1996.

[20] Vergalli J, Bodrenko I V., Masi M, Moynié L, Acosta-Gutiérrez S, Naismith JH, et al. Porins and small-molecule translocation across the outer membrane of Gram-negative bacteria. Nature Reviews Microbiology 2019 18:3 2019;18:164–76. https://doi.org/10.1038/s41579-019-0294-2.

[21] Ramos MADS, Silva PB Da, Spósito L, Toledo LG De, vidal Bonifácio B, Rodero CF, et al. Nanotechnology-based drug delivery systems for control of microbial biofilms: A review. Int J Nanomedicine 2018;13:1179–213. https://doi.org/10.2147/IJN.S146195.

[22] Carter DM, Miousse IR, Gagnon JN, Martinez É, Clements A, Lee J, et al. Interactions between TonB from Escherichia coli and the periplasmic protein FhuD. Journal of Biological Chemistry 2006;281:35413–24. https://doi.org/10.1074/jbc.M607611200.

[23] Nikaido H. Molecular Basis of Bacterial Outer Membrane Permeability Revisited. Microbiology and Molecular Biology Reviews 2003;67:593–656. https://doi.org/10.1128/mmbr.67.4.593-656.2003.

[24] Nikaido H, Vaara M. Molecular basis of bacterial outer membrane permeability. Microbiol Rev 1985;49:1–32. https://doi.org/10.1128/mmbr.49.1.1-32.1985.

[25] Schauer K, Rodionov DA, de Reuse H. New substrates for TonB-dependent transport: do we only see the “tip of the iceberg”? Trends Biochem Sci 2008;33:330–8. https://doi.org/10.1016/j.tibs.2008.04.012.

[26] Straubinger M, Blenk H, Naber KG, Wagenlehner FME. Urinary concentrations and antibacterial activity of bal30072, a novel siderophore monosulfactam, against uropathogens after intravenous administration in healthy subjects. Antimicrob Agents Chemother 2016;60:3309–15. https://doi.org/10.1128/AAC.02425-15.

[27] FDA. Drug Approval Package: FETROJA (cefiderocol) 2019. https://www.accessdata.fda.gov/drugsatfda_docs/nda/2019/209445Orig1s000TOC.cfm (accessed April 14, 2023).

[28] Masi M, Réfregiers M, Pos KM, Pagès J-MM. Mechanisms of envelope permeability and antibiotic influx and efflux in Gram-negative bacteria. Nat Microbiol 2017;2:1–7. https://doi.org/10.1038/nmicrobiol.2017.1.

[29] Skwarczynski M, Bashiri S, Yuan Y, Ziora ZM, Nabil O, Masuda K, et al. Antimicrobial Activity Enhancers: Towards Smart Delivery of Antimicrobial Agents. Antibiotics 2022;11:1–28. https://doi.org/10.3390/antibiotics11030412.

[30] Vaara M. Polymyxin Derivatives that Sensitize Gram-negative Bacteria to Other Antibiotics. Molecules 2019;24:249. https://doi.org/10.3390/MOLECULES24020249.

[31] Scheller A, Oehlke J, Wiesner B, Dathe M, Krause E, Beyermann M, et al. Structural requirements for cellular uptake of α-helical amphipathic peptides. Journal of Peptide Science 1999;5:185–94. https://doi.org/10.1002/(SICI)1099-1387(199904)5:4<185::AID-PSC184>3.0.CO;2-9.

[32] Dwyer DJ, Collins JJ, Walker GC. Unraveling the physiological complexities of antibiotic lethality. Annu Rev Pharmacol Toxicol 2015;55:313–32. https://doi.org/10.1146/annurev-pharmtox-010814-124712.

[33] Koo HB, Seo J. Antimicrobial peptides under clinical investigation. Peptide Science 2019;111. https://doi.org/10.1002/pep2.24122.

[34] Oikawa K, Islam MM, Horii Y, Yoshizumi T, Numata K. Screening of a Cell-Penetrating Peptide Library in Escherichia coli: Relationship between Cell Penetration Efficiency and Cytotoxicity. ACS Omega 2018;3:16489–99. https://doi.org/10.1021/acsomega.8b02348.

[35] Krishnamoorthy G, Wolloscheck D, Weeks JW, Croft C, Rybenkov V V., Zgurskaya HI. Breaking the permeability barrier of Escherichia coli by controlled Hyperporination of the outer membrane. Antimicrob Agents Chemother 2016;60:7372–81. https://doi.org/10.1128/AAC.01882-16.

[36] Ye M, Zhao Y, Wang Y, Yodsanit N, Xie R, Gong S. pH-Responsive Polymer–Drug Conjugate: An Effective Strategy to Combat the Antimicrobial Resistance. Adv Funct Mater 2020;30:2002655. https://doi.org/10.1002/adfm.202002655.

[37] Ji C, Miller MJ. Chemical syntheses and in vitro antibacterial activity of two desferrioxamine B-ciprofloxacin conjugates with potential esterase and phosphatase triggered drug release linkers. Bioorg Med Chem 2012;20:3828–36. https://doi.org/10.1016/j.bmc.2012.04.034.

[38] Haktaniyan M, Bradley M. Polymers showing intrinsic antimicrobial activity. Chem Soc Rev 2022;51:8584–611. https://doi.org/10.1039/D2CS00558A.

[39] Barman S, Konai MM, Samaddar S, Haldar J. Amino Acid Conjugated Polymers: Antibacterial Agents Effective against Drug-Resistant Acinetobacter baumannii with No Detectable Resistance. ACS Appl Mater Interfaces 2019;11:33559–72. https://doi.org/10.1021/ACSAMI.9B09016/SUPPL_FILE/AM9B09016_SI_001.PDF.

[40] Blazyk J, Wiegand R, Klein J, Hammer J, Epand RM, Epand RF, et al. A Novel Linear Amphipathic β-Sheet Cationic Antimicrobial Peptide with Enhanced Selectivity for Bacterial Lipids. Journal of Biological Chemistry 2001;276:27899–906. https://doi.org/10.1074/jbc.M102865200.

[41] Manabe T, Kawasaki K. D-form KLKLLLLLKLK-NH2 peptide exerts higher antimicrobial properties than its L-form counterpart via an association with bacterial cell wall components. Scientific Reports 2017 7:1 2017;7:1–10. https://doi.org/10.1038/srep43384.

[42] Nam HY, Choi J, Kumar SD, Nielsen JE, Kyeong M, Wang S, et al. Helicity Modulation Improves the Selectivity of Antimicrobial Peptoids. ACS Infect Dis 2020;6:2732–44. https://doi.org/10.1021/ACSINFECDIS.0C00356/.

[43] Saint Jean KD, Henderson KD, Chrom CL, Abiuso LE, Renn LM, Caputo GA. Effects of Hydrophobic Amino Acid Substitutions on Antimicrobial Peptide Behavior. Probiotics Antimicrob Proteins 2018;10:408–19. https://doi.org/10.1007/S12602-017-9345-Z/METRICS.

[44] Matthyssen T, Li W, Holden JA, Lenzo JC, Hadjigol S, O'Brien-Simpson NM. The Potential of Modified and Multimeric Antimicrobial Peptide Materials as Superbug Killers. Front Chem 2022;9:795433. https://doi.org/10.3389/FCHEM.2021.795433/BIBTEX.

[45] Tam JP, Lu YA, Yang JL. Antimicrobial dendrimeric peptides. Eur J Biochem 2002;269:923–32. https://doi.org/10.1046/J.0014-2956.2001.02728.X.

[46] Sahariah P, Sørensen KK, Hjálmarsdóttir MA, Sigurjónsson ÓE, Jensen KJ, Másson M, et al. Antimicrobial peptide shows enhanced activity and reduced toxicity upon grafting to chitosan polymers. Chemical Communications 2015;51:11611–4. https://doi.org/10.1039/C5CC04010H.

[47] Chan LW, Hern KE, Ngambenjawong C, Lee K, Kwon EJ, Hung DT, et al. Selective Permeabilization of Gram-Negative Bacterial Membranes Using Multivalent Peptide Constructs for Antibiotic Sensitization. ACS Infect Dis 2021;7:721–32. https://doi.org/10.1021/acsinfecdis.0c00805.

[48] Lehn JM. Toward complex matter: Supramolecular chemistry and self-organization. Proceedings of the National Academy of Sciences 2002;99:4763–8. https://doi.org/10.1073/PNAS.072065599.

[49] Cousins GRL, Poulsen SA, Sanders JKM. Molecular evolution: dynamic combinatorial libraries, autocatalytic networks and the quest for molecular function. Curr Opin Chem Biol 2000;4:270–9. https://doi.org/10.1016/S1367-5931(00)00088-0.

[50] Lehn JM. Dynamers: dynamic molecular and supramolecular polymers. Prog Polym Sci 2005;30:814–31. https://doi.org/10.1016/J.PROGPOLYMSCI.2005.06.002.

[51] Liu Y, Lehn JM, Hirsch AKH. Molecular Biodynamers: Dynamic Covalent Analogues of Biopolymers. Acc Chem Res 2017;50:376–86. https://doi.org/10.1021/ACS.ACCOUNTS.6B00594/ASSET/IMAGES/LARGE/AR-2016-005942_0008.JPEG.

[52] Hirsch AKHH, Buhler E, Lehn JM. Biodynamers: Self-organization-driven formation of doubly dynamic proteoids. J Am Chem Soc 2012;134:4177–83. https://doi.org/10.1021/ja2099134.

[53] Wang L, Liu L, Wu L, Liu L, Wang X, Yang S, et al. Environmentally responsive amino acid-bioconjugated dynamic covalent copolymer as a versatile scaffold for conjugation. RSC Adv 2015;5:30456–63. https://doi.org/10.1039/C5RA00192G.

[54] Oba M, Nagano Y, Kato T, Tanaka M. Secondary structures and cell-penetrating abilities of arginine-rich peptide foldamers. Sci Rep 2019;9:1–9. https://doi.org/10.1038/S41598-018-38063-8.

[55] Popella L, Jung J, Do PT, Hayward RJ, Barquist L, Vogel J. Comprehensive analysis of PNA-based antisense antibiotics targeting various essential genes in uropathogenic Escherichia coli. Nucleic Acids Res 2022;50:6435–52. https://doi.org/10.1093/nar/gkac362.

[56] Bennett CF, Swayze EE. RNA targeting therapeutics: Molecular mechanisms of antisense oligonucleotides as a therapeutic platform. Annu Rev Pharmacol Toxicol 2010;50:259–93. https://doi.org/10.1146/ANNUREV.PHARMTOX.010909.105654.

[57] Misson LE, Mindrebo JT, Davis TD, Patel A, Andrew McCammon J, Noel JP, et al. Interfacial plasticity facilitates high reaction rate of E. coli FAS malonyl-CoA:ACP transacylase, FabD. Proc Natl Acad Sci U S A 2020;117:24224–33. https://doi.org/10.1073/PNAS.2009805117.

[58] Yavari N, Goltermann L, Nielsen PE. Uptake, Stability, and Activity of Antisense Anti- acpP PNA-Peptide Conjugates in Escherichia coli and the Role of SbmA. ACS Chem Biol 2021;16:471–9. https://doi.org/10.1021/ACSCHEMBIO.0C00822.

[59] Story S, Bhaduri S, Ganguly S, Dakarapu R, Wicks SL, Bhadra J, et al. Understanding Antisense Oligonucleotide Efficiency in Inhibiting Prokaryotic Gene Expression. ACS Infect Dis 2024;10:971–87. https://doi.org/10.1021/ACSINFECDIS.3C00645.

[60] Angrish N, Khare G. Antisense oligonucleotide based therapeutics and its applications against bacterial infections. Med Drug Discov 2023;20:100166. https://doi.org/10.1016/J.MEDIDD.2023.100166.

[61] Hutchings M, Truman A, Wilkinson B. Antibiotics: past, present and future. Curr Opin Microbiol 2019;51:72–80. https://doi.org/10.1016/J.MIB.2019.10.008.

[62] Walker DK. The use of pharmacokinetic and pharmacodynamic data in the assessment of drug safety in early drug development. Br J Clin Pharmacol 2004;58:601–8. https://doi.org/10.1111/J.1365-2125.2004.02194.X.

6. List of Publications

6.1 Publications in Peer-Reviewed Journals

Research Papers

1. Menina, S., Eisenbeis, J., **Kamal, M. A. M.**, Koch, M., Bischoff, M., Gordon, S., Loretz, B., Lehr, C. Bioinspired Liposomes for Oral Delivery of Colistin to Combat Intracellular Infections by Salmonella enterica. *Advanced Healthcare Materials*, *8*(17), 2019, https://doi.org/10.1002/adhm.201900564 (Research paper)
2. Richter, R., **Kamal, M. A. M.**, García-Rivera, M. A., Kaspar, J., Junk, M., Elgaher, W. A., Srikakulam, S. K., Gress, A., Beckmann, A., Grißmer, A., Meier, C., Vielhaber, M., Kalinina, O., Hirsch, A. K., Hartmann, R. W., Brönstrup, M., Schneider-Daum, N., Lehr, C.M.. A hydrogel-based in vitro assay for the fast prediction of antibiotic accumulation in Gram-negative bacteria. *Materials Today Bio*, *8*, 100084, 2020, https://doi.org/10.1016/j.mtbio.2020.100084 (Research paper)
3. Richter, R., **Kamal, M. A. M.**, Koch, M., Niebuur, B., Huber, A., Goes, A., Volz, C., Vergalli, J., Kraus, T., Müller, R., Schneider-Daum, N., Fuhrmann, G., Pagès, J., Lehr, C.M.. An Outer Membrane Vesicle-Based Permeation Assay (OMPA) for assessing bacterial bioavailability. *Advanced Healthcare Materials*, *11*(5), 2021, https://doi.org/10.1002/adhm.202101180 (Research paper)
4. Sousa, C. F., **Kamal, M. A. M.**, Richter, R., Elamaldeniya, K., Hartmann, R. W., Empting, M., Lehr, C.M., Kalinina, O. V. Modeling the Effect of Hydrophobicity on the Passive Permeation of Solutes across a Bacterial Model Membrane. *Journal of Chemical Information and Modeling*, *62*(20), 5023–5033, 2022, https://doi.org/10.1021/acs.jcim.2c00767 (Research paper)
5. Wu, Y., Zoller, B. G. E., **Kamal, M. A. M.**, Hotop, S., Lehr, C.M., Brönstrup, M., Dersch, P., Empting, M. Establishment of an in bacterio assay for the assessment of carbon storage regulator A (CSRA) inhibitors. *ChemBioChem*, *24*(16), 2023. https://doi.org/10.1002/cbic.202300369 (Research paper)
6. Zeroug-Metz, L., **Kamal, M. A. M.**, Bassil, J., Elamaldeniya, K., Ryu, B. H., Buhler, E., Lee, S. Fluorescent histidine-derived biodynamers as biocompatible and highly water-soluble copper(ii)-sensors. *RSC Applied Polymers*, 2024, https://doi.org/10.1039/d4lp00126e (Research paper)
7. **Kamal, M. A. M.**, Bassil, J., Loretz, B., Hirsch, A. K., Lee, S., Lehr, C.M.. Arg-biodynamers as antibiotic potentiators through interacting with Gram-negative outer membrane lipopolysaccharides. *European Journal of Pharmaceutics and Biopharmaceutics*, *200*, 114336, 2024, https://doi.org/10.1016/j.ejpb.2024.114336 (Research paper)
8. Liu, Y., Biesel, A., **Kamal, M.A.M**., Latta, L., Loretz, B., Hirsch, A.K.H., Lee, S., Lehr, C.M. Tobramycin crosslinking improves the colloidal stability of arginine chitosan biodynamers for safe and efficient siRNA delivery. *International Journal of Biological Macromolecules*, 311, 1, 2025, https://doi.org/10.1016/j.ijbiomac.2025.143420. (Research paper)

Perspective Papers

9. Bali, A.*, **Kamal, M. A. M.***, Mulla, G.*, Loretz, B., Lehr, C.M. Functional materials to overcome bacterial barriers and models to advance their development. *Advanced Functional Materials*, *33*(45), 2023, https://doi.org/10.1002/adfm.202304370

*Equal first co-authorship

Articles to be Submitted/Accepted

10. **Kamal, M. A. M.**, Bassil, J., Niebuur, B.-J., Kraus, T., Herrmann, J., Koch, M., Hirsch, A. K. H., Loretz, B., Lee, S., & Lehr, C.M. A multivalent TAT–Arginine-Biodynamer conjugate to overcome the bacterial cell envelope barrier by Bacteria-Specific membrane interactions. *Advanced Functional Materials*, 2025
11. **Bassil, J.**, Kamal, M.A.M., Gabelmann, A., Christoulaki, A., Koch, M., Loretz, B., Gallei, M., Behler, E., Lehr, C.M., Hirsch, A.K.H., Lee, S. Direct Monitoring of Intracellular Polymer Degradation via BODIPY Dynamic Dequenching. *Materials & Design*, 2025

6.2 Presentations at Conferences

12. **Kamal, M. A. M.**, Loretz, B., Lee, S., Lehr, C.M., Biodynamers functionalized with cell-penetrating peptides as tools to permeabilize Gram-negative Bacteria, TANDEM meeting, Homburg, Germany, 2022. (Podium)
13. **Kamal, M. A. M.**, Basil, J., Loretz, B., Hirsch, A. K. H., Lee, S., Lehr, C.M., Biodynamers as antimicrobial polymers against Escherichia coli, CRS Germany Local Chapter Meeting, Würzburg, Germany, 2023. (Poster)
14. **Kamal, M. A. M.**, Basil, J., Loretz, B., Hirsch, A. K. H., Lee, S., Lehr, C.M., Molecular stents as antibiotics potentiators through β-sheet formation in LPS microenvironment, CRS Germany Local Chapter Meeting, Bad Dürkheim, Germany, 2024 (Poster)
15. **Kamal, M. A. M.**, Basil, J., Loretz, B., Lee, S., Lehr, C.M., Potentiating the efficacy of antibiotics in Escherichia coli by α-helical nanorods, DZIF Annual Meeting, Hannover, Germany, 2023. (Poster)
16. **Kamal, M. A. M.**, Basil, J., Loretz, B., Hirsch, A. K. H., Lee, S., Lehr, C.M., Breaking in through bacterial barriers: Enhancing Antibiotics by molecular stents in Gram-negative bacteria, Merzig, Germany, 2023. (Poster)
17. **Kamal, M. A. M.**, Basil, J., Loretz, B., Lee, S., Lehr, C.M., β-sheet forming polymeric peptidomimetics as molecular stents in LPS microenvironments as antibiotics delivery adjuvants, CRS Annual Meeting and Expo, Bologna, Italy, 2024. (Poster)
18. Lee, Sangeun , **Kamal, M. A. M.,** Lehr, C.M., Hirsch, A. K. H., Biodynamers as novel materials to improve Drug Delivery across biological barriers, Program-Oriented Funding of Topic 3 in Helmholtz Center for Infection Research, 2025. (Poster)
19. Koumou-Okandze, M., Mulla, G., **Kamal, M.A.M.,** Schneider-Daum, N., Loretz, B., Lehr, C.M., Functional Nanomaterials to Overcome Bacterial Barriers and Resistance, Internation Conference on Anti-Infectives, 2025. (Poster)

6.3 Ongoing Patent Application

20. Biodynamer conjugates as versatile tools for biological applications
    Inventors: **Mohamed A. M. Kamal**, Brigitta Loretz, Sangeun Lee, Claus-Michael Lehr

7. Curriculum Vitae

Mohamed Ashraf Mostafa Kamal

Date of birth: 27/11/1996 **Phone number:** (+49) 1702841950
Email address: mohamedashraf.kamal96@gmail.com
LinkedIn: https://www.linkedin.com/in/mohamed-ashraf-kamal/
Website: https://www.scopus.com/authid/detail.uri?authorId=57210213964
Home: Sulzbachtalstraße 61, 66280 Sulzbach (Germany)

ABOUT ME

Motivated pharmacist and scientist with expertise in leading drug discovery projects and formulation development. Experienced in designing and implementing lab-scale experiments, managing external collaborations, and driving interdisciplinary projects that address global challenges.

SKILLS

Core Skills

Can-do Attitude, Eagerness to self-develop and stay informed, Project Management, Interdisplinary Collaboration, Team Leadership, Problem Solving, Time-effective Project Completion, Technical Report Writing and Presentation.

Technical Skills

Skin models, human and bacterial metabolism, Bacterial Culture (BSL-2) and Antimicrobial Assaying, Mammalian Cell Culture, Analytical Techniques (HPLC, SEC, 2D NMR, qNMR, FTIR, DLS, SLS, GPC, ITC, UV-Vis, Circular Dichorism), Western blot, SDS-PAGE, Analytical Method Development and Validation, Statistical Analysis (GraphPad Prism, MS Excel, R Programming), Molecular Modeling and Docking.

WORK EXPERIENCE

Doctoral Scientist
Helmholtz Institute for Pharmaceutical Research Saarland (HIPS) [14/08/2021 – Current]

City: Saarbrücken | **Country:** Germany

- Led Drug Discovery projects of antimicrobial macromolecules with hands-on experience both in the biological as well as the chemical fields.
- Conducting a number of complex assays to conclude a novel mechanism of action against bacteria.
- Conducting antibacterial assays in BSL-2 lab as well as cytotoxicity assays on mammalian cells.

Graduate Student Researcher
Helmholtz Institute for Pharmaceutical Research Saarland (HIPS) [14/02/2021 – 22/11/2021]

City: Saarbrücken | **Country:** Germany | **Website:** https://www.helmholtz-hzi.de/en/research/research-topics/anti-infectives/biological-barriers-and-drug-delivery/claus-michael-lehr/ | **Name of unit or department:** Department of Biological Barriers and Drug Delivery

- Developed and validated a complex *in vitro* model with a bioanalytical method allowing for *in situ* monitoring of different compartments simultaneously for evaluating the permeability and bioavailability of biologics, ensuring compliance with FDA and EMA industrial guidlines.

Pharmaceutical Chemistry Teaching Assistant
German International University of Applied Sciences (GIU-AS) [30/09/2020 – 30/01/2021]

City: New Admin Capital | **Country:** Egypt | **Website:** http://www.giu-uni.de/ | **Name of unit or department:** Department of Chemistry and Biology

- Set up a new laboratory for students and ensuring GLP compliance
- Participation in curriculum and exams creation

Undergraduate Research Fellow
Helmholtz Centre for Infection Research [31/05/2019 – 29/08/2019]

City: Braunschweig | **Country:** Germany

1 / 2

• Generation of novel recombinant reporter cytomegalovirus for humans and mice via genetic engineering aiming for its use as a potential vaccine vector.

Undergraduate Research Fellow
Helmholtz Institute for Pharmaceutical Research Saarland (HIPS) [31/05/2018 – 29/08/2018]

City: Saarbrücken | **Country:** Germany

• Modeling the structure and permeability of the Gram-negative bacterial cell envelope *in vitro* using lipids and bacterial outer membrane vesicles.

Undergraduate Research Fellow
Helmholtz Institute for Pharmaceutical Research Saarland (HIPS) [25/06/2017 – 02/09/2017]

City: Saarbrücken | **Country:** Germany

• Development of bacterial injection system functionalized drug-loaded liposomes for oral drug delivery against GIT infections.

EDUCATION AND TRAINING

Planned: Qualitätsmanagement in der Medizin- und Pharmaindustrie (GMP) "ISO 13485" und "ISO 9001"
alfatraining

PhD (Doctorate) in Pharmaceutical Technology
Saarland University [14/08/2021 – Current]

City: Saarland University | **Country:** Germany

telc Deutsch B2 (allgemein)
[21/10/2023]

Country: Germany

MSc in Pharmacy
Saarland University [14/02/2021 – 22/11/2021]

City: Saarbrücken | **Country:** Germany | **Final grade:** 1.0

Data Science: Foundations using R (programming language) Specialization
Johns Hopkins University [01/02/2020 – 30/04/2020]

Website: https://www.coursera.org/specializations/data-science-foundations-r | **Final grade:** 96%

Bachelor in Pharmacy
German University in Cairo [30/09/2015 – 29/07/2020]

City: Kairo | **Country:** Egypt | **Website:** https://www.guc.edu.eg/ | **Final grade:** 0,79 (A+)

Egyptian general secondary school leaving certificate
Maadi Language School [30/09/2012 – 30/06/2015]

City: Kairo | **Country:** Egypt | **Final grade:** 99.5%

LANGUAGES

English - Fluent

Arabic - Fluent

German - Upper intermediate (B2) - actively improving

8. Acknowledgements

Reaching the completion of this thesis has been a challenging yet rewarding journey, made possible by the unwavering support, guidance, and encouragement of many remarkable individuals. I would like to take this moment to express my deepest gratitude to everyone who contributed to this milestone.

First and foremost, I extend my heartfelt thanks to my Doktorvater, Prof. Dr. Claus-Michael Lehr. Ihre unerschütterliche Führung, Ihr wertvolles Feedback und Ihre inspirierende Mentorenschaft haben mein akademisches Wachstum entscheidend geprägt – angefangen bei meinen Praktika in den Jahren 2017 und 2018, über meine Masterarbeit im Jahr 2021 bis hin zu meiner Doktorarbeit im Jahr 2025. Ihre konstruktiven Ratschläge während wissenschaftlicher Diskussionen, gepaart mit Ihrer Ermutigung und Unterstützung in schwierigen Momenten, haben stets ein Umfeld der Neugierde und Exzellenz geschaffen. Ihre Leidenschaft für Wissenschaft und Ihre menschliche Art sind für mich eine Inspiration. Ich bin zutiefst dankbar für die Möglichkeit, von Ihnen lernen zu dürfen.

I am also deeply grateful to Jun.-Prof. Dr. Sangeun Lee, for your invaluable feedback, no matter the time or urgency. Your attention to detail, scientific expertise, and tireless support have been a constant source of guidance throughout my journey. You have always been there to provide clarity and encouragement, and your mentorship has enriched this thesis in more ways than I can express.

A special word of appreciation goes to Dr. Brigitta Loretz, whose guidance and unwavering mentorship were pivotal to overcoming numerous challenges. Your kindness, patience, and dedication inspired me to push my boundaries, both scientifically and personally. Thank you for being a reliable source of expertise and for helping me navigate even the toughest moments with confidence.

I would also like to express my sincere gratitude to the technical and administrative staff at DDEL, particularly Pascal Paul, Petra König, and Annette Boese, for their dedication and behind-the-scenes contributions. Your hard work ensured the smooth progression of my experiments and the organizational flow of my work. I truly appreciate all your efforts.

To my colleagues and collaborators in DDEL and AK Lee, thank you for creating such a supportive and intellectually stimulating environment. A special mention goes to Dr. Robert Richter, whose guidance during my early days set me on the path toward scientific exploration. I would also like to thank Aghiad Bali, whose positivity and encouragement kept me motivated, even during the longest lab days. Working alongside all of you has been an enriching and memorable experience.

On a personal note, I owe an immeasurable debt of gratitude to my family. To my beloved father and mother, thank you for your unwavering support, endless encouragement, and boundless love. Your belief in me and your inspiring role model have been my greatest strength throughout this journey. To my brother, thank you for being my unwavering supporter and for always cheering me on, no matter the distance.

Lastly, my deepest gratitude goes to Maryam and our daughter, Sophia. Maryam, your patience, love, and support have been my anchor, especially during the most demanding moments of this journey. Sophia, your smile and energy have brought me joy and reminded me of the importance of balance. Thank you both for being my inspiration and my greatest source of happiness.

To everyone who played a role in this journey, whether mentioned here or not, thank you for your contributions, kindness, and belief in me. This thesis is as much a reflection of your efforts as it is of mine.

9. Reprints of Original Publications:

9.1 Perspective Paper

Subchapter is the following publication:

Abstract and section 2.2 of Paper 1: “Functional Materials to Overcome Bacterial Barriers and Models to Advance Their Development”

Aghiad Bali*, **Mohamed A. M. Kamal***, Glorjen Mulla*, Brigitta Loretz, Claus-Michael Lehr

DOI: 10.1002/adfm.202304370

*Authors contributed equally to this work

Contributions: A.B, M.A.M.K, and G.M. contributed mainly to sections 3, 2.2, 2.1, respectively. B.L. and C.M.L contributed to the supervision. All authors contributed to conceptualization, writing the manuscript.

ADVANCED FUNCTIONAL MATERIALS
www.afm-journal.de

Functional Materials to Overcome Bacterial Barriers and Models to Advance Their Development

*Aghiad Bali, Mohamed A. M. Kamal, Glorjen Mulla, Brigitta Loretz, and Claus-Michael Lehr**

With the emerging problem of antimicrobial resistance, the world is facing a slow but dangerous pandemic. While the discovery of novel antibiotics is reaching a nearly exhaustive end, new concepts for anti-infective drugs are emerging. So-called pathoblockers aim to de-weaponize bacteria rather than just killing them. As the target of these molecules is typically located intracellularly, however, hitherto almost unnoticed biological barriers are emerging such as the biofilm matrix, the bacterial cell envelope, efflux pumps, and eventual bacterial metabolism. This leads to a new paradigm that is to maximize bacterial bioavailability. To overcome the bacterial barriers, especially when further optimization of the active molecules is not possible, functional materials are needed to engineer innovative delivery systems. Those may not only enable novel anti-infective molecules to reach their targets, but will also improve the bacterial bioavailability of existing anti-infectives. Additionally, there is a need for better infection models that allow studying drug effects on both the bacteria and the host in a relevant manner as needed for rational anti-infective drug development.

1. Introduction

1.1. The Threat of Bacterial Resistance and the Need for Novel Anti-Infectives

Antimicrobial resistance (AMR) is the ability of a microbe to learn how to avoid being killed by antimicrobials. Reports of this global health threat are increasing, and it is estimated that 700000 deaths per year worldwide are attributed to AMR. The number of fatalities is predicted to increase to 10 million per year by 2050, making AMR the leading cause of death if no action is taken. The World Health Organization has categorized the different critical pathogen groups into priority lists. Notably, priority list 1 comprises exclusively multiple drug-resistant (MDR) Gram-negative bacteria (*Acinetobacter baumannii*, *Pseudomonas aeruginosa*, *Enterobacteriaceae*). This emphasizes the difficulty of combating these bacteria with conventional antimicrobials, mainly due to the complex Gram-negative bacterial cell envelope. The usual workflow in clinical settings starts with using some first-line agent(s), followed by second and third lines, reaching last resort alternatives that often have serious effects on the life quality of the patient. Nevertheless, time is always not in favor of the patients as confirming the resistance and initiating the new treatment protocol can happen in a very late stage after the infection has built its fortresses and castles (for instance in the form of biofilms), rendering it both resistant and tolerant to antibiotic treatment.[1] In this perspective, we will have a special emphasis on the Gram-negative cell envelope and bacterial biofilms as biological barriers. As regards the human body, we shall pay some special attention to the lungs, which are one of the organs most seriously affected by infectious diseases.

AMR is a phenomenon that occurs naturally but is propagated by extensive and inappropriate use of antibiotics. Moreover, the increasing emergence of multidrug-resistant bacteria has made the search for new antibiotics even more critical. The lack of new classes of antibiotics to fight against these resistant bacteria is a major concern. The pipeline for new antibiotics has slowed down in recent years, and the discovery void for new classes of antibiotics is becoming more and more apparent. It is noteworthy, that none of the potential antibiotics in current clinical trials represents a novel class against Gram-negative bacteria. On the other hand, there are many reasons for the lack of research on novel antibiotics, which include a lack of satisfactory return on investment, insufficient cooperation between academia, industry, and still limited public awareness and funding. However, there have been some initiatives recently, such as the "Global Antibiotic Research and Development Partnership" (GARDP).[2] To combat the problem of AMR, there is an urgent need for more

A. Bali, M. A. M. Kamal, G. Mulla, B. Loretz, C.-M. Lehr
Department of Biological Barriers and Drug Delivery
Helmholtz Centre for Infection Research (HZI)
Helmholtz Institute for Pharmaceutical Research Saarland (HIPS)
66123 Saarbrücken, Germany
E-mail: claus-michael.lehr@helmholtz-hzi.de
A. Bali, M. A. M. Kamal, G. Mulla, C.-M. Lehr
Department of Pharmacy
Saarland University
66123 Saarbrücken, Germany

The ORCID identification number(s) for the author(s) of this article can be found under https://doi.org/10.1002/adfm.202304370

DOI: 10.1002/adfm.202304370

instance, PEG-coated nanoparticles previously reported to display decreased mucoadhesive behavior would theoretically also show decreased biofilm adhesion.[63] In a study, it was found that the acidic mucus milieu promotes the interaction between the surface of nanoparticles and mucins, which are the main component of the mucus layer and have been reported to attenuate the virulence of *P. aeruginosa*.[64] On one hand, surface-PEGylated solid nanoparticles exhibited the advantage of mucus penetration, while on the other side positively charged amine-modified solid nanoparticles and carboxyl-modified particles were trapped in the negatively charged mucus.[65] In another study, it was found that ultra-small (< 100 nm) solid lipid nanoparticles with hydrophilic surface properties enhance mucus penetration.[66] If the claim that mucus and biofilms display similar rheological properties stands, then it can be speculated that lipid nanoparticles and PEG-shell-modified nanocarrier could potentially facilitate biofilm penetration. Indeed, a recent study showed that PEG–PLGA nanoparticles had enhanced biofilm penetration.[67]

Materials and Strategies for Biofilm Penetration: Different nanoparticles have been shown to display biofilm penetration activity (Figure 3). Among them, polymeric nanoparticles display the greatest potential.[68] For instance, cationic polymer conjugates could penetrate through biofilm layers.[69] Likewise, biofilm-responsive caged guanidine nanoparticles could penetrate and accumulate in bacterial biofilm.[70] Other examples include CS, poly(lactic-co-glycolic acid, and polycaprolactone nanoparticles. CS is a polymer of special interest due to its intrinsic antibacterial activity.[71,72] The overall positive charge enables it to electrostatically bind to the negatively charged outer membrane of the bacteria and negatively charged biofilm EPS. Therefore, many nanoparticles were designed to be coated with CS to facilitate the biofilm diffusion of both drugs and nanoparticles.[73,74] For instance, a chitosan-polyethylene glycol-peptide conjugate with a size of ≈100 nm resulted in an increased biofilm penetration.[75] Alternatively, lipid nanoparticles could enhance the penetration of biofilms. A recent study showed that tobramycin-loaded lipid liquid crystal nanoparticles could significantly enhance the penetration and eradication of *P. aeruginosa* biofilm infections.[76]

In the context of biofilm penetration, an alternative approach might be to treat the biofilm matrix as an "ally" and employ agents that display similar characteristics to EPS polymers to coat and make loaded drugs "invisible" to the biofilm surface. The latter could be considered a biomimetic drug delivery strategy. To advance this hypothesis, several steps must be taken. First, potential materials such as polymers of the biofilm matrix should be identified and characterized. Afterward, polymeric analogs of these materials must be found or synthesized. Lastly, once available the newly identified EPS-mimetic compound can be employed as a coating agent to merge with the biofilm matrix as part of its structure and to release the cargo in the immediate vicinity of its bacterial targets.

2.2. Overcoming the Bacterial Cell Envelope

A major cause of bacterial resistance to antibiotics is attributed to the bacterial cell envelope, which represents with its complex structure a significant barrier for the internalization and accumulation of antibiotics in bacterial cells and thereby limits bacterial bioavailability (**Figure 4**). Depending on the structure of their envelope, bacteria are classified as Gram-positive and Gram-negative. The cell envelope of Gram-positive bacteria is constituted of an inner lipid membrane and a thick peptidoglycan layer representing a gel-like mesh structure. In contrast to their Gram-positive counterparts, Gram-negative bacteria have a much thinner peptidoglycan layer and confine an additional outer membrane made of an inner leaflet of lipids and an outer leaflet of lipopolysaccharide (LPS). Some Gram-negative bacteria might also have an extra outer layer called the S-layer, made of proteins or glycoproteins.[77,78] Different proteins are embedded within the bacterial cell membrane to coordinate the facilitated diffusion and transport through the membrane.

Targeting intracellular components requires the active molecule to possess the size and other physiochemical properties needed for uptake while still maintaining binding affinity and activity at the target. Besides optimizing the transport properties of anti-infective molecules, an alternative strategy is to look for materials that can serve as carriers, adjuvants, or are even antimicrobials by themselves. Such material has to interact with the bacterial membrane to either selectively target it or destroy it. It can be as little as small molecules or polymers or even much larger, such as nanoparticles, fibers, membranes or coatings, and scaffolds.[79] We will focus more on zero-dimensional materials, e.g., nanoparticles, which are favored to overcome biological barriers.

Simple Passive Diffusion: The transport of small molecules across the outer membrane of Gram-negative bacteria may occur through protein channels and/or the membrane lipids. The latter is referred to as simple passive diffusion. As with any other diffusion barrier, the main determinants are the concentration gradients and the size of the molecule in the host settings. LPS is the main limiter of simple passive diffusion, which is absent in Gram-positive bacteria. LPS consists of lipid A, inner core sugars, outer core sugars and O-antigen tightly bound together with divalent cations (Ca^{+2} and Mg^{+2}). The next layer is the peptidoglycan that is a gel-like mesh, then the lipid bilayer of the inner membrane. Only small hydrophilic neutral molecules like amino acids, water, and soluble gases are most likely to readily pass through the LPS layer.[80,81]

Facilitated Passive Diffusion: Facilitated passive diffusion is a process by which the bacteria use non-active channels to transport molecules from the outside to the inside of the bacterium without the expense of energy in the form of ATP or any potential gradient. The process depends primarily on the concentration gradient of the molecules of interest. Additionally, mutations can alter the function of these channels or porins resulting in reduced effectivity of the small organic molecules. This phenomenon has been observed in different strains, especially in *P. aeruginosa*, *A. baumannii*, and *Klebsiella pneumoniae*.[82]

Active Transport: Active transport refers to a process by which certain molecules are transported across the cell membrane independent of the concentration gradient. In bacteria, the so-called TonB-dependent transport system has evolved to internalize molecules that cannot translocate by facilitated diffusion, but at the expense of energy in the form of ATP or proton gradient. TonB transport is initiated when the substrate binds to one of its receptors at the OM (e.g., FhuA (binds ferrichrome),

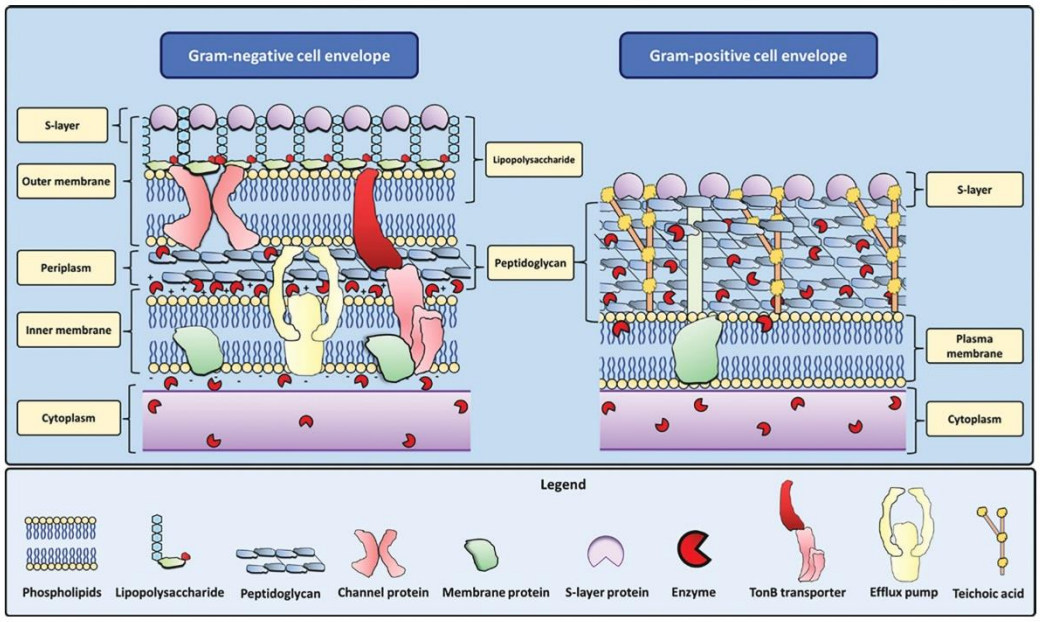

Figure 4. The different structures of Gram-positive and Gram-negative bacterial cell envelopes, illustrating the unique LPS structure as well as efflux pumps as the main limiters of simple passive diffusion. Adapted with permission.[6] Copyright 2023, Elsevier.

FepA (binds ferric enterobactin), and BtuB (binds vitamin B12)). Subsequently, the TonB system uses ATP or proton gradient for transport through the outer and inner membranes as well as the periplasm.[84]

As shown in **Table 1**, it is quite noticeable that the affinity of these channels to their substrates is variable and relatively low compared to the TonB transporter, which involves specific receptors as well as higher molecular weight cutoff. This affinity advantage of TonB-dependent transporters makes it more promising for the Trojan Horse approach for better intra-bacterium drug delivery.

Efflux Pumps: Efflux pumps are energy-dependent membrane-bound transporters that actively pump out toxic substances, drugs, and other antimicrobial agents. Notoriously they play a major role in bacterial resistance.[84] This is especially true for hydrophobic compounds (clogD7.4 > 3). On the other side, highly charged compounds with low molecular weight (<400 Da) are not affected by efflux pumps. The latter stands

Table 1. Different passive channels and TonB-dependent transporter (active transporter) in bacteria showing the substrates, the affinity (K_D) of the channel to its substrates, and an estimated size cut-off for molecules that can pass through.

Name	Substrate	K_D for a known substrate	Size cutoff [daltons]	References
Porins	Unspecific: hydrophilic molecules and ions	No/little affinity	600	[77,83–85]
LamB	Maltose, maltodextrins	10 μM for maltose	850	
BglH	Aryl-ß-D-glucoside	1–3 mM for 2-hydroxymethylphenyl-ß-glucoside	Expected as LamB due to homology	
Tsx	Nucleotides	Not determined	850	
FadL	Long-chain fatty acids	0.2 μM for oleate	300	
CymA	Cyclodextrin	28 μM for cyclodextrin	980	
TonB-dependent Transporters	Siderophores	300 nM for ferricrocin	1360	

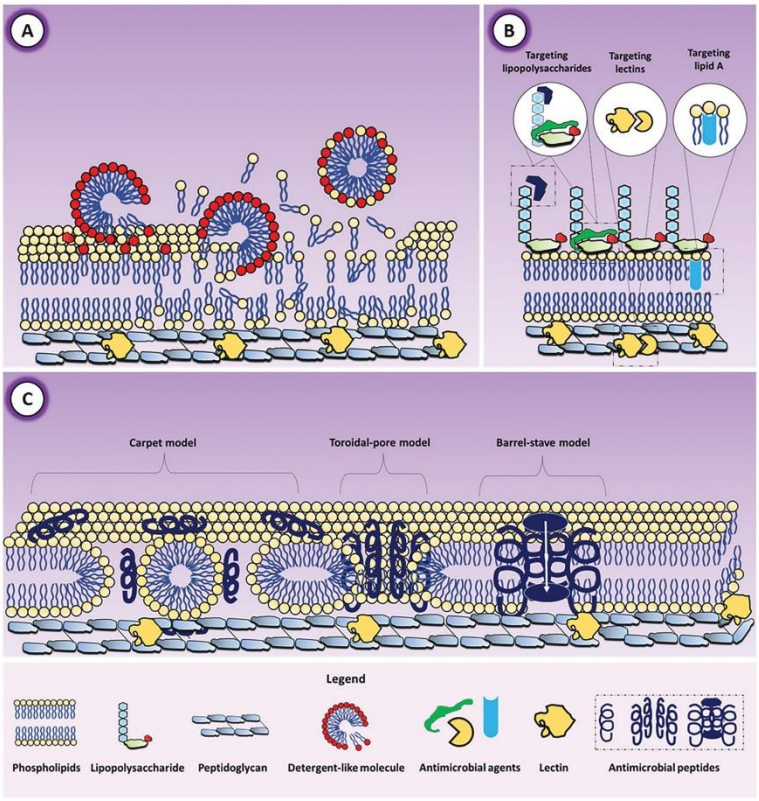

Figure 5. Strategies to enhance the permeability of anti-microbial agents across the Gram-negative bacterial cell envelope by A) Demolishment of the bacterial cell envelope (e.g., by detergent-like molecules). B) Specific bioadhesion to certain components (e.g., binding to lectins, lipid A, LPS) within the bacterial cell envelope. C) Permeabilization of the bacterial cell envelope (e.g., by membrane-active AMPs).

true also for polar zwitterions with a high molecular weight (400–600 Da). However, variations in the efflux systems among different bacterial strains like *E. coli* and *P. aeruginosa* exist, therefore, these generalizations are not absolute. Further understanding of the molecular descriptors that can be utilized to avoid efflux is important for improving bacterial bioavailability.[86] Alternatively, researchers could enhance the MIC of tetracycline by 4-fold when it was combined with efflux pump inhibitors.[87]

2.2.1. Enhancing the Permeability of the Bacterial Cell Envelope

Permeability through the bacterial cell envelope is the main delimiter of the activity of different potential anti-infectives. The permeation of small organic molecules through the bacterial cell envelope has been extensively covered in literature.[88,89] In this subsection, membrane-active materials will be discussed. We differentiate between two concepts; demolishment, and permeabilization. Demolishment refers to destroying the cell envelope to an extent that causes leakage of the intracellular components (**Figure 5**A). This is common for most disinfectants and leads to blunt killing of the bacteria. This again, however, just increases the chances of developing AMR. On the other hand, permeabilization refers to only inducing some structural changes (e.g., pore formation), rather than destroying the cell envelope. The aim is not to kill the bacterium but to facilitate the uptake of anti-infectives (e.g., modern pathoblockers) in its vicinity (Figure 5C).[90]

Demolishment: Most antibiotics that are active against Gram-negative bacteria act on intracellular targets, which requires the internalization of these molecules as a prerequisite for their activity. On the contrary, molecules that act on the bacterial cell envelope, do not require to be taken up by the bacterium to become active. Understanding this could encourage the scientific community to give more attention to membrane-directed strategies. Approaches that can be employed to demolish cellular membranes include:

- Detergents that have a hydrophobic part that sticks with the lipids and a hydrophilic part that stays in contact with the water outside the bacterium.[91]
- Peptides that can acquire α-helical conformation inside the membrane, permeabilizing the membrane.[92]
- Metal ions that can form complexes with the membrane of the bacteria, disrupting the membrane.[90]
- Gas generation within the membrane like hydrogen sulfide and H_2O_2 (which also can produce ROS to destroy the membrane).[93]

These membrane-destructive strategies need, however, to be adopted to avoid damage to the mammalian cell membrane, i.e., to target structures that are only found in bacteria, but not in mammalian cells. Such approaches include divalent cations, bacterial membrane-specific lipids and polysaccharides, and membrane overall charge. For instance, polymyxins (in use since 1964) belong to a class of antibiotics that interact with the LPS and compromise the membrane integrity of the bacteria. Nowadays, it is used as a last resort in the clinical setting because of its toxicity.[91]

So far, some detergent-like and α-helical peptides have reached advanced clinical development or are on the market. For instance, teixobactin, in addition to being a peptide-like molecule and not an AMP, targets lipid II in the bacterial membrane, inhibits peptidoglycan synthesis, and compromises the membrane integrity.[94] Other membrane-acting peptides with the ability to destroy the membrane have been isolated, e.g., melittin and maginin (reached clinical phase 3 and rejected). Melittin exhibits a detergent-like mechanism, while maginin forms an α-helix inside the lipid membrane of the bacteria. The usage of AMPs, however, is still quite limited due to the cost of production and the relatively high toxicity due to interactions with mammalian cell membranes.[95]

Nevertheless, membrane-active AMPs have enormous potential. Peptides have the highest degree of freedom and thus offer much potential to adjust the molecule toward bacterial, but not mammalian toxicity. Also, AMPs are not split structurally into a targeting moiety and an activity moiety, which therefore maximizes the antimicrobial activity normalized by molecular weight. Developing AMPs for clinical applications requires first screening against both mammalian cells and bacteria, ideally also leading to a better understanding of what governs this selectivity that has not been done until very recently.[96,97] Peptide modifications such as using D-amino acids and cyclization must also be taken into consideration. They can significantly influence the activity and selectivity of bacterial cells. In addition to peptides, synthetic oligomers, and polymers can also serve the same purpose, but more research is required to optimize their pharmacokinetics and pharmacodynamics.

Permeabilization: Permeabilization refers to the introduction of pores in the bacterial cell envelope by the employment of different pore-inducing agents. This process would therefore lead to enhanced drug uptake. Initial research could demonstrate that in some strains of Gram-negative bacteria, which had high pore expression, the minimum inhibitory concentration (MIC) of some antibiotics was decreased up to 128fold.[98] Increasing the permeability of the bacterial cell envelope would also open the perspective to convert narrow-spectrum antibiotics, acting on Gram-positive bacteria only, to broad-spectrum Gram-negative acting antibiotics. More importantly, it may enable to design agents against intracellular targets that are above 600 Daltons as long as the created pores allow their uptake.

Well-known pore-forming molecules are proteins like α-hemolysin and peptides like melittin (bee venom). Nevertheless, the proteins can cause collateral damage to mammalian cells, which limits their translation to the clinic.[99,100] However, recent studies discovered more biocompatible membrane-acting potentiators, such as polycations, cell-penetrating peptides, artificially-quaternized polymers, and combinations of the two approaches like peptide-functionalized polycationic polymers.[101–103] Others developed a relatively simple structure with two positively charged groups that interact with the bacterial membrane and were able to potentiate pre-existing antibiotics by up to 512-folds against MDR *E. coli*.[104]

Silver nanoparticles have been used for so long as antimicrobial materials because of their many involved mechanisms of action such as the inactivation of proteins (disrupting bacterial metabolism), production of reactive oxygen species, and contact interactions with the bacterial cell envelope. However, safety concerns and difficulty in excreting metal-based nanoparticles halted their further development.[105] Nevertheless, the door stays open for employing silver nanoparticles in lower doses as an adjuvant to other anti-infectives such as carbenicillin.[106]

There seem to be three crucial factors that contribute to such adjuvanted effects. First, the more cationic a molecule, the more likely it is to have antimicrobial activity. Second, the higher the alpha-helical structure of a peptide, the more rigid it will be to thus disrupt the membrane and enhance the permeation effect.[107] Third, the collective effect of more than one acting unit on the membrane can increase the activity in a near-exponential manner up to a certain limit.[108] It is worth noting that the first two factors are correlated with increased mammalian toxicity that makes it tricky to translate such materials to the clinic. In our perspective, multivalent membrane-active drug conjugates can have a much higher collective potency as all units get to exert their effect simultaneously in analogy to membrane attack complexes (MAC) embracing the biomimetic approaches.[109]

2.2.2. Binding to the Bacterial Cell Envelope (Bio-Adhesion)

Finding molecules that specifically bind to bacteria but not to mammalian cells is usually the bottleneck in developing targeted anti-infective therapies. As shown in Figure 5B, some features of the bacterial cell envelope have already been identified as targets, which may allow the development of "magic bullets" especially for Gram-negative bacteria.[110] Potential targets for achieving bio-adhesion to bacteria are:

- The overall pronounced anionic character
- LPS molecules, which form the outer leaflet of the outer membrane
- Divalent cations that are needed to stabilize the LPS
- Lipid A, as a specific component of LPS which is not found in mammalian cells
- The lectins; LecA and LecB

In addition to more or less specific binding, some molecules can also destroy the bacterial, but not the mammalian cell

Table 2. Examples of innovative materials and applications involving specific binding (bio-adhesion) to Gram-negative bacteria.

Target	Localization	Material	Regulatory status	Mechanism	Application	Reference
Lipid A	Inner leaflet of the LPS	Lipid A analogs, e.g., eritoran	Failed in phase 3	Mimics Lipid A to disrupt the outer membrane	Gold clusters	[113,114]
LPS	Outer membrane	Polymyxins, e.g., colistin and polymyxin B	Approved	Binds to and compromises the LPS	PMB-loaded cubosomes	[115,116]
LecA and LecB	Periplasmic space	Carbohydrates	Investigational	Blocks LecA and LecB	Surface modified polymeric nanoparticles	[117,118]
Peptide-membrane interactions	In between the lipid molecules	Membrane-active peptides, e.g., PEGylated LL-37	Clinical phase 2	Interact with the bacterial membrane	Photodynamic NP decorated with TAT	[103,119,120]

membranes. The selective destruction of membranes takes place by crystallization,[111] hydrophobic interactions with membrane lipids, formation of ion-permeable channels in the bacterial membrane by peptide-assemblies, and peroxidase-like activity via the release of H_2O_2 into the membrane.[101,112]

As **Table 2** illustrates, such specific binding materials are often employed to decorate the surface of nanocarriers to make them bio-adhesive to bacteria and to release their cargo in close vicinity to their target. Researchers can design a carrier compatible with the cargo and the needed loading capacity, as shown in **Figure 6**. A wide variety of nanoparticles have been created with different combinations and increased complexity, for example by loading a second active molecule in the coating or by using the polymeric core as an active antimicrobial.

Among pharmaceutical polymers, CS is widely used both as a carrier and because of its bioadhesive and antimicrobial properties. Due to its pKa 6.5, it has the advantage to acquire a positive charge in slightly acidic pH that is likely to happen in the inflammation sites (pH 5–6). The combination of CS with other

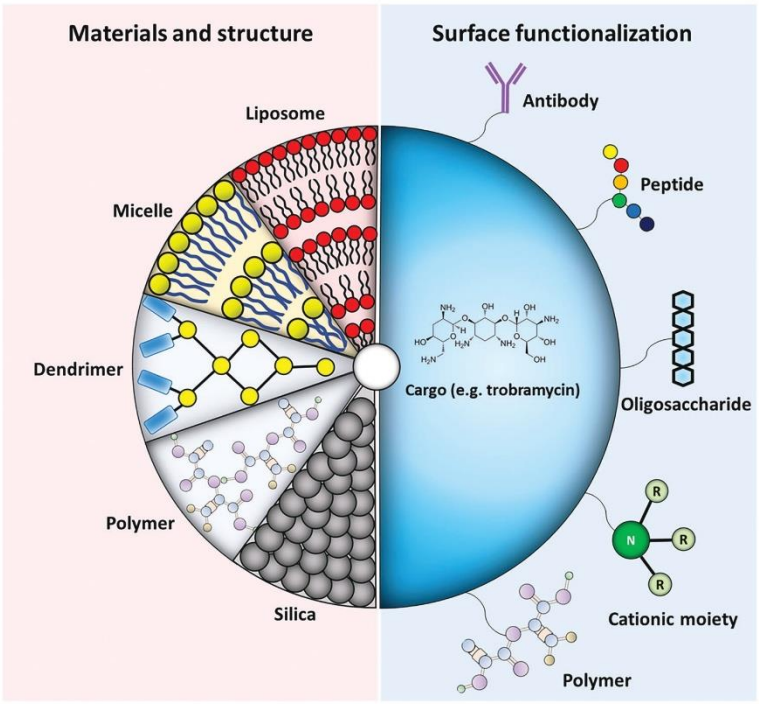

Figure 6. Nanocarriers can be made of different structures and materials (e.g., polymers, micelles, liposomes, inorganic materials) and functionalized on their surface (e.g., with antibodies, lectin-binding oligosaccharides, peptides, cationic moieties, etc.,) for targeted delivery of anti-infective cargos (e.g., tobramycin as shown here) across bacterial barriers.

materials can also increase the stability of a drug carrier to deliver other anti-infective molecules.[105,121]

A recent study showed that it is possible to harness the natural machinery found in *Photorhabdus asymbiotica* to inject macromolecules into cells. Although this was so far demonstrated for the delivery of CRISPR-CAS9 into mouse cells, such an approach would have enormous potential for anti-infective therapies if it could be translated also to bacteria.[122]

2.2.3. Exploitation of Specific Transport Pathways (Trojan Horse Approach)

The Trojan horse approach refers to conjugating one or more antimicrobials to a carrier molecule to achieve uptake by bacteria in a camouflaged manner via nutrient transporters. The drug either exhibits its action in the conjugated form or is released from the carrier molecule to become active. The transporters should be expressed mainly in bacteria with no or little expression in mammalian cells.

The most investigated transporters for this approach are the Ton-B-dependent transporters by utilizing siderophores as the carrier molecules. Researchers could have known approved antibiotics conjugated to native or artificial siderophores and show increased activity. The same approach is being further investigated by targeting the bacterio-specific siderophore receptor FepA.[123,124] Recently, another research could conjugate siderophores to TonB box peptides to allow better uptake into the bacteria, resulting in a superior antimicrobial activity in iron-limited growth media.[125] However, conjugating drugs with siderophores comes also with some drawbacks. Most importantly, bacteria can develop resistance by down-expressing the transporter leading to reduced uptake of the conjugate in the first place. A handful of molecules have been tested preclinically and clinically in this regard such as pirazmonam (Squibb), U-78608 (Upjohn), SMC-3176 (Astra-Zeneca), BAL30072 (Basilea), and cefiderocol (Shionogi). For the majority of them, the components of the iron transporter system got mutated or downregulated. This was avoided in the case of BAL30072 when using iron-limited media.[126] The latter may be indeed relevant for clinical settings like urinary tract infections due to low levels of iron in urine. Nevertheless, resistance is likely to develop elsewhere in the human body and render the potential antibiotic inactive.[127] Furthermore, cefiderocol was approved as a drug product in 2020 by both EMA and FDA.[128,129]

Alternatively, the Trojan Horse approach can also be implemented for passive transporters like the, e.g., LamB channel for maltose. Researchers have conjugated trimethoprim to maltose with a disulfide bridge as a release mechanism and proved that this leads to better accumulation inside the bacteria. However, they failed to demonstrate the superiority of the conjugate to free trimethoprim in terms of antibacterial activity that is expected because trimethoprim is a small molecule and permeability is not the limiter for its activity.[130] Additionally, others used a maltotriose conjugate, which was validated to be taken up by bacteria using the LamB channel.[131]

2.3. Infection-Triggered Drug Delivery

A promising strategy to selectively deliver potent anti-infectives to their bacterial targets is by conjugating the active agent to moieties that can only be bio-degraded by microenvironmental conditions related to the infection or under specific biochemical stimuli to release the drug. Most relevant strategies rely on materials that can be cleaved in the acidic pH found at the infection site or by an enzyme that is secreted either by the pathogen or the host as a response to the infection. The key to accomplishing this is a very good understanding of disease-related pathology and microbiology as well as the provoked microenvironment.

Bacterial-selective targeting was achieved by conjugating the antibiotic colistin to a modified fragment of the human AMP (ubiquicidin) by introducing a linker that is cleaved at infection sites by neutrophil elastase to release colistin.[132] Similarly, a desferrioxamine B-ciprofloxacin conjugate with "trimethyl-lock"-based linkers designed to release the antibiotic after exposure to bacterial esterase was reported to exhibit good antimicrobial activity against different bacterial strains.[133] Bacterial enzymes secreted into the biofilm matrix can also trigger drug release. Enzymatic release via bacterial gelatinase and hyaluronidase was also achieved by doxycycline-loaded core-shell nanoparticles. The gelatin core was surrounded by a double coating of CS and hyaluronic acid from the inside out. The nanoparticles were applied to an in vitro and ex vivo wound infection model of *Vibrio vulnificus* biofilms. Upon exposure, the outermost shell layer composed of hyaluronic acid was degraded by hyaluronidase present in the EPS. The underlying CS layer enhanced the penetration and retention of the nanoparticles into the EPS. Eventually, swelling of the CS core increased access of bacterial gelatinase to the gelatin causing subsequent core degradation and drug release leading to high biofilm penetration and eradication efficacy in comparison to the free drug.[134]

The concept of infection-triggered drug delivery can also be synergistically combined with adjuvanted carrier molecules. A pH-responsive polymer-drug conjugate made of a biodegradable cationic polymer HEX-Cys-DET and streptomycin was designed for this purpose.[135] The conjugate is neutral under normal physiological conditions but becomes positively charged in infected tissues with low pH, resulting in antibiotic release as well as enhanced activity of streptomycin because the polymer can induce pores in the bacterial membrane that improves the transport of the antibiotic into the bacteria. In addition to its effect on planktonic bacteria, the conjugate was found to effectively penetrate bacterial biofilms as well as being taken up by mammalian cells that might be needed to combat intracellular infections. Subsequently, this supports the conclusion that acidic pH in biofilms can be utilized for the concept of infection-triggered release. In this regard, cationic farnesol-loaded nanoparticles were formulated to have the ability to retain at the infection site for longer times due to their affinity to biofilm and pellicle. The pH-responsive core, made of 2-(di-methylamino)ethyl methacrylate, butyl methacrylate, and 2-propylacrylic acid, released the loaded drug inside the biofilm. This led to an 80% reduction of the biomass of S. mutants in vitro and attenuate the number and severity of carious lesions in vivo. This system was further modified and enhanced by the same research group to achieve a higher acid sensitivity and enhance the biofilm

reduction capacity.[136–138] Responsiveness to pH is one of the most frequently used triggering strategies. However, this concept can also be implemented to deliver non-drug species. For instance, nanoparticles were designed to release radicals in the proximity of the bacteria to allow for membrane destruction and thus bacterial killing at very low concentrations.[139]

Infection-triggered drug release can be combined with biofilm penetrating approaches to further enhance biofilm eradication and decrease off-target effects. To combat chronic lung infections, azithromycin-conjugated nanoparticles were produced with the ability to form size and charge adaptive clusters. These clusters are negatively charged in physiological pH enabling long circulation and accumulation in infected lung tissues. However, in acidic microenvironments as found in biofilms, these NP clusters can disassemble and release azithromycin-conjugated PAMAM nanoparticles. This conversion is accompanied by a size decrease from 112 to 6.5 nm and a charge reversal from −2.2 to +23.8 mV. The released nanoparticles with small size and positive surface charge exhibited excellent penetration and retention capabilities accompanied by an antibacterial effect against *P. aeruginosa* biofilms in vitro and in vivo.[140] Intensive research in the field of infection-triggered drug delivery will not necessarily require the development of novel anti-infective molecules. By boosting their antimicrobial activity and reducing undesired off-target effects it may even be possible to improve the potency of existing anti-infectives that could not yet reach clinical applications so far.

3. Advanced In Vitro Models for Developing Anti-Infective Therapies, Especially by Improving their Delivery

The need for novel anti-infectives and the problem of AMR has been well recognized by the scientific community and already led to many novel concepts and approaches in the last decade. Nevertheless, to facilitate the translation from bench to bed, predictive infection models for the preclinical development of such drug products are a necessity. Similar to the development of new anti-infective molecules, the development of novel drug carriers and formulations requires testing for both safety and efficacy. For the purpose of this perspective, we will discuss in particular preclinical models with a focus on pulmonary infections and drug delivery.

Animal models are considered essential, mainly because of the necessity of investigating immune responses as well as host-pathogen interactions. For many years, the known physiological differences between animals and humans in addition to their different responses and sensitivity to human pathogens have raised great concerns regarding the predictivity of such animal models for clinical outcomes.[141,142] Furthermore, the use of in vivo models for experimental reasons is restricted by legal regulations because of ethical concerns.[143] Each project that includes the use of animal models must be evaluated by ethics committees to confirm that it follows the "3R-rule": Replace, Reduce, and Refine.[144]

Animal models for chronic infections implicate an additional challenge due to the timelapse needed to develop the infection.[145] For instance, a classic model to mimic chronic *P. aeruginosa* lung infections starts with an inoculum of bacteria embedded in agarose or alginate beads to prolong the survival of the animal and hence the life span of the experiment.[146] Apart from the open question of whether the biofilm is really growing on the pulmonary mucosa rather than only in the agar beads, this model is problematic, because some of the animals do not even get sick while others die immediately, and only a small fraction of the animals develop symptoms that can be used to measure the anti-infective effect of a given treatment. Moreover, for this group of animals, the course of the experiment is extremely painful.

All these concerns, drawbacks, and restrictions necessitate the use and development of alternative methods to animal testing. An important milestone in this field is probably the recent *FDA Modernization Act 2.0*.[147] By replacing the former law from 1938, animal experiments are no longer mandatory for testing new drugs before entering clinical trials. This development already has and will still further stimulate the research on alternative models. Those are typically based on advanced in vitro techniques like, e.g., native or reconstituted tissues, novel cell lines, organs-on-chip, micro-physiological systems (MPS), and other CIVMs. In the future, in silico approaches like computer models, simulations and artificial intelligence will become increasingly important.

3.1. Biofilm Models

For modeling chronic infections, typically involving bacterial biofilms, there is no "gold standard" as each model may provide an answer to a specific question. In vivo models always implicate the suffering and killing of animals and at the same time are limited by (patho-)physiological differences to humans. In contrast, in vitro models may be based on human cells and tissues, allowing to reduce the complexity of a living organism to the biological factors of interest. Making reliable observations in a controlled environment is essential for the necessary validation of any model – either in vivo or in vitro – to eventually predict clinical outcomes.

3.1.1. "Biofilm-Only" Models

The first biofilm models were based on bacteria seeded on plastic surfaces either under static conditions, e.g., microtiter plates, or dynamic conditions, e.g., flow cells.[148] Such relatively simple in vitro models offer high reproducibility, reliable read-outs, and a rather high throughput, which is essential in early drug development. However, the lack of any host factors or even host-pathogen interactions makes it difficult to draw further-going conclusions based on these studies. Moreover, such simple models are often based on laboratory bacterial strains like *P. aeruginosa* PAO1. The latter has the advantage of being rather robust and relatively safe to work with, but its mushroom-like structures are not observed in clinical situations. Assays with laboratory strains may therefore cause a technical bias and were found to be of limited relevance for the clinical situation, e.g., in cystic fibrosis patients [149] The problem with clinically relevant strains, on the other hand, is that they don't adhere well to plastic surfaces and are easily washed away in these experiments.[150]

[35] M. Yasir, M. D. P. Willcox, D. Dutta, *Materials* **2018**, *11*, 2468.
[36] F. Xie, Y. Zan, X. Zhang, H. Zhang, M. Jin, W. Zhang, Y. Zhang, S. Liu, *Int. J. Mol. Sci.* **2020**, *21*, 1871.
[37] J. Overhage, A. Campisano, M. Bains, E. C. W. Torfs, B. H. A. Rehm, R. E. W. Hancock, *Infect. Immun.* **2008**, *76*, 4176.
[38] G. Batoni, G. Maisetta, F. L. Brancatisano, S. Esin, M. Campa, *Curr. Med. Chem.* **2011**, *18*, 256.
[39] S. Fahimirad, E. Ghaznavi-Rad, H. Abtahi, N. Sarlak, *Int. J. Pept. Res. Ther.* **2021**, *27*, 2505.
[40] N. Rezaei, H. G. Hamidabadi, S. Khosravimelal, M. Zahiri, Z. A. Ahovan, M. N. Bojnordi, B. S. Eftekhari, A. Hashemi, F. Ganji, S. Darabi, M. Gholipourmalekabadi, *Int. J. Biol. Macromol.* **2020**, *164*, 855.
[41] I. Castillo-Juárez, T. Maeda, E. A. Mandujano-Tinoco, M. Tomás, B. Pérez-Eretza, S. J. García-Contreras, T. K. Wood, R. García-Contreras, *World J Clin Cases* **2015**, *3*, 575.
[42] M. Duplantier, E. Lohou, P. Sonnet, *Pharmaceuticals* **2021**, *14*, 1262.
[43] K. Jiang, Y. Xu, B. Yuan, Y. Yue, M. Zhao, R. Luo, H. Wu, L. Wang, Y. Zhang, J. Xiao, F. Lin, *Front Microbiol* **2022**, *13*, https://doi.org/10.3389/fmicb.2022.791802.
[44] D. Tielker, S. Hacker, R. Loris, M. Strathmann, J. Wingender, S. Wilhelm, F. Rosenau, K. E. Jaeger, *Microbiology* **2005**, *151*, 1313.
[45] R. Sommer, S. Wagner, K. Rox, A. Varrot, D. Hauck, E. C. Wamhoff, J. Schreiber, T. Ryckmans, T. Brunner, C. Rademacher, R. W. Hartmann, M. Brönstrup, A. Imberty, A. Titz, *J. Am. Chem. Soc.* **2018**, *140*, 2537.
[46] J. Fong, K. T. Mortensen, A. Nørskov, K. Qvortrup, L. Yang, C. H. Tan, T. E. Nielsen, M. Givskov, *Front Cell Infect. Microbiol.* **2019**, *9*, 443.
[47] S. Li, S. Chen, J. Fan, Z. Cao, W. Ouyang, N. Tong, X. Hu, J. Hu, P. Li, Z. Feng, X. Huang, Y. Li, M. Xie, R. He, J. Jian, B. Wu, C. Xu, W. Wu, J. Guo, J. Lin, P. Sun, *Eur. J. Med. Chem.* **2018**, *145*, 64.
[48] S. L. Elshaer, M. I. Shaaban, *Antibiotics* **2021**, *10*, 1461.
[49] B. R. Singh, B. N. Singh, A. Singh, W. Khan, A. H. Naqvi, H. B. Singh, *Sci. Rep.* **2015**, *5*, 1.
[50] K. Forier, K. Raemdonck, S. C. De Smedt, J. Demeester, T. Coenye, K. Braeckmans, *J. Controlled Release* **2014**, *190*, 607.
[51] B. Ozcelik, K. K. K. Ho, V. Glattauer, M. Willcox, N. Kumar, H. Thissen, *ACS Biomater. Sci. Eng.* **2017**, *3*, 78.
[52] M. Nag, D. Lahiri, D. Mukherjee, R. Banerjee, S. Garai, T. Sarkar, S. Ghosh, A. Dey, S. Ghosh, S. Pattnaik, H. A. Edinur, Z. A. Kari, S. Pati, R. R. Ray, *Polymers* **2021**, *13*, 2533.
[53] N. Singh, M. Romero, A. Travanut, P. F. Monteiro, E. Jordana-Lluch, K. R. Hardie, P. Williams, M. R. Alexander, C. Alexander, *Biomater. Sci.* **2019**, *7*, 4099.
[54] L. A. Damiati, M. P. Tsimbouri, V. L. Hernandez, V. Jayawarna, M. Ginty, P. Childs, Y. Xiao, K. Burgess, J. Wells, M. R. Sprott, R. M. D. Meek, P. Li, R. O. C. Oreffo, A. Nobbs, G. Ramage, B. Su, M. Salmeron-Sanchez, M. J. Dalby, *Biomaterials* **2022**, *280*, 121263.
[55] D. K. Ho, X. Murgia, C. De Rossi, R. Christmann, A. G. Hüfner de Mello Martins, M. Koch, A. Andreas, J. Herrmann, R. Müller, M. Empting, R. W. Hartmann, D. Desmaele, B. Loretz, P. Couvreur, C. M. Lehr, *Angew. Chem. – Int. Ed.* **2020**, *59*, 10292.
[56] C. De las Heras Alarcón, S. Pennadam, C. Alexander, *Chem. Soc. Rev.* **2005**, *34*, 276.
[57] C. Lu, C. K. Maurer, B. Kirsch, A. Steinbach, R. W. Hartmann, *Angew. Chem. – Int. Ed.* **2014**, *53*, 1109.
[58] C. Schütz, D. K. Ho, M. M. Hamed, A. S. Abdelsamie, T. Röhrig, C. Herr, A. M. Kany, K. Rox, S. Schmelz, L. Siebenbürger, M. Wirth, C. Börger, S. Yahiaoui, R. Bals, A. Scrima, W. Blankenfeldt, J. C. Horstmann, R. Christmann, X. Murgia, M. Koch, A. Berwanger, B. Loretz, A. K. H. Hirsch, R. W. Hartmann, C. M. Lehr, M. Empting, *Adv. Sci.* **2021**, *8*, 2004369.
[59] A. V. Gannesen, E. L. Zdorovenko, E. A. Botchkova, J. Hardouin, S. Massier, D. S. Kopitsyn, M. V. Gorbachevskii, A. A. Kadykova, A. S. Shashkov, M. V. Zhurina, A. I. Netrusov, Y. A. Knirel, V. K. Plakunov, M. G. J. Feuilloley, *Front Microbiol* **2019**, *10*, 1284.
[60] R. Bansil, B. S. Turner, *Adv. Drug Deliv. Rev.* **2018**, *124*, 3.
[61] K. R. Rouillard, W. J. Kissner, M. R. Markovetz, D. B. Hill, *mSphere* **2022**, *7*, https://doi.org/10.1128/msphere.00345-22.
[62] X. Murgia, P. Pawelzyk, U. F. Schaefer, C. Wagner, N. Willenbacher, C. M. Lehr, *Biomacromolecules* **2016**, *17*, 1536.
[63] J. Kirch, A. Schneider, B. Abou, A. Hopf, U. F. Schaefer, M. Schneider, C. Schall, C. Wagner, C. M. Lehr, *Proc. Natl. Acad. Sci. U S A* **2012**, *109*, 18355.
[64] K. M. Wheeler, G. Cárcamo-Oyarce, B. S. Turner, S. Dellos-Nolan, J. Y. Co, S. Lehoux, R. D. Cummings, D. J. Wozniak, K. Ribbeck, *Nat. Microbiol.* **2019**, *4*, 2146.
[65] Y. Guo, Y. Ma, X. Chen, M. Li, X. Ma, G. Cheng, C. Xue, Y. Y. Zuo, B. Sun, *ACS Nano* **2023**, *17*, 2813.
[66] N. Nafee, A. Husari, C. K. Maurer, C. Lu, C. De Rossi, A. Steinbach, R. W. Hartmann, C. M. Lehr, M. Schneider, *J. Controlled Release* **2014**, *192*, 131.
[67] M. S. Deepika, R. Thangam, S. Sundarraj, T. S. Sheena, S. Sivasubramanian, J. Kulandaivel, R. Thirumurugan, *ACS Appl Bio Mater* **2020**, *3*, 385.
[68] Y. Sheng, Z. Chen, W. Wu, Y. Lu, *Drug Discov. Today* **2023**, *28*, 103455.
[69] F. Soukarieh, P. Gurnani, M. Romero, N. Halliday, M. Stocks, C. Alexander, M. Cámara, *ACS Macro Lett.* **2023**, *12*, 314.
[70] C. Wang, W. Zhao, B. Cao, Z. Wang, Q. Zhou, S. Lu, L. Lu, M. Zhan, X. Hu, *Chem. Mater.* **2020**, *32*, 7725.
[71] V. Pawar, H. Topkar, R. Srivastava, *Int. J. Biol. Macromol.* **2018**, *115*, 1131.
[72] E. M. Costa, S. Silva, S. Vicente, M. Veiga, F. Tavaria, M. M. Pintado, *Carbohydr. Polym.* **2017**, *178*, 347.
[73] S. Scutera, M. Argenziano, R. Sparti, F. Bessone, G. Bianco, C. Bastiancich, C. Castagnoli, M. Stella, T. Musso, R. Cavalli, *Antibiotics* **2021**, *10*, 57.
[74] A. D. Permana, M. Mir, E. Utomo, R. F. Donnelly, *Int J Pharm X* **2020**, *2*, 100047.
[75] X. Ju, J. Chen, M. Zhou, M. Zhu, Z. Li, S. Gao, J. Ou, D. Xu, M. Wu, S. Jiang, Y. Hu, Y. Tian, Z. Niu, *ACS Appl. Mater. Interfaces* **2020**, *12*, 13731.
[76] C. R. Thorn, C. d. S. Carvalho-Wodarz, J. C. Horstmann, C. M. Lehr, C. A. Prestidge, N. Thomas, *Small* **2021**, *17*, 2100531.
[77] M. A. D. S. Ramos, P. B. Da Silva, L. Spósito, L. G. De Toledo, B. vidal Bonifácio, C. F. Rodero, K. C. Dos Santos, M. Chorilli, T. M. Bauab, P. B. Da Silva, L. G. De Toledo, B. vidal Bonifácio, *Int J Nanomedicine* **2018**, *13*, 1179.
[78] U. B. Sleytr, B. Schuster, E. M. Egelseer, D. Pum, *FEMS Microbiol. Rev.* **2014**, *38*, 823.
[79] H. Luo, X. Q. Yin, P. F. Tan, Z. P. Gu, Z. M. Liu, L. Tan, *J. Mater. Chem. B* **2021**, *9*, 2802.
[80] R. S. Santos, C. Figueiredo, N. F. Azevedo, K. Braeckmans, S. C. De Smedt, S. C. De Smedt, S. C. De Smedt, *Adv Drug Deliv Rev* **2018**, *136*, 28.
[81] P. Demchick, A. L. Koch, *J. Bacteriol.* **1996**, *178*, 768.
[82] J. Vergalli, I. V. Bodrenko, M. Masi, L. Moynié, S. Acosta-Gutiérrez, J. H. Naismith, A. Davin-Regli, M. Ceccarelli, B. van den Berg, M. Winterhalter, J. M. Pagès, *Nat. Rev. Microbiol.* **2019**, *18*, 164.
[83] D. M. Carter, I. R. Miousse, J. N. Gagnon, É. Martinez, A. Clements, J. Lee, M. A. Hancock, H. Gagnon, P. D. Pawelek, J. W. Coulton, *J. Biol. Chem.* **2006**, *281*, 35413.
[84] H. Nikaido, *Microbiology and Molecular Biology Reviews* **2003**, *67*, 593.
[85] H. Nikaido, M. Vaara, *Microbiol Rev* **1985**, *49*, 1.

[86] D. G. Brown, T. L. May-Dracka, M. M. Gagnon, R. Tommasi, *J. Med. Chem.* **2014**, *57*, 10144.
[87] J. Mehta, R. Rolta, K. Dev, *J. Ethnopharmacol.* **2022**, *282*, 114589.
[88] M. F. Richter, P. J. Hergenrother, *Ann. N. Y. Acad. Sci.* **2019**, *1435*, 18.
[89] M. Masi, M. Réfregiers, K. M. Pos, J.-M. M. Pagès, *Nat. Microbiol.* **2017**, *2*, 17001.
[90] M. Skwarczynski, S. Bashiri, Y. Yuan, Z. M. Ziora, O. Nabil, K. Masuda, M. Khongkow, N. Rimsueb, H. Cabral, U. Ruktanonchai, M. A. T. Blaskovich, I. Toth, *Antibiotics* **2022**, *11*, 412.
[91] M. Vaara, *Molecules* **2019**, *24*, 249.
[92] A. Scheller, J. Oehlke, B. Wiesner, M. Dathe, E. Krause, M. Beyermann, M. Melzig, M. Bienert, *J. Pept. Sci.* **1999**, *5*, 185.
[93] D. J. Dwyer, J. J. Collins, G. C. Walker, *Annu. Rev. Pharmacol. Toxicol.* **2015**, *55*, 313.
[94] R. Shukla, F. Lavore, S. Maity, M. G. N. Derks, C. R. Jones, B. J. A. Vermeulen, A. Melcrová, M. A. Morris, L. M. Becker, X. Wang, R. Kumar, J. Medeiros-Silva, R. A. M. van Beekveld, A. M. J. J. Bonvin, J. H. Lorent, M. Lelli, J. S. Nowick, H. D. MacGillavry, A. J. Peoples, A. L. Spoering, L. L. Ling, D. E. Hughes, W. H. Roos, E. Breukink, K. Lewis, M. Weingarth, *Nature* **2022**, *608*, 390.
[95] H. B. Koo, J. Seo, *Biopolymers* **2019**, *111*, https://doi.org/10.1002/pep2.24122.
[96] K. Oikawa, M. M. Islam, Y. Horii, T. Yoshizumi, K. Numata, *ACS Omega* **2018**, *3*, 16489.
[97] H. M. Lee, J. Ren, K. M. Tran, B. M. Jeon, W. U. Park, H. Kim, K. E. Lee, Y. Oh, M. Choi, D. S. Kim, D. Na, *Commun Biol* **2021**, *4*, 205.
[98] G. Krishnamoorthy, D. Wolloscheck, J. W. Weeks, C. Croft, V. V. Rybenkov, H. I. Zgurskaya, *Antimicrob. Agents Chemother.* **2016**, *60*, 7372.
[99] A. D. Kennedy, J. B. Wardenburg, D. J. Gardner, D. Long, A. R. Whitney, K. R. Braughton, O. Schneewind, F. R. DeLeo, *J. Infect. Dis.* **2010**, *202*, 1050.
[100] A. Gupta, S. Mumtaz, C. H. Li, I. Hussain, V. M. Rotello, *Chem. Soc. Rev.* **2019**, *48*, 415.
[101] L. Lin, J. Chi, Y. Yan, R. Luo, X. Feng, Y. Zheng, D. Xian, X. Li, G. Quan, D. Liu, C. Wu, C. Lu, X. Pan, *Acta Pharm. Sin. B* **2021**, *11*, 2609.
[102] Y. Zhao, L. Chen, Y. Wang, X. Song, K. Li, X. Yan, L. Yu, Z. He, *Nano Res.* **2021**, *14*, 4417.
[103] M. M. Konai, B. Bhattacharjee, S. Ghosh, J. Haldar, *Biomacromolecules* **2018**, *19*, 1888.
[104] B. Yu, M. Roy Choudhury, X. Yang, S. L. Benoit, E. Womack, K. Van Mouwerik Lyles, A. Acharya, A. Kumar, C. Yang, A. Pavlova, M. Zhu, Z. Yuan, J. C. Gumbart, D. W. Boykin, R. J. Maier, Z. Eichenbaum, B. Wang, *ACS Infect. Dis.* **2022**, *8*, 1491.
[105] B. Balasubramaniam, Prateek, S. R., M. Saraf, P. Kar, S. P. Singh, V. K. Thakur, A. Singh, R. K. Gupta, *ACS Pharmacol. Transl. Sci.* **2021**, *4*, 8.
[106] L. D'Lima, M. Phadke, V. D. Ashok, *New J. Chem.* **2020**, *44*, 4935.
[107] H. Gong, X. Hu, M. Liao, K. Fa, D. Ciumac, L. A. Clifton, M. A. Sani, S. M. King, A. Maestro, F. Separovic, T. A. Waigh, H. Xu, A. J. Mcbain, J. R. Lu, *ACS Appl. Mater. Interfaces* **2021**, *13*, 16062.
[108] S. P. Liu, L. Zhou, R. Lakshminarayanan, R. W. Beuerman, *Int. J. Pept. Res. Ther.* **2010**, *16*, 199.
[109] D. A. C. Heesterbeek, R. M. Muts, V. P. van Hensbergen, P. de Saint Aulaire, T. Wennekes, B. W. Bardoel, N. M. van Sorge, S. H. M. Rooijakkers, *PLoS Pathog.* **2021**, *17*, e1009227.
[110] K. Klobucar, E. D. Brown, *Curr. Opin. Chem. Biol.* **2022**, *66*, 102099.
[111] S. Manioglu, S. M. Modaresi, N. Ritzmann, J. Thoma, S. A. Overall, A. Harms, G. Upert, A. Luther, A. B. Barnes, D. Obrecht, D. J. Müller, S. Hiller, *Nat. Commun.* **2022**, *13*, 6195.
[112] Y. Liu, L. Shi, L. Su, H. C. Van der Mei, P. C. Jutte, Y. Ren, H. J. Busscher, H. C. van der Mei, *Chem. Soc. Rev.* **2019**, *48*, 428.
[113] F. H. Liao, T. H. Wu, Y. T. Huang, W. J. Lin, C. J. Su, U. S. Jeng, S. C. Kuo, S. Y. Lin, *Nano Lett.* **2018**, *18*, 2864.
[114] S. M. Opal, P. F. Laterre, B. Francois, S. P. LaRosa, D. C. Angus, J. P. Mira, X. Wittebole, T. Dugernier, D. Perrotin, M. Tidswell, L. Jauregui, K. Krell, J. Pachl, T. T. C. Peckelsen, E. Cordasco, C. S. Chang, S. Oeyen, N. Aikawa, T. Maruyama, R. Schein, A. C. Kalil, M. Van Nuffelen, M. Lynn, D. P. Rossignol, J. Gogate, M. B. Roberts, J. L. Wheeler, J. L. Vincent, *JAMA, J. Am. Med. Assoc.* **2013**, *309*, 1154.
[115] L. Poirel, A. Jayol, P. Nordmanna, *Clin. Microbiol. Rev.* **2017**, *30*, 557.
[116] X. Lai, M. L. Han, Y. Ding, S. H. Chow, A. P. Le Brun, C. M. Wu, P. J. Bergen, J. hang Jiang, H. Y. Hsu, B. W. Muir, J. White, J. Song, J. Li, H. H. Shen, *Nat. Commun.* **2022**, *13*, 343.
[117] Y. Zhao, Q. Guo, X. Dai, X. Wei, Y. Yu, X. Chen, C. Li, Z. Cao, X. Zhang, *Adv. Mater.* **2019**, *31*, 1806024.
[118] T. R. Flockton, L. Schnorbus, A. Araujo, J. Adams, M. Hammel, L. J. Perez, *Pathogens* **2019**, *8*, 55.
[119] Z. Li, W. Pan, E. Shi, L. Bai, H. Liu, C. Li, Y. Wang, J. Deng, Y. Wang, *ACS Biomater. Sci. Eng.* **2021**, *7*, 772.
[120] C. J. Morris, K. Beck, M. A. Fox, D. Ulaeto, G. C. Clark, M. Gumbleton, *Antimicrob. Agents Chemother.* **2012**, *56*, 3298.
[121] M. T. Yilmaz, A. Yilmaz, P. K. Akman, F. Bozkurt, E. Dertli, A. Basahel, B. Al-Sasi, O. Taylan, O. Sagdic, *Innovative Food Sci. Emerging Technol.* **2019**, *52*, 166.
[122] J. Kreitz, M. J. Friedrich, A. Guru, B. Lash, M. Saito, R. K. Macrae, F. Zhang, *Nature* **2023**, *616*, 357.
[123] L. Pinkert, Y. H. Lai, C. Peukert, S. K. Hotop, B. Karge, L. M. Schulze, J. Grunenberg, M. Brönstrup, *J. Med. Chem.* **2021**, *64*, 15440.
[124] T. Zheng, E. M. Nolan, *J. Am. Chem. Soc.* **2014**, *136*, 9677.
[125] C. Peukert, V. Gasser, T. Orth, S. Fritsch, V. Normant, O. Cunrath, I. J. Schalk, M. Brönstrup, *J. Med. Chem.* **2023**, *66*, 553.
[126] K. Bush, M. G. P. Page, *J. Pharmacokinet. Pharmacodyn.* **2017**, *44*, 113.
[127] M. Straubinger, H. Blenk, K. G. Naber, F. M. E. Wagenlehner, *Antimicrob. Agents Chemother.* **2016**, *60*, 3309.
[128] FDA, *Drug Approval Package: FETROJA (cefiderocol)*, **2019**, https://www.accessdata.fda.gov/drugsatfda_docs/nda/2019/209445Orig1s000TOC.cfm.
[129] European Medicines Agency, *Fetcroja* **2020**, https://www.ema.europa.eu/en/medicines/human/EPAR/fetcroja.
[130] X. Wang, C. A. Borges, X. Ning, M. Rafi, J. Zhang, B. Park, K. Takemiya, C. Lo Sterzo, W. R. Taylor, L. Riley, N. Murthy, *Bioconjug Chem* **2018**, *29*, 1729.
[131] E. Dumont, J. Vergalli, J. Pajovic, S. P. Bhamidimarri, K. Morante, J. Wang, D. Lubriks, E. Suna, R. A. Stavenger, M. Winterhalter, M. Réfrégiers, J. M. Pagès, *Life Sci Alliance* **2019**, *2*, e201800242.
[132] W. Tegge, G. Guerra, A. Höltke, L. Schiller, U. Beutling, K. Harmrolfs, L. Gröbe, H. Wullenkord, C. Xu, H. Weich, M. Brönstrup, *Angew. Chem., Int. Ed.* **2021**, *60*, 17989.
[133] C. Ji, M. J. Miller, *Bioorg. Med. Chem.* **2012**, *20*, 3828.
[134] Y. Wang, A. Shukla, *Biomater. Sci.* **2022**, *10*, 2831.
[135] M. Ye, Y. Zhao, Y. Wang, N. Yodsanit, R. Xie, S. Gong, *Adv. Funct. Mater.* **2020**, *30*, 2002655.
[136] B. Horev, M. I. Klein, G. Hwang, Y. Li, D. Kim, H. Koo, D. S. W. Benoit, *ACS Nano* **2015**, *9*, 2390.
[137] J. Zhou, B. Horev, G. Hwang, M. I. Klein, H. Koo, D. S. W. Benoit, *J. Mater. Chem. B* **2016**, *4*, 3075.
[138] K. R. Sims, Y. Liu, G. Hwang, H. I. Jung, H. Koo, D. S. W. Benoit, *Nanoscale* **2019**, *11*, 219.
[139] P. Das, M. Maruthapandi, A. Saravanan, M. Natan, G. Jacobi, E. Banin, A. Gedanken, *ACS Appl. Nano Mater.* **2020**, *3*, 11777.

[140] Y. Gao, J. Wang, M. Chai, X. Li, Y. Deng, Q. Jin, J. Ji, *ACS Nano* **2020**, *14*, 5686.
[141] M. B. Bracken, *J. R. Soc. Med.* **2009**, *102*, 120.
[142] H. S. Warren, C. Fitting, E. Hoff, M. Adib-Conquy, L. Beasley-Topliffe, B. Tesini, X. Liang, C. Valentine, J. Hellman, D. Hayden, J. Cavaillon, *J. Infect. Dis.* **2010**, *201*, 223.
[143] D. B. Morton, *Clin. Microbiol. Infect.* **1998**, *4*, 613.
[144] R. C. Hubrecht, E. Carter, *Animals (Basel)* **2019**, *9*, 754.
[145] K. P. Rumbaugh, N. L. Carty, *Biofilm Infections* **2011**, 267, https://link.springer.com/chapter/10.1007/978-1-4419-6084-9_16.
[146] S. S. Pedersen, G. H. Shand, B. L. Hansen, G. N. Hansen, *APMIS* **1990**, *98*, 203.
[147] J. J. Han, *Artif. Organs* **2023**, *47*, 449.
[148] T. Coenye, H. J. Nelis, *J Microbiol Methods* **2010**, *83*, 89.
[149] A. Penesyan, S. S. Kumar, K. Kamath, A. M. Shathili, V. Venkatakrishnan, C. Krisp, N. H. Packer, M. P. Molloy, I. T. Paulsen, *PLoS One* **2015**, *10*, e0138527.
[150] T. Bjarnsholt, M. Alhede, M. Alhede, S. R. Eickhardt-Sørensen, C. Moser, M. Kühl, P. Ø. Jensen, N. Høiby, *Trends Microbiol.* **2013**, *21*, 466.
[151] D. D. Sriramulu, H. Lünsdorf, J. S. Lam, U. Römling, *J Med Microbiol* **2005**, *54*, 667.
[152] B. C. Huck, O. Hartwig, A. Biehl, K. Schwarzkopf, C. Wagner, B. Loretz, X. Murgia, C.-M. Lehr, *Biomacromolecules* **2019**, *20*, 3504.
[153] S. Frisch, A. Boese, B. Huck, J. C. Horstmann, D.-K. Ho, K. Schwarzkopf, X. Murgia, B. Loretz, C. de Souza Carvalho-Wodarz, C.-M. Lehr, *J. Antimicrob. Chemother.* **2021**, *76*, 1472.
[154] J. Juntke, X. Murgia, N. G. Türeli, A. E. Türeli, C. R. Thorn, M. Schneider, N. Schneider-Daum, C. de Souza Carvalho-Wodarz, C.-M. Lehr, *Drug Deliv Transl Res* **2021**, *11*, 1752.
[155] B. A. Woodworth, E. Tamashiro, G. Bhargave, N. A. Cohen, J. N. Palmer, *Am J Rhinol* **2008**, *22*, 235.
[156] A. J. Carterson, K. Höner Zu Bentrup, C. M. Ott, M. S. Clarke, D. L. Pierson, C. R. Vanderburg, K. L. Buchanan, C. A. Nickerson, M. J. Schurr, *Infect. Immun.* **2005**, *73*, 1129.
[157] S. Moreau-Marquis, C. V. Redelman, B. A. Stanton, G. G. Anderson, *J Vis Exp* **2010**, *44*, e2186.
[158] L. L. Bowler, T. B. Ball, L. L. Saward, *J Microbiol Methods* **2014**, *101*, 49.
[159] J. C. Horstmann, A. Laric, A. Boese, D. Yildiz, T. Röhrig, M. Empting, N. Frank, D. Krug, R. Müller, N. Schneider-Daum, C. de Souza Carvalho-Wodarz, C.-M. Lehr, *ACS Infect. Dis.* **2022**, *8*, 137.
[160] E. Ning, G. Turnbull, J. Clarke, F. Picard, P. Riches, M. Vendrell, D. Graham, A. W. Wark, K. Faulds, W. Shu, *Biofabrication* **2019**, *11*, 045018.
[161] R. Richter, M. A. M. Kamal, M. Koch, B. J. Niebuur, A. L. Huber, A. Goes, C. Volz, J. Vergalli, T. Kraus, R. Müller, N. Schneider-Daum, G. Fuhrmann, J. M. Pagès, C. M. Lehr, *Adv. Healthcare Mater.* **2022**, *11*, 2101180.
[162] E. J. Geddes, Z. Li, P. J. Hergenrother, *Nat. Protoc.* **2021**, *16*, 4833.
[163] R. Richter, M. A. M. Kamal, M. A. García-Rivera, J. Kaspar, M. Junk, W. A. M. Elgaher, S. K. Srikakulam, A. Gress, A. Beckmann, A. Grißmer, C. Meier, M. Vielhaber, O. Kalinina, A. K. H. Hirsch, R. W. Hartmann, M. Brönstrup, N. Schneider-Daum, C. M. Lehr, *Mater Today Bio* **2020**, *8*, 100084.
[164] C. F. Sousa, M. A. M. Kamal, R. Richter, K. Elamaldeniya, R. W. Hartmann, M. Empting, C. M. Lehr, O. V. Kalinina, *J. Chem. Inf. Model.* **2022**, *62*, 5023.
[165] P. Kudela, S. Paukner, U. B. Mayr, D. Cholujova, Z. Schwarczova, J. Sedlak, J. Bizik, W. Lubitz, *J. Immunother.* **2005**, *28*, 136.
[166] F. Graef, R. Richter, V. Fetz, X. Murgia, C. De Rossi, N. Schneider-Daum, G. Allegretta, W. Elgaher, J. Haupenthal, M. Empting, F. Beckmann, M. Brönstrup, R. Hartmann, S. Gordon, C. M. Lehr, *ACS Infect. Dis.* **2018**, *4*, 1188.
[167] F. Graef, B. Vukosavljevic, J. P. Michel, M. Wirth, O. Ries, C. De Rossi, M. Windbergs, V. Rosilio, C. Ducho, S. Gordon, C. M. Lehr, *J. Controlled Release* **2016**, *243*, 214.
[168] M. F. Richter, B. S. Drown, A. P. Riley, A. Garcia, T. Shirai, R. L. Svec, P. J. Hergenrother, *Nature* **2017**, *545*, 299.
[169] J. D. Prajapati, C. J. Fernández Solano, M. Winterhalter, U. Kleinekathöfer, *J. Chem. Theory Comput.* **2017**, *13*, 4553.
[170] R. Talandashti, H. Mahdiuni, M. Jafari, F. Mehrnejad, *J. Chem. Inf. Model.* **2019**, *59*, 3262.
[171] B. G. Hall, M. Barlow, *J. Antimicrob. Chemother.* **2005**, *55*, 1050.
[172] J. M. Stokes, A. J. Lopatkin, M. A. Lobritz, J. J. Collins, *Cell Metab.* **2019**, *30*, 251.
[173] M. S. Islam, A. Aryasomayajula, P. R. Selvaganapathy, *Micromachines* **2017**, *8*, 83.

Aghiad Bali is a PhD student with a background in pharmacy and biotechnology. During his master's studies, he focused on the development and testing of various pharmaceutical formulations using intracellular in vitro infection models. In his doctoral research, he is currently engaged in the development of chronic infection model by bioprinting bacterial biofilms on pulmonary human epithelial cells.

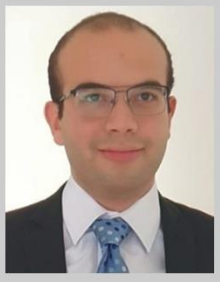

Mohamed A. M. Kamal, is a pharmacist by training. During his undergraduate studies, he completed two internships in the Department of Drug Delivery, HIPS and one internship in the Department of Viral Immunology, HZI. From February 2021, he completed his Master's degree at Prof. Claus-Michael Lehr group on the use of cell-penetrating peptides as tools to overcome the Gram-negative bacterial cell envelope. Currently, he is a doctoral researcher and his PhD topic is "Cell-penetrating peptides as drug delivery tools to overcome the Gram-negative cell envelope and biofilms as prominent bacterial barriers".

Glorjen Mulla is currently a PhD candidate with Prof. Claus Michael-Lehr in the Helmholtz Institute for Pharmaceutical Research Saarland (HIPS), Helmholtz Centre for Infection Research (HZI), Saarland University. He received his first MS degree in 2019 at University of Medicine, Tirana. In 2022 he obtained his second MS degree at Saarland University. His current research focuses on Intracellular metabolism and extracellular polymeric substances as biological barriers in Gram-negative bacteria.

Brigitta Loretz is a senior scientist at the Helmholtz Institute for Pharmaceutical Research Saarland (HIPS). She studied microbiology and did her Ph.D. at the University of Innsbruck, Department of Pharmaceutical Technology. She is author/coauthor of >60 research articles as well as several reviews and book chapters. Her scientific interests are nanocarriers for the delivery of biopharmaceutics and anti-infectives, with a particular focus on nucleotide delivery.

Claus-Michael Lehr is Professor of Pharmacy at Saarland University, Germany, as well as cofounder and head of the department "Drug Delivery and Biological Barriers" at the Helmholtz Institute for Pharmaceutical Research Saarland (HIPS). A major line of his research is on the lungs and pulmonary drug delivery. His group works on innovative carrier systems capable of safely and efficiently delivering drugs and vaccines to their targets, especially against infectious diseases. In this context, the lab has pioneered human-cell and tissue models with the aim of better predicting clinical outcomes as an alternative to animal testing.

9.2 First Research Paper

"Arg-biodynamers as antibiotic potentiator through interacting with Gram-negative outer membrane lipopolysaccharides"

Mohamed A.M. Kamal, Justine Bassil, Brigitta Loretz, Anna K.H. Hirsch, Sangeun Lee, Claus-Michael Lehr

DOI: 10.1016/j.ejpb.2024.114336

Contributions: M.A.M.K conceived the project, designed and performed the experiments (except chemical synthesis of the monomer starting materials), analyzed the data, and wrote the first draft of the manuscript. J.B. performed the chemical synthesis of the monomers of the polymer. M.A.M.K, B.J., S.L, and C.M.L interpret the results. B.J., S.L, A.K.H.H. and C.M.L secured funding, supervised the research, and provided critical revisions of the manuscript.

European Journal of Pharmaceutics and Biopharmaceutics 200 (2024) 114336

Contents lists available at ScienceDirect

European Journal of Pharmaceutics and Biopharmaceutics

journal homepage: www.elsevier.com/locate/ejpb

Research paper

Arg-biodynamers as antibiotic potentiators through interacting with Gram-negative outer membrane lipopolysaccharides

Mohamed A.M. Kamal [a,b], Justine Bassil [a,b], Brigitta Loretz [a], Anna K.H. Hirsch [a,b], Sangeun Lee [a,b,*], Claus-Michael Lehr [a,b,*]

[a] Helmholtz Institute for Pharmaceutical Research Saarland (HIPS), Helmholtz Centre for Infection Research (HZI), Saarland University, 66123 Saarbrücken, Germany
[b] Saarland University, Department of Pharmacy, 66123 Saarbrücken, Germany

ARTICLE INFO

Keywords:
Biodegradable polymers
Bacterial bioavailability
Bacterial cell envelope
Secondary structure
Membrane-active polymers
Supramolecular interactions

ABSTRACT

Antimicrobial resistance is becoming more prominent day after day due to a number of mechanisms by microbes, especially the sophisticated biological barriers of bacteria, especially in Gram-negatives. There, the lipopolysaccharides (LPS) layer is a unique component of the outer leaflet of the outer membrane which is highly impermeable and prevents antibiotics from passing passively into the intracellular compartments. Biodynamers, a novel class of dynamically bio-responsive polymers, may open new perspectives to overcome this particular barrier by accommodating various secondary structures and form supramolecular structures in such bacterial microenvironments. Generally, bio-responsive polymers are not only candidates as bio-active molecules against bacteria but also carriers via their interactions with the cargo. Based on their dynamicity, design flexibility, biodegradability, biocompatibility, and pH-responsiveness, we investigated the potential of two peptide-based biodynamers for improving antimicrobial drug delivery. By a range of experimental methods, we discovered a greater affinity of Arg-biodynamers for bacterial membranes than for mammalian membranes as well as an enhanced LPS targeting on the bacterial membrane, opening perspectives for enhancing the delivery of antimicrobials across the Gram-negative bacterial cell envelope. This could be explained by the change of the secondary structure of Arg-biodynamers into a predominant β-sheet character in the LPS microenvironment, by contrast to the α-helical structure typically observed for most lipid membrane-permeabilizing peptides. In comparison to poly-L-arginine, the intrinsic antibacterial activity of Arg-biodynamers was nearly unchanged, but its toxicity against mammalian cells was >128-fold reduced. When used in bacterio as an antibiotic potentiator, however, Arg-biodynamers improved the minimum inhibitory concentration (MIC) against Escherichia coli by 32 times compared to colistin alone. Similar effect has also been observed in two stains of Pseudomonas aeruginosa. Arg-biodynamers may therefore represent an interesting option as an adjuvant for antibiotics against Gram-negative bacteria and to overcome antimicrobial resistance.

1. Introduction

Antimicrobial resistance (AMR) is a process where microbes, especially bacteria, are rendered insusceptible to antimicrobial agents. Frequently, bacterial species tend to become resistant to a whole class of antibiotics once they learned to resist one member of the class. This brings the endpoint of research from developing new derivatives of existing antibiotic classes to developing rather chemically distant new classes of antibiotics. There are no novel classes of antibiotics against Gram-negative bacteria in advanced clinical trials so far, meaning that for now we have to rely on the current classes on the market. The search for novel antibiotics, especially against Gram-negative bacteria, faces many hurdles. New antibiotics have inadequate investment returns due to the use as a last resort upon approval while preferring the well-established antibiotics while also the discovery of new antibiotics is technically very challenging. To combat this problem, researchers are trying to extend the lifetime of the current antibiotics classes and to keep them in use for as long as possible without significant emergence of resistance. To achieve this, research must extend beyond drug discovery to innovative drug delivery systems and combination therapy. As a

* Corresponding authors at: Helmholtz Institute for Pharmaceutical Research Saarland (HIPS), Helmholtz Centre for Infection Research (HZI), Saarland University, 66123 Saarbrücken, Germany. Saarland University, Department of Pharmacy, 66123 Saarbrücken, Germany.
E-mail addresses: sangeun.lee@uni-saarland.de (S. Lee), claus-michael.lehr@helmholtz-hips.de (C.-M. Lehr).

https://doi.org/10.1016/j.ejpb.2024.114336
Received 18 April 2024; Received in revised form 18 May 2024; Accepted 20 May 2024
Available online 23 May 2024

solution, the concept of antibiotic enhancers or potentiators is promoted. An antibiotic potentiator is a molecule that is not antimicrobial by itself but rather enhances the activity of an antibiotic restoring its susceptibility against resistant bacteria.[1–4] Small organic molecules were long investigated in this field, especially in synergy with colistin aiming to reduce the required dose to avoid resistance. [4,5] Larger macromolecules were also recently shown to be increase the efficacy of many antibiotics, opening doors for potential uses in drug delivery field. [6–9]

The World Health Organization has classified resistant bacteria into priority lists. All three bacterial organisms in the critical list are Gram-negative. Due to the high complexity of the membrane of Gram-negative bacteria along with other factors, they have developed resistance against most of the classes of antibiotics, resulting in case reports for multi-drug resistant organisms (MDRs), especially in nosocomial settings. The complex cell envelope of Gram-negative bacteria represents a special barrier controlling the bacterium's incoming substances. This Gram-negative bacterial cell envelope consists of a lipid bilayer as the inner membrane, a periplasmic space made of peptidoglycan, and finally an outer membrane made of two leaflets; an inner leaflet of lipids and an outer leaflet of lipopolysaccharide (LPS) molecules. For some bacterial species, there is also the S-layer, composed of glycoproteins. The essential element of the Gram-negative bacteria cell envelope are the LPS. An LPS molecule consists of three main elements, namely, lipid A, core sugars, and O-antigen. LPS are tightly bound together by the divalent cations interacting with neighboring molecules, leading to a very tight biological membrane. Very few types of molecules can pass through the LPS barrier, namely small neutral hydrophilic molecules like amino acids, water, and soluble gases. Almost all of the classes of antibiotics have intracellular targets in the bacteria, meaning that the uptake is a prerequisite for activity. This leaves few uptake mechanisms for an active antimicrobial to be taken up, e.g., porins, simple passive diffusion, and active transporters. However, the structural features that would favor uptake rarely align with structure–activity prerequisites for antimicrobial activity. This gap, however, can perhaps be overcome by identifying compounds that selectively interact with the LPS leading to an enhanced permeability of the bacterial but not mammalian cell membranes.[9] Yet so far, membrane-active antibiotics, e.g., colistin and polymyxin B, may skip the uptake prerequisite for antimicrobial activity, but with collateral damage to the mammalian membrane due to their surfactant-like nature resulting in serious side effects. Therefore, they are a last resort in infection management guidelines and extensive research is ongoing to find safer alternatives.[9,10]

Here, we describe biodynamers as candidate potentiators for antibiotics. Biodynamers have been extensively researched and already been characterized in literature. [11–15] They are polymerized between amino acid hydrazides and hexaethyleneglycol-conjugated carbazole dialdehydes by dynamic covalent chemistry, leading to the ability to dynamically polymerize and depolymerize upon certain chemical stimuli. When made of amino acids, biodynamers can be considered a mimic of polypeptides. Due to their amphiphilic nature, they form single-chain nanorod structures, with a carbazole core and a polyethylene glycol (PEG) shell. In comparison to plain poly-L-arginine, Arg-biodynamers have some special features. Besides the aforementioned formation of supramolecular nanorod structures, their reduced charge density leads to favor their biocompatibility. Additionally, their PEG shell improves solubility as well as stability against enzymatic degradation in biological settings. Also, the biodynamers discussed in this manuscript are expected to have decreased protein adsorption on its surface due to the presence of 6 units of PEG. [15] In contrast to static conventional biopolymers, biodynamers can prioritize structural adaptability through reversible covalent bonds and supramolecular interactions to rearrange their areas and monomers in response to environmental factors. Recently, cationic lysine-based biodynamers gained interest due to their pH-dependent morphological and optical properties. Since pH can impact both size and structure of these biodynamers, a great potential for applications can be unlocked.[12,13]

In this study, we explore the potential of biodynamers as adjuvants to antibiotics to potentiate their effect against Gram-negative bacteria. Due to the previous evidence and research which show that arginine and lysine-rich peptides could target LPS, we focused our research on those two derivatives. [16] For this purpose, a combination of biological as well as chemical, and physical methods is needed. We also investigated their membrane interactions via high-resolution techniques, e.g., scanning electron microscopy and circular dichroism spectrometry. Our aim is to provide a first-reported potentiation mechanism.

2. Materials and methods

2.1. Materials

A549 cells (ATCC ACL107) were obtained from the DSMZ (Braunschweig, Germany). Monocytic cell line THP-1 (ACC 16) was obtained from DSMZ (Braunschweig, Germany). RAW264.7 cell line was obtained from ECACC (Salisburg, UK). *E. coli* DSM 6897, PA01 (DSMZ 22644), and PA14 (DSMZ 19882) were obtained from DSMZ (Braunschweig, Germany). *E. coli* ClearColi BL21 cells were obtained from LGC Genomics GmbH (Berlin, Germany). RPMI 1640 medium, DMEM, FCS, and Trypsin-EDTA were obtained from Thermofisher scientific (Waltham, USA). Hanks' Balanced Salt Solution (HBSS) was obtained from Gibco™ (Paisley, Scotland). 3-(4,5-Dimethylthiazol-2-yl)-2,5-diphenyltetrazoliumbromid "MTT reagent" (CAS: 298–93-1) was obtained from Sigma-Aldrich (St. Louis, USA). PMA (phorbol-12-myristate-13-acetate) (CAS: 16561–29-8) was obtained from Sigma Aldrich (St. Louis, USA). Mueller Hinton broth (MHB) was obtained from Scharlau microbiology (Barcelona, Spain). M9 Minimal salts 5x Powder was obtained from SERVA (Heidelberg, Germany). Poly-L-arginine (CAS: 26982–20-7) was obtained from Sigma-Aldrich (St. Louis, USA). Poly-L-lysine (CAS: 25988–63-0) was obtained from Sigma-Aldrich (St. Louis, USA). TritonX-100 (CAS: 9036–19-5) was obtained from Sigma-Aldrich (St. Louis, USA). Cys-TAT peptide was obtained from GenScript (Rijswijk, Netherlands). Colistin sulfate (CAS: 1264–72-8), Novobiocin (CAS: 1476–53-5), Fusidic acid (CAS: 751–94-0), Linezolid (CAS: 165800–03-3), Clindamycin (CAS: 21462–39-5), Rifampin (CAS: 13292–46-1), Vancomycin (CAS: 123409–00-7), Trimethoprim (CAS: 738–70-5) were obtained from Adipogen (Fuellinsdorf, Switzerland), Cayman chemical (Michigan, USA), Sigma-Aldrich (St. Louis, USA), Activate Scientific (Prien, Germany), USBiological (Massachusetts, USA), MP Biomedicals (Eschwege, Germany), Sigma-Aldrich (St. Louis, USA) respectively. Paraformaldehyde solution (16 %) was obtained from Thermofisher scientific (Waltham, USA). 488 NHS-ester was obtained from FluoProbes (Arizona, USA).

2.2. Synthesis of Arg- and Lys- biodynamers and their respective quality controls

The biodynamers were synthesized following the previously reported protocol with some modifications. [11] In detail, it took place by mixing 1 equivalent of carbazole hexaglycol dialdehyde with 1 equivalent arginine or lysine hydrazide in deutrated acetic acid solution at pD 3.4 acidified deuterium oxide making a 10 mM solution of both reactants. The mixture was left reacting overnight with occasional mixing and wet sonication to make sure that everything is well dissolved. As quality controls, two methods (HNMR and Dynamic Light Scattering) were applied to control for successful replication of the biodynamers previously reported. [11–14] Reaction completion was monitored by observing a depletion of the aldehyde protons as well as the broadening of the protons on the HNMR due to successful polymerization, as shown in Figures S12 and S13 at 10.2 ppm. Also, Dynamic light scattering was conducted check for the size of the biodynamers using Zetasizer ZS Series (Malvern Instruments Limited, Malvern, UK) at 1 mg/mL concentration, as shown in Figure S1. Afterwards, the mixture was washed with

MilliQ water using Pall 3 kDa centrifugal filters three times. The synthesized biodynamers were then stored at −20 °C. The biodynamers were always neutralized before assays by having high dilution factors in neutral media. The detailed chemical synthesis of the starting materials and the corresponding NMRs can be found in the supplementary materials (Figures S6-S12). For the sake of comparability, the molarity was calculated using the molecular weight of the repeating unit of all the polymers. The molecular weight of Arg- and Lys-biodynamers are 653.8 and 625.8 g/mol respectively.

2.3. Bacterial culture

To prepare an overnight culture of *E. coli* DSM 6897, a single uniform colony was picked from any agar plate and put into 50 mL of Mueller Hinton Broth (MHB) and left to grow overnight in an incubator at 37 °C with 180 rpm. After overnight incubation, 50 μL of the cultured bacteria were inoculated into 50 mL of fresh broth. When the bacteria reached log phase (OD_{600} 0.6–0.8), they were used and inoculate the microbial assays. This strain was chosen for its comparability with previous studies and follow up studies with resistant strains. [17,18]

2.4. Minimum inhibitory concentration (MIC) determination

The substance dilutions (2x dilution per step) were prepared in 96-well plates (50 μL) in MHB with Tween 80 (0.002 %). Bacteria inoculum (50 μL of 2*10^4 CFU/mL) was added to all of the wells to make the final bacteria concentration 10^4 CFU/mL. The MIC value was determined as the lowest concentration that showed no OD_{600} difference from the medium control after overnight incubation shaking at 180 rpm at 37 °C. Two replicates were done.

For LPS decoy experiment, LPS vesicles were pre-formed in the same manner as for the circular dichroism experiments and then diluted to the respective concentrations.

For experiments in different growth media, overnight cultures were grown in MHB, then the bacteria was inoculated and assayed in M9 medium or RPMI 1640 supplemented with 20 mM of Glucose.

In order to calculate the w/v concentration to molar concentration, the molecular weight of the one repeating unit of the polymers (Arg-biodynamers, Lys-biodynamers, poly-L-arginine, poly-L-lysine) were used. The molar concentration was used in this experiment as it corresponds to the normality of the molecules to avoid any bias in the presentation of the data.

2.5. Synergy of combination treatments in bacterio

A dilution of substance A was performed along the 96-well plate rows starting with 50 μL of 4x the target final concentration of substance A diluted into 25 μL of plain medium each dilution step. Substance B dilutions were prepared independently into LoBind tubes at 4x the target dilutions and then added on substance A in 96-well plate. Bacterial suspension (50 μL of 4*10^4 CFU/mL) was added to all of the wells. All the wells were prepared with MHB. Bacterial inhibition was indicated in the wells that had no bacterial growth as per OD_{600} after incubation for overnight shaking at 180 rpm at 37 °C. Vancomycin and trimethoprim generated turbidity due to precipitation when substance A and B were mixed, otherwise OD_{600} was used. In these plates, 10 μL of PrestoBlue was added to the well after the overnight incubation and the fluorescence (ex.: 560 nm, em.: 590 nm) of the wells was measured after 2 h of shaking at 37 °C.

Fractional inhibitory concentration index (FICI) was calculated as following:

$$FICI = \frac{MICofArgBDsincombination}{MICofArgBDsalone} + \frac{MICoftheantibioticincombination}{MICoftheantibioticalone}$$

2.6. Biocompatibility determination using MTT assay

A549 or RAW264.7 cells were seeded on 96-well plates in RPMI medium supplemented with 10 % FCS (20,000 cells per well). The plates were then incubated until cells reached confluency with fresh medium added every 2 days. For THP-1, 80,000 cells per well were seeded into 96 well plates with DMEM medium supplemented with 10 % FCS and 30 ng/mL of PMA, so that differentiated THP-1 cells can adhere to the wells. Then for all types of cells, they were washed twice with HBSS buffer followed by the addition of sample substances in HBSS. For the dead control, it was 1 % TritonX-100 in HBSS and the live control was HBSS. The cells were incubated on 150 rpm shaking at 37 °C with 5 % CO_2. After 4 h, sample solutions were removed and the cells were washed once with HBSS. MTT solution (10 μL pf 5 mg/mL Thiazolyl Blue Tetrazolium Bromide stock diluted with 100 μL HBSS) were added to the cells for 4 h while shaking. After another 4 h of incubation, the MTT solution was removed and 100 μL of DMSO were added to dissolve the MTT crystals for 30 min. Viability was calculated using the measured absorbance at 550 nm as following:

$$\%viability = \frac{Abs_{550}ofsample - Abs_{550}ofdeadcontrol}{Abs_{550}oflivecontrol - Abs_{550}ofdeadcontrol} * 100\%$$

Three replicates were performed. The CC_{50} (A549) was calculated using GraphPad Prism 9 by fitting the data after assuming that the 7.8 μM represents 100 % viability by nonlinear regression. Since no complete killing of the cells with Lys- and Arg-biodynamers took place, CC_{50} of the biodynamers was approximated. The molar concentration was used in this experiment as it corresponds to the normality of the molecules to avoid any bias in the presentation of the data.

2.7. Visualization of bacteria permeabilization with PI

First, Arg-biodynamers were synthesized using the standard way as described before, with the following adjustments: The hydrazide content added for the reaction was 70 w/w% arginine hydrazide and 30 w/w% lysine hydrazide. To label the Arg-biodynamers, 20 w/w% of FluoProbes 488 NHS-ester was added after adjusting the pH to 8 using triethanolamine and placed at room temperature for a day. Afterwards, the mixture was washed with MilliQ water using Pall 3 kDa centrifugal filters until the ultrafilterate had fluorescence signal-to-noise ratio of less than 2 compared to MilliQ water.

Using a log phase culture in MHB, a bacterial suspension of 10^8 CFU/mL of *E. coli* in sterile PBS (1 mL). Three different treatments were applied to three different bacterial suspension in LoBind tubes. The first was a negative control of untreated bacteria with 30 μM of PI. The second treatment was 0.1 w/w% final concentration of TritonX-100 with 30 μM of PI serving as a positive control. The third treatment was labeled Arg-biodynamers with a final concentration of 128 μg/mL, which represents a concentration at which synergy with colistin was shown, with 30 μM of PI. The samples were incubated for 15 min followed by precipitation in a centrifuge cooled to 4 °C at 5,000 g for 5 min, washed twice with PBS and resuspended in 1 mL 4 % paraformaldehyde (PFA) in PBS for 15 min. For the low-dose (10 μg/mL) Arg-biodynamers-treated bacteria, the fixing by PFA was done on the second day of the experiment. At this low concentration, the arrangement of the Arg-biodynamers on the surface is expected to be shown when the surface is not saturated with Arg-biodynamers. The bacteria were again washed once with PBS. Then the bacteria pellet was suspended in a low volume 20 μL, one drop was added to a glass slide, and mixed with a drop of DAKO fluorescence mounting media and covered with a glass slide.

The slides were then visualized with Leica TC SP8 (Leica Microsystems, Wetzler, Germany) with a 63x water objective (HC PL APO CS2 63x/1.20 WATER). The specifications of the measurement were as follows: argon laser intensity = 30 %, wavelength laser for excitation for labeled Arg-bioynamers = 488 nm (intensity of 4 %), emission for

labeled Arg-bioynamers = 494–563 nm, wavelength laser for excitation of PI = 514 nm (intensity of 0.3 %), emission for PI = 608–725 nm. The signal was measured in sequence not simultaneously using HyD detector with a gain of 100, and pinhole 111.4 μm. A line average of 2 was applied. Resolution was 1024 × 1024. A z-stack was created over a span of around 9 μm above and below the bacteria. Scan speed was 400 Hz.

For the low-dose sample (treated with 10 μg/mL Arg-biodynamers), the imaging was performed similar described above with the following adjustments: wavelength laser for excitation for labeled Arg-biodynamers = 488 nm (intensity of 20 %), wavelength laser for excitation of PI = 514 nm (intensity 1 %) to be able to visualize the low amount of labeled Arg-biodynamers and low amount of taken up PI. The PI signal was later increased to be able to see the bacteria morphology as the taken-up amount is negligible with 10 μg/mL of Arg-biodynamers.

2.8. Visualization of morphological changes of the bacterial membrane upon treatment

E. coli suspension (190 μL) in the log phase (OD 0.4–0.8) was incubated for 2 h in PBS in a 96-well plate with the treatment 200 μg/mL (final concentration) of Arg-biodynamers suspended in 10 μL or without treatment by adding the respective volume of MilliQ water as the Arg-biodynamers (10 % of the total volume). There was no in-between washing to keep the Arg-biodynamers on the bacteria surface. Shortly, sterilized silicon wafers were put at the bottom of the 96 well plate. After 2 h, 50 μL of 16 % paraformaldehyde was added for 1.5 h without shaking the well to cross-link the bacterial cells. The cells were then washed very carefully with increasing amounts of ethanol starting from 30 % to 100 % using 10 % steps and then all solution was removed to keep only the pellet. Finally, hexamethyldisilazane was added for 10 min to dry the sample and then removed. The wafers were left under the hood for overnight to completely dry. The wafers were then gold-sputtered using Quorum Q150R ES sputter-coater (Gala Instrumente GmbH, Germany) and visualized under the SEM using Zeiss EVO HD15 (Zeiss, Germany) with voltage of 5 kV.

2.9. Molecular interactions and conformational changes determination in different bacterial microenvironments

The method was adapted from a previously reported protocol with some changes.[19] In detail, a Jasco 1500 spectropolarimeter (Gross-Umstadt, Germany) was used to measure the CD spectra were obtained at 24 °C in 1 mm path length quartz cell. The setting for the measurements were as following: Bandwidth = 1 nm, Range = 175–600 nm, No. of accumulations = 16 (which were averaged to give the resulting spectrum), Scanning speed 20 nm/min. All samples were suspended in 50 mM phosphate buffer. The concentrations of Arg-biodynamers, LPS, POPG were 300 μM, 10 mg/mL, 3.4 mM, respectively. After the environment background subtractions, the spectra were analyzed with CONTIN algorithm only between 175 and 260 nm to get the secondary structure information. α-helical = H(r) + H(d), β-sheet = S(r) + S(d), Turns = Trn, and Unrd = random.

3. Results

3.1. Biocompatibility of biodynamers

To avoid the pitfall of designing some non-selective, unsafe antibiotic potentiator, we determined the biocompatibility of the Arg- and Lys-biodynamers with mammalian cells (A549 cells), compared to their non-dynamic analogs poly-L-arginine and poly-L-lysine, respectively. The evaluation of the biocompatibility was determined via an MTT assay. At low concentrations, poly-L-arginine and poly-L-lysine appear to first increase viability to > 100 %, hinting that the cationic poly-amino acids have a respiratory stimulating effect on the cells. As shown in Fig. 1, Arg- and Lys-biodynamers showed a much better biocompatibility with A549 cells, especially Arg-biodynamers, which had a good safety profile until 4000 μM (2.7 mg/mL). Compared to its non-dynamic poly-amino acid analog, we observed some > 128-fold improvement in biocompatibility for Arg-biodynamers. Additionally, Arg-biodynamers was shown to be safe for longer exposure times in previous studies. [11]

3.2. Antimicrobial effects and selectivity of biodynamers

The antimicrobial activity was determined using MIC assay against *E. coli* as a representative of Gram-negative bacteria. As shown in Table 1, Arg- and Lys-biodynamers showed some slightly decreased antimicrobial ability by about 3–6 times compared to poly-L-arginine and poly-L-lysine, indicating a limited potential of biodynamers as stand-alone antimicrobials.

However, calculating the selectivity index (SI) by the ratio of mammalian CC_{50} over bacterial MIC, the favorable safety profile of biodynamers becomes evident, as shown in Table 1. By comparing the Arg-biodynamers with poly-L-arginine, it is at least 21-fold more selective towards bacteria. This observation hints that Arg-biodynamers are capable of undergoing some specific interaction with the bacteria, not

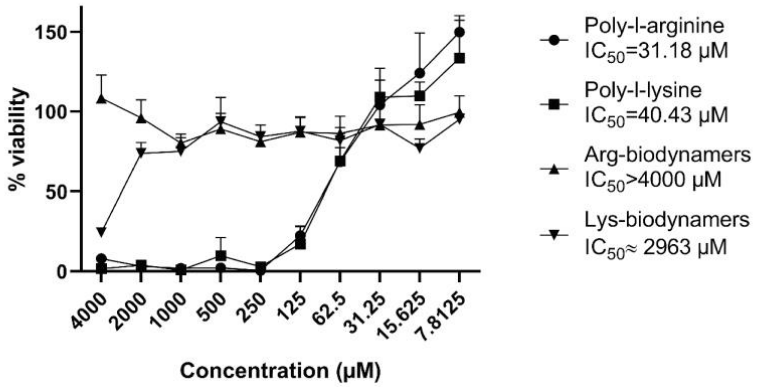

Fig. 1. Cytotoxicity (MTT assay) of different polymers on A549 cells incubated for 4 h in HBSS showing the relative safety of biodynamers on the mammalian cells compared to their poly-amino acid analogs. Molar concentration represents the molar concentration of the repeating units of the polymers. Three replicates were conducted. Datapoints represent the average and error bars represent standard deviation.

Table 1
Selectivity index (SI) calculations of different polymers showing the superiority of the biodynamers over their poly-amino acids analogs. Molar concentration represents the molar concentration of the repeating units of the polymers.

Polymer	MIC in *E. coli* (μM)	CC_{50} in A549 (μM)	SI (A549/*E. coli*)	Fold improvement of SI*
Arg-biodynamers	3061	>4000	>1.3	21
Poly-L-arginine	1000	62.53	0.062	
Lys-biodynamers	1598	2570	1.6	12
Poly-L-lysine	250	32.25	0.129	

Minimum inhibitory concentrations (MIC), Cytotoxic concentration (CC_{50}), Selectivity index (SI).
* Calculated by the ratio between $SI_{BD}/SI_{poly\text{-}amino\ acid}$.

solely depending on their positive charge. Since Arg-biodynamers are polymers, it is more plausible that they interact with the bacterial cell envelope rather than an intracellular target. [13] In order to unravel those complex interactions, we chose to study them with the isolated components of the bacterial cell envelope. For its superior improvement (21x) of the SI compared to that of Lys-biodynamers (12x) over their non-dynamic analogs, we decided to concentrate our subsequent investigations on Arg-biodynamers.

3.3. Antibacterial synergy of Arg-biodynamers with different antibiotics

Antibacterial checkerboard assay was conducted to assess the synergistic effect of Arg-biodynamers. The antibacterial checkerboard assay was performed for combinations with a variety of antibiotics, representing a wide variety of physicochemical properties, antimicrobial spectra, and mechanisms of actions to explore different influences of Arg-Biodynamers on different categories of antibiotics. Sub-MIC concentrations of Arg-biodynamers, ranging from 64 μg/mL to 1024 μg/mL, and Sub-MIC concentrations of antibiotics (colistin, novobiocin, fusidic acid, linezolid, clindamycin, rifampicin, vancomycin, and trimethoprim) were combined to observe bacterial growth inhibition after overnight incubation to investigate the effect of titrating different Arg-Biodynamers concentrations on the efficacy of antibiotics in combination.

The additive effect was plotted as a red line in Fig. 2, while anything below is a hint towards synergistic effect. As shown in Fig. 2, the most benefiting antibiotic from such synergy was shown to be colistin with a staggering 32-fold improvement at inhibiting bacterial growth and a fractional inhibitory concentration index (FICI) of 0.125. A FICI below 0.5 is considered synergistic, meaning that colistin, linezolid, and novobiocin were synergistic with Arg-biodynamers while fusidic acid, rifampin, and clindamycin are borderline ($0.5 < FICI < 1.0$). On the other hand, vancomycin and trimethoprim were shown to be antagonistic ($FICI > 1.0$), as summarized in Table 2.

3.4. Bacterial membrane and Arg-biodynamers interaction

To further probe the interaction between Arg-biodynamers and the LPS-rich bacterial membrane, we first visualized its impact on membrane structure using scanning electron microscopy (SEM). As shown in Fig. 3, one can observe a few structural changes. Most obviously, the surface roughness of *E. coli* was increased when treated with sub-MIC concentrations of Arg-biodynamers. This suggests a tendency for Arg-biodynamers to directly affect the outer membrane of the Gram-negative bacteria. Furthermore, the size of the bacteria seems to be shrunk, which could align with an increased water leakage due to membrane permeabilization.

To further confirm that Arg-biodynamers is acting on the bacterial cell envelope, *E. coli* were treated with 128 μg/mL of labeled Arg-biodynamers (L-Arg-bioynamers) and PI to investigate the membrane

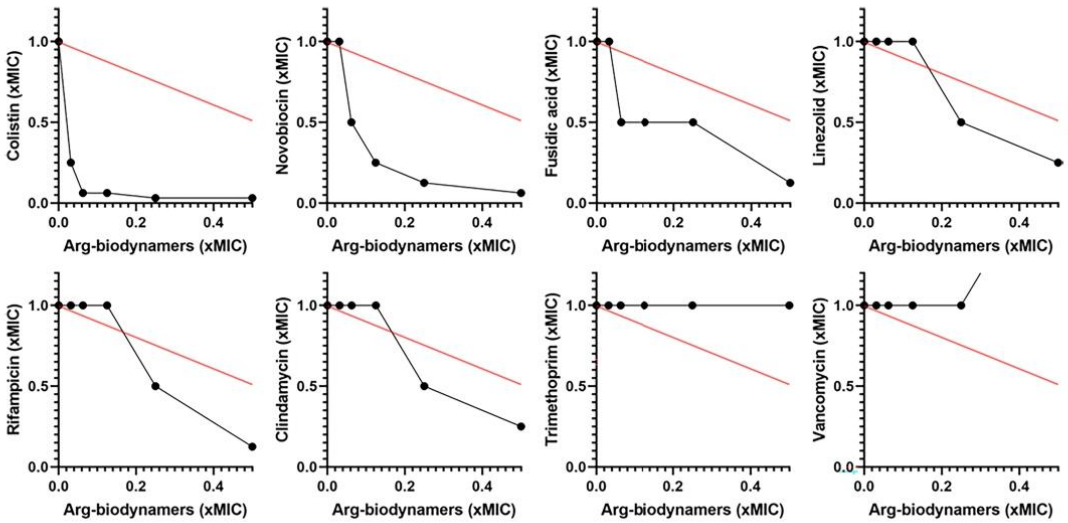

Fig. 2. Checkerbaord assays using *E. coli* for different antibiotics in combination with Arg-biodynamers. Every black point represents complete inhibition of bacterial growth. The red line represents a perfect additive effect meaning that below this line, synergy is probable and above this line, antagonism is probable. The MICs of Arg-biodynamers, colisitin, fusidic acid, linezolid, clindamycin, rifampicin, vancomycin, trimethoprim were 2048, 0.5, 128, 256, 128, 128, 16, 32, 512 μg/mL respectively. (For interpretation of the references to color in this figure legend, the reader is referred to the web version of this article.)

Table 2
Tested antibiotics in combination with Arg-biodynamers highlighting the achieved improvement of the MIC value compared to MIC for the antibiotic alone in *E. coli*.

Antibiotics	Target	Maximum fold improvement of MIC	FICI	LPS-related mechanism	References
Colistin	Cell membrane	32	0.125	Yes	[38]
Novobiocin	DNA gyrase	16	0.375	Yes (LptB agonism)	[39,40]
Fusidic acid	Protein synthesis	8	0.563	N/A	[41]
Rifampin	Polymerase	8	0.625	N/A	[42]
Linezolid	Protein synthesis	4	0.625	N/A	[43]
Clindamycin	Protein synthesis	4	0.75	N/A	[44]
Trimethoprim	Folate pathway	N/A	1	N/A	[45]
Vancomycin	Cell wall synthesis	N/A	>1	N/A	[46]

Fractional inhibitory concentration index (FICI), Lipopolysaccharide (LPS).

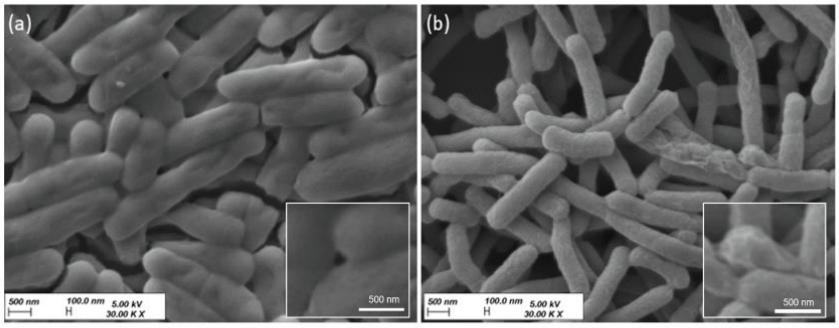

Fig. 3. Scanning electron microcopy of *E. coli* after sample preparation (a) without treatment and (b) with 200 μg/mL Arg-biodynamers, with zoom in on each panel.

permeabilization degree using confocal laser scanning microscopy (CLSM). Note that the PI is not membrane penetrable, so only it penetrates the cell membranes in the presence of a permeabilizing agent. As shown in Fig. 4 (a), the negative control showed no autoflorescence or background for the measured channels while the positive control was 0.1 % TritonX surfactant which permeabilized the bacteria successfully and formed a structure known as "Bacterial Spheroplasts" (Fig. 4 (b)). [20] Meanwhile, we visualized the localization of the L-Arg-biodynamers in the bacteria. As shown in Fig. 4 (c), after very transient incubation (15 min) with the L-Arg-biodynamers followed by immediate cross-linking, we could observe a green signal (L-Arg-bioynamers) in all of the cells. For the red signal (PI), it was also observed in most of the bacteria treated with L-Arg-biodynamers.

If L-Arg-biodynamers internalized with the PI, the merged images should exhibit yellow color. However, most bacteria can show a dominating red signal (internalized PI) engulfed with green borders (L-Arg-biodynamers) which suggests that L-Arg-biodynamers primarily localize on the cell membrane. Nevertheless, colocalization of the red and green signal inside the bacteria could be attributed to partial degradation of saturation of the florescence signal on the surface of the bacteria or partial degradation of Arg-biodynamers via pH-dependent dynamic covalent chemistry allowing its internalization into the bacteria. [12] It is worth noting that *E. coli* bacterial cultures pH was around 6 after overnight growth by a simple litmus paper test although the growth medium was originally neutral.

Additionally, we performed imaging after a longer time without cross-linking until one day later to see how L-Arg-bioynamers would look like after a while on the surface of the bacteria, meaning that bacterial cells were left with no cross-linking and the Arg-biodynamers treatment was removed, as shown in Fig. 4 (d). A very interesting observation was to see assemblies of Arg-biodynamers on the surface of the bacteria as if L-Arg-bioynamers molecules assembled into agglomerated structures on the outer membrane of the *E. coli* cells, leaving some uncovered areas. As shown on Figure S2, just 25 % of the PI was found to be taken up into the bacteria which indicates only a mild damage to the membrane, which aligns with the relatively higher MIC of Arg-biodynamers.

3.5. Molecular interactions of Arg-biodynamers with the bacterial membrane components

Circular dichroism (CD) spectroscopy was performed for Arg-biodynamers in different microenvironments to determine the conformation of the Arg-biodynamers on the molecular level. Arg-biodynamers was measured in plain buffer, POPG, and LPS solutions while subtracting the background composes of each solution, and the resulting spectra are shown in Fig. 5. Arg-biodynamers in POPG seem to a flatter spectrum but maintain a similar CD spectrum as the plain buffer with no significant changes in absorption pattern. LPS induces a major change in the Arg-biodynamers spectrum resulting indicating a different secondary structure. [21]

Since biodynamers are peptide mimetics, the CONTIN algorithm was applied on the spectra to determine the secondary structure of Arg-biodynamers, as shown in Fig. 6. It can be noted that the Arg-biodynamers secondary structure changes minimally when it is with POPG. However, Arg-biodynamers with LPS changes to β-sheets with a substantial decrease of the unordered portion (from 38 to 8 %) hinting that such change is thermodynamically favorable.

CD is a powerful technique which also allows a more than just knowing the secondary structure by looking at the longer wavelength region of the spectrum to gain information about the tertiary structure or even the side chains environment for proteins, peptides or even DNA. Arg-biodynamers have aromatic systems with nitrogen atoms in hydrazones/imines on their backbone and the carbazole core, which interact with the polarized UV light at regions higher than 240 nm as shown in Figure S3. Analyzing CD findings in the 240–300 nm region can be of relevance as reported in literature. It has been noted in literature that an absorption pattern, having a minimum at 260 nm and a maximum at 295 nm, is associated with the formation of what is known as "Anti-parallel G-quadruplex". Interestingly, the Arg-biodynamers

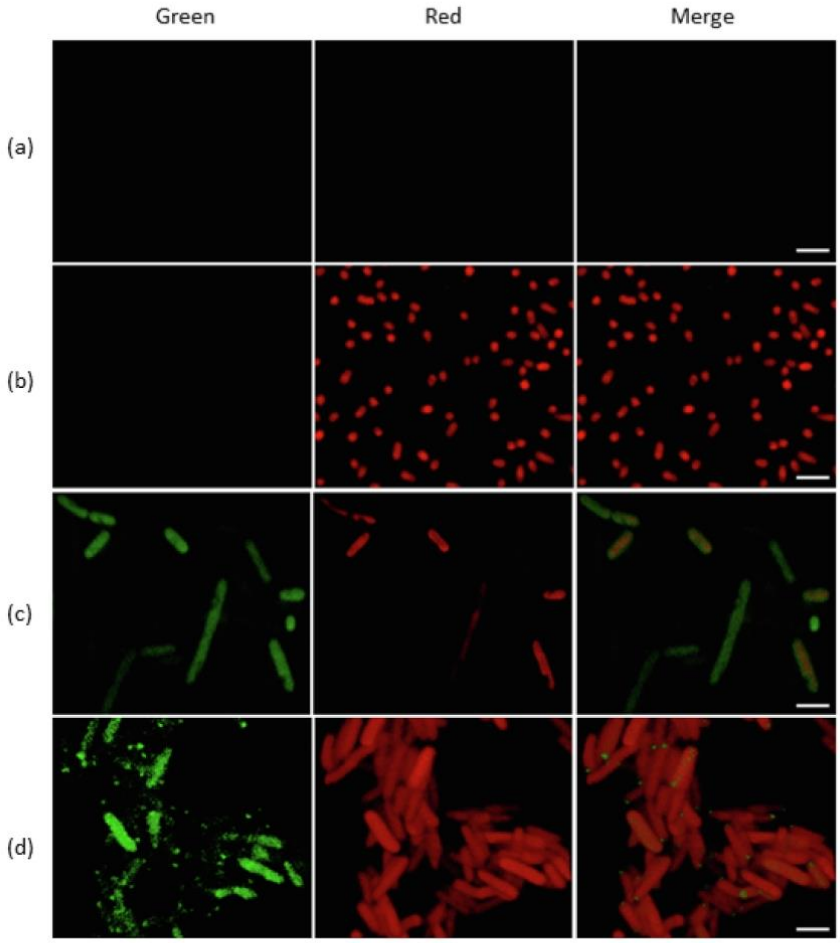

Fig. 4. Permeabilization of propidium iodide (red) into E. coli in the presence different treatment; (a) blank, (b) 0.1 % TritonX, (c) 128 μg/mL labeled Arg-biodynamers (green) with immediate cross-linking, (d) 10 μg/mL (low-dose) labeled Arg-biodynamers (green) with delayed cross-linking. The first three treatments were done for 15 min, cross-linked immediately, while the low-dose Arg-biodynamers was treated for 15 min, but left without cross-linking for overnight to allow for membrane-polymer arrangement. Also, the low-dose Arg-biodynamers treatment green and especially the red signals were increased using the software to be able to see the bacterial morphology, however the uptake PI amount was negligible with the low-dose treatment. The scale bar is 2 μm. Arg-biodynamers; ArgBD. (For interpretation of the references to color in this figure legend, the reader is referred to the web version of this article.)

show such a particular CD spectrum in the presence of LPS (Fig. 6), which can be explained by the arrangement of the Arg-biodynamers around the phosphate moiety on the LPS in quadruplexes [22,23].

4. Discussion

From the results of MTT and MIC, we demonstrated that cationic biodynamers, especially Arg-biodynamers, are more selective to bacteria than cationic polyaminoacids. By looking into the potential of Arg-biodynamers as bacterial potentiators, one could calculate the *in vitro* therapeutic index, where Arg-biodynamers can achieve colistin potentiation at concentrations of just 64 μg/mL, while it is toxic to A549 lung cells at > 2700 μg/mL. This is an improvement in the safety by a factor of 128 compared to poly-L-arginine. While still Arg-biodynamers and Lys-biodynamers kept a very good safety profile in immune cells, which are typically more sensitive to macromolecules (Figure S4). Regarding the electivity index for Arg-biodynamers as an adjuvant with colistin, the ratio CC_{50} (with A549) and the lowest concentration which synergizes colistin, yields a selectivity index of > 41, which is rather acceptable for further development and potential *in vivo* applications.[24]

Arg-biodynamers appeared to be effective as a potentiator at mass concentrations ≥ 64 μg/mL. However, as reported small molecule potentiators have molecular weights in the range of hundreds of daltons only, the molecular weight of Arg-Biodynamers was found to be 15–70 kDa depending on the synthesis and measurement methods which translates to an activity in the μM range. [14] Interestingly enough, the MIC of Arg-Biodynamers was found to be 64x more active (32 μg/mL) in protein-free growth media (M9 and RPMI) compared to the complex Mueller Hinton Broth (Table S2), which makes Arg-biodynamers appear particularly promising for topical applications.

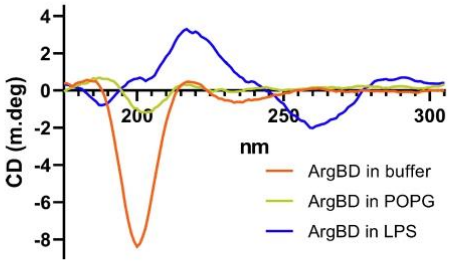

Fig. 5. Circular dichroism of Arg-biodynamers in phosphate buffer, POPG, or LPS using circular dichroism spectrometry. The spectra of Arg-biodynamers in addition to buffer only, POPG in buffer, or LPS in buffer were subtracted from the spectra without Arg-biodynamers to get the pure signal of the Arg-biodynamers. Arg-biodynamers; ArgBD.

It is reported that the more arginine a peptide contains, the more antimicrobial, but also the more cytotoxic it is.[25] On the other hand, the secondary structure of a peptide is also known to play a major role for the membrane activity of the peptide.[26] We hypothesize that the biodegradability of the biodynamers, their decreased charge density, and the PEG chain of Arg- and Lys-biodynamers are the reasons for reduced mammalian cytotoxicity compared to poly-L-arginine or poly-L-lysine. Especially, the PEG chain is expected to shield the charges of the biodynamers, which can be shown by the zeta potential of Arg-biodynamers, which was shown to be + 1.34 mV (+/- 0.203) hinting a relatively neutral surface charge. The later reasons are thought as well to be contributing to the superior antimicrobial efficacy of poly-aminoacids. By favoring the interaction with the LPS-containing bacterial over the LPS-free mammalian membrane, the capacity to dynamically adopt their secondary structure to those different substrates may explain the favorable safety profile of the biodynamers.

To further investigate the selectivity of biodynamers to bacterial membranes, we conducted a few additional experiments. First, it is evident from the SEM images that sub-MIC Arg-biodynamers influences the surface roughness and structure. Our SEM findings are very similar to an earlier study,[27] showing developed peptides (Pa-MAP2) to interact with anionic components of the bacterial cell envelope. Their atomic force microscopy (AFM) data show a similar increase of surface roughness with Pa-MAP2 peptide, which was proven to interact with LPS, POPG, and POPS. As we could show by SDS-PAGE (Figure S5), our Arg-biodynamers has a molecular weight (15 kDa), which corresponds to 25 repeating units and is well above the size limit of any known bacterial transporters, which is typically around 600 Da.[28,29] Therefore, Arg-biodynamers may interact with the outer bacterial membrane only while it is still in its polymeric form. It can also be seen in literature that relatively hydrophilic and cationic molecules are more probable to interact with the outer membrane than the inner membrane.[5]

Secondly, to further investigate their impact on bacterial membranes, we observed the Arg-biodynamers on the *E. coli* membranes using CLSM. Our CLSM data show that Arg-biodynamers can be assembled on *E. coli* membrane when in low amounts and kept for long enough on the bacterial membrane large enough to be detectable by a 63x objective on a CLSM. This is similar to a recent discovery on the mechanism of action of teixobactin. Shukla *et al.* could prove that teixobactin can form β-sheets on the bacterial membrane of Gram-positive bacteria, specifically the lipid II component of the membrane.[30] Additionally, β-sheet assemblies were found to also have membrane-specific interactions with the lipid bilayer with peptides designed for this purpose.[31] The Arg-biodynamers presented a similar tendency but with the LPS. It has been shown recently that the formation of such rigid ordered structures on the membrane of bacteria can lead to antimicrobial activity, even in an established class of antibiotics like polymyxins, which was never discovered earlier during their development.[32] However, to the best of our knowledge, our present study is the first to report such an increased β-sheet formation as well as an antiparallel quadruplex on the membranes of Gram-negative bacteria mediated by an interaction with LPS. The tested LPS was extracted from *E. coli*, so a validation for activity in other Gram-negative bacteria had to be proven via MIC reduction assay in PA01 and PA14 (Table S1), this interaction can be extended to different strains of Gram-negatives. We propose that β-sheet-forming polymers/peptides, which antagonize the LPS barrier, could lead to a new path in antimicrobial research, analogously to α-helical peptides, which destroy membranes by forming rigid structures embedded inside lipid bilayers.[33]

We explored which factors on the bacterial membranes could interact with Arg-biodynamers. The LPS is made of lipid A, core saccharides, and O antigen. Furthermore, lipid A is negatively charged and has two sugars as well as a lipid tail. As per our CD results, charged anionic POPG seems to not influence much the Arg-biodynamers' secondary structure. As a support towards this hypothesis, we performed combination treatment of normal *E. coli* and mutated ClearColi *E. coli* having only the lipid A part (including the glucosamine sugars with the charged phosphate) with colistin or colistin in addition to Arg-biodynamers and even better synergy was observed than with the normal *E. coli* (Table S1). Thus, it can be concluded that lipid A is the key part of the LPS, responsible for the interaction. Additionally, the better synergy hints that could be attributed to the lack of steric hinderance of the LPS against Arg-biodynamers. It can be hinted that the interaction with the LPS is not due to the lipid part of the charged lipid A because

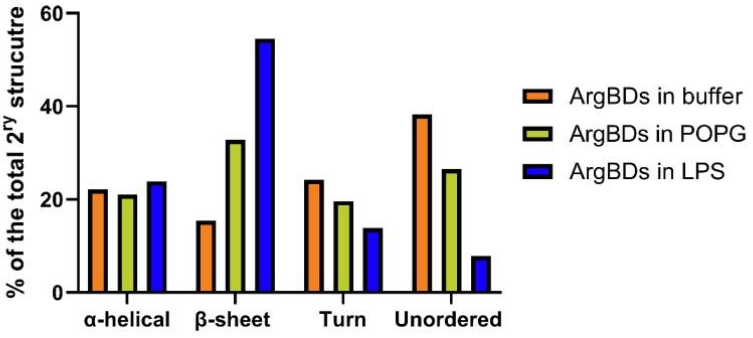

Fig. 6. Secondary structure for as determined by circular dichroism spectropolarimeter showing drastic change of the secondary structure when incubated in different media (buffer, POPG, and LPS). Arg-biodynamers; ArgBD.

POPG does not show much interaction with Arg-biodynamers. Since the charge of LPS is mainly attributed to the phosphate groups on the glucosamine sugars of lipid A, we hypothesize that the primary interaction takes place between the positively charged guanidino groups of Arg-biodynamers and negatively charged phosphate groups of lipid A. As a secondary evidence of the interaction Arg-biodynamers with LPS, decoy LPS could be observed to decrease the antimicrobial activity of Arg-biodynamers indicating a confirmed ArgBD-LPS coupling (Table S2).

It has been already shown that the antimicrobial protein colicin N is likely to interact with lipid A in between the core sugars of the LPS, which agrees as well with our hypotheses.[34,35] On the other hand, peptidomimetics targeting LPS core-sugars were shown to not have synergistic effects with colistin. This is in contrast with our results for Arg-biodynamers, but fully aligned with our hypothesis that β-sheet formation is essential for such synergy.[36] If additional experiments, such as 2D ^{1}H NMR or in silico simulations on the atomic level, are conducted, this hypothesis may become more solid. However, broadened and merged ^{1}H NMR signals of Arg-biodynamers (Figure S13) and the complicated structure of their repeating units causing tremendous computing volumes will be limitations of any technique that needs to be addressed.[19,27,37]

The tested antibiotics have a variety of action spectra as well as different targets within a bacterium and very different physicochemical properties. The most noted feature of the antibiotics with the highest synergy was their mechanism of action, which has the LPS as a target (colistin and novobiocin, Table 2). This has given us the motivation to investigate the ArgBD–LPS interactions.

Aside from LPS-targeting antibiotics, we hypothesized that these antibiotics are synergized due to their enhanced uptake passively through the LPS layer. Although it is known that colistin can break down the LPS layer integrity, Arg-biodynamers is thought to embed in between the LPS molecules so that colistin enabled to interact with inner parts of the LPS layer (Lipid A) and exert its surfactant-like effect. Another potential mechanism of potentiation of the Arg-biodynamers for colistin is that they facilitate colistin to interact with the inner membrane of the bacterial cell envelope at higher local concentrations.[47]

Regarding novobiocin, it is not the first time that this antibiotic was found to have synergistic effects with membrane-active molecules. Synergy has been reported between novobiocin and colistin, however, the underlying mechanism remains unanswered. Novobiocin happens to be a LptB agonist. LptB is an LPS transporter, which transports LPS to the bacterial membrane. This synergy is puzzling because if the LPS molecules on the membrane increase via novobiocin, this can overwhelm the colistin as an LPS-targeting antibiotic and decrease its efficiency in contrast to what was observed.[39] Novobiocin was found to utilize yddB porin for uptake into bacteria, however, it has been found a significant portion can still take the passive non-facilitated uptake pathway into the bacteria to its target (DNA gyrase). We hypothesize that one reason for limited novobiocin antimicrobial activity is that novobiocin increases LPS on the surface and, thus, has less passive non-facilitated uptake of novobiocin itself.[48–52] We speculate that Arg-biodynamers were able to synergize with novobiocin by decreasing the MIC from 128 to just 8 μg/mL, bringing the MIC at only two folds the MIC breakpoint in *E. coli*.[52] Therefore, colistin or Arg-biodynamers could be the solution to break this loop of novobiocin decreasing its own activity. This finding highlights the importance of the non-porin dependent uptake pathway of novobiocin as a potential research area to increase their spectrum to include Gram-negative bacteria.

5. Conclusions

In this study, we demonstrated that biodynamers, such as Arg-biodynamers, may improve the delivery of antibiotics across the Gram-negative bacterial cell envelope. In contrast to their non-dynamic analogs (poly-L-arginine), they undergo selective interactions with the LPS-containing outer bacterial membrane without damaging mammalian cells. In combination with different antibiotics, we thus observed a potentiating effect, up to 32-fold in the case of colistin. As a mechanism of action, Arg-biodynamers was shown to form assemblies with the bacterial membrane aligned with a change of the secondary structure with the LPS. Similar to the recently discovered interaction of teixobactin with lipid II in Gram-positive bacteria, Arg-biodynamers interacts with LPS, which makes up the outer-most leaflet of the Gram-negative bacterial cell envelope. The formation of weak points, but without destroying this notoriously tight barrier, results in an improved activity of LPS-hindered antibiotics in Gram-negative bacteria. This qualifies Arg-biodynamers as an interesting potentiator/adjuvant with a novel mechanism for existing antibiotics in the battle against the notoriously hard-to-treat Gram-negative bacteria and antimicrobial resistance.

Credit authorship contribution statement

Mohamed A.M. Kamal: Writing – review & editing, Writing – original draft, Visualization, Validation, Investigation, Methodology, Formal analysis, Data curation, Conceptualization. **Justine Bassil:** Writing – review & editing, Validation, Methodology. **Brigitta Loretz:** Writing – review & editing, Supervision, Resources, Project administration, Investigation, Conceptualization. **Anna K.H. Hirsch:** Writing – review & editing, Supervision, Resources, Project administration, Funding acquisition, Conceptualization. **Sangeun Lee:** Writing – review & editing, Visualization, Supervision, Project administration, Investigation, Data curation, Conceptualization. **Claus-Michael Lehr:** Writing – review & editing, Supervision, Resources, Project administration, Funding acquisition, Conceptualization.

Declaration of competing interest

The authors declare that they have no known competing financial interests or personal relationships that could have appeared to influence the work reported in this paper.

Data availability

Data will be made available on request.

Acknowledgment

The authors would like to thank Dr. Annette Boese, Pascal Paul, Neha Bankar, and Petra König for guidance and help with the confocal microscopy, scanning electron microscopy, its sample preparation, and cell culture, respectively.

Author contributions

The manuscript was written through contributions of all authors. All authors have given approval to the final version of the manuscript.

Appendix A. Supplementary data

Size measurement of Arg-Biodynamers. Quantification of permeabilized PI. Absorbance scan of Arg-biodynamers and an example peptide. Cytotoxicity assays in stimulated THP-1 and RAW267.4. SDS PAGE of Arg-biodynamers. MIC reduction experiments in *Escherichia coli* and *Pseudomonas aeruginosa*. LPS as a decoy and medium effect for Arg-biodynamers. Chemical synthesis and NMRs. Supplementary data to this article can be found online at https://doi.org/10.1016/j.ejpb.2024.114336.

References

[1] A.H. Holmes, L.S.P. Moore, A. Sundsfjord, M. Steinbakk, S. Regmi, A. Karkey, P. J. Guerin, L.J.V. Piddock, Understanding the Mechanisms and Drivers of Antimicrobial Resistance, Lancet 387 (10014) (2016) 176–187, https://doi.org/10.1016/S0140-6736(15)00473-0.

[2] D.M.P. De Oliveira, B.M. Forde, T.J. Kidd, P.N.A. Harris, M.A. Schembri, S. A. Beatson, D.L. Paterson, M.J. Walker, Antimicrobial Resistance in ESKAPE Pathogens, Clin. Microbiol. Rev. 33 (3) (2020), https://doi.org/10.1128/CMR.00181-19.

[3] S. Walesch, J. Birkelbach, E.J. Ez, G. Equel, J. Haeckl, J.D. Hegemann, T. Hesterkamp, A.K.H. Hirsch, P. Hammann, R. MŁller, Fighting Antibiotic Resistance—Strategies and (Pre)Clinical Developments to Find New Antibacterials, EMBO Rep. 24 (1) (2023) e56033.

[4] J.M. Stokes, C.R. Macnair, B. Ilyas, S. French, J.P. Côté, C. Bouwman, M.A. Farha, A.O. Sieron, C. Whitfield, B.K. Coombes, E.D. Brown, Pentamidine Sensitizes Gram-Negative Pathogens to Antibiotics and Overcomes Acquired Colistin Resistance, Nature Microbiol. 2 (5) (2017) 1–8, https://doi.org/10.1038/nmicrobiol.2017.28.

[5] K. Klobucar, E.D. Brown, New Potentiators of Ineffective Antibiotics: Targeting the Gram-Negative Outer Membrane to Overcome Intrinsic Resistance, Curr. Opin. Chem. Biol. 66 (2022) 102099, https://doi.org/10.1016/j.cbpa.2021.102099.

[6] S. Wu, Y. Huang, J. Yan, Y. Li, J. Wang, Y.Y. Yang, P. Yuan, X. Ding, Bacterial Outer Membrane-Coated Mesoporous Silica Nanoparticles for Targeted Delivery of Antibiotic Rifampicin against Gram-Negative Bacterial Infection In Vivo, Adv. Funct. Mater. 31 (35) (2021) 2103442, https://doi.org/10.1002/ADFM.202103442.

[7] X. Ding, C. Yang, W. Moreira, P. Yuan, B. Periaswamy, P. Florez de Sessions, H. Zhao, J. Tan, A. Lee, K. Xun Ong, N. Park, Z. Chang Liang, J.L. Hedrick, Y. Yan Yang, X. Ding, P. Yuan, H. Zhao, C. Yang, B. Periaswamy, J. Tan, A. Lee, Z.C. Liang, Y.Y. Yang, W. Moreira, K.X. Ong, P.F. de Sessions, N. Park, J.L. Hedrick, A Macromolecule Reversing Antibiotic Resistance Phenotype and Repurposing Drugs as Potent Antibiotics, Adv. Sci. 7 (17) (2020) 2001374, https://doi.org/10.1002/ADVS.202001374.

[8] L.W. Chan, K.E. Hern, C. Ngambenjawong, K. Lee, E.J. Kwon, D.T. Hung, S. N. Bhatia, Selective Permeabilization of Gram-Negative Bacterial Membranes Using Multivalent Peptide Constructs for Antibiotic Sensitization, ACS Infect. Dis. 7 (4) (2021) 721–732, https://doi.org/10.1021/acsinfecdis.0c00805.

[9] A. Bali, M.A.M. Kamal, G. Mulla, B. Loretz, C.M. Lehr, Functional Materials to Overcome Bacterial Barriers and Models to Advance Their Development, Adv. Funct. Mater. (2023) 2304370, https://doi.org/10.1002/ADFM.202304370.

[10] B. Yu, M. Roy Choudhury, X. Yang, S.L. Benoit, E. Womack, K. Van Mouwerik Lyles, A. Acharya, A. Kumar, C. Yang, A. Pavlova, M. Zhu, Z. Yuan, J.C. Gumbart, D.W. Boykin, R.J. Maier, Z. Eichenbaum, B. Wang, Restoring and Enhancing the Potency of Existing Antibiotics against Drug-Resistant Gram-Negative Bacteria through the Development of Potent Small-Molecule Adjuvants, ACS Infect. Dis. 8 (8) (2022) 1491–1508, https://doi.org/10.1021/acsinfecdis.2c00121.

[11] S. Lee, S. Nasr, S. Rasheed, Y. Liu, O. Hartwig, C. Kaya, A. Boese, M. Koch, J. Herrmann, R. Müller, B. Loretz, E. Buhler, A.K.H.H. Hirsch, C.-M.-M. Lehr, Proteoid Biodynamers for Safe MRNA Transfection via PH-Responsive Nanorods Enabling 1 Endosomal Escape Introductory Paragraph 20, J. Control. Release 353 (2023) 915–929, https://doi.org/10.1016/J.JCONREL.2022.12.018.

[12] Y. Liu, J.M. Lehn, A.K.H. Hirsch, Molecular Biodynamers: Dynamic Covalent Analogues of Biopolymers, Acc. Chem. Res. 50 (2) (2017) 376–386, https://doi.org/10.1021/acs.accounts.6b00594.

[13] S. Lee, C. Kaya, H. Jang, M. Koch, B. Loretz, E. Buhler, C.M. Lehr, A.K.H. Hirsch, PH-Dependent Morphology and Optical Properties of Lysine-Derived Molecular Biodynamers, Mater. Chem. Front. 4 (3) (2020) 905–909, https://doi.org/10.1039/c9qm00651f.

[14] Y. Liu, M.C.A. Stuart, E. Buhler, J.M. Lehn, A.K.H. Hirsch, Proteoid Dynamers with Tunable Properties, Adv. Funct. Mater. 26 (34) (2016) 6297–6305, https://doi.org/10.1002/ADFM.201601612.

[15] R. Gref, M. Lück, P. Quellec, M. Marchand, E. Dellacherie, S. Harnisch, T. Blunk, R. H. Müller, 'Stealth' Corona-Core Nanoparticles Surface Modified by Polyethylene Glycol (PEG): Influences of the Corona (PEG Chain Length and Surface Density) and of the Core Composition on Phagocytic Uptake and Plasma Protein Adsorption, Colloids Surf. B Biointerfaces 18 (3–4) (2000) 301–313, https://doi.org/10.1016/S0927-7765(99)00156-3.

[16] S.A. Muhle, J.P. Tam, Design of Gram-Negative Selective Antimicrobial Peptides†, Biochemistry 40 (19) (2001) 5777–5785, https://doi.org/10.1021/BI0100384.

[17] M. Borowiak, J. Fischer, J.A. Hammerl, R.S. Hendriksen, I. Szabo, B. Malorny, Identification of a Novel Transposon-Associated Phosphoethanolamine Transferase Gene, Mcr-5, Conferring Colistin Resistance in d-Tartrate Fermenting Salmonella Enterica Subsp. Enterica Serovar Paratyphi B, J. Antimicrob. Chemother. 72 (12) (2017) 3317–3324, https://doi.org/10.1093/JAC/DKX327.

[18] M. Moosavian, N. Emam, D. Pletzer, M. Savari, Rough-Type and Loss of the LPS Due to Lpx Genes Deletions Are Associated with Colistin Resistance in Multidrug-Resistant Clinical Escherichia Coli Isolates Not Harbouring Mcr Genes, PLoS One 15 (5) (2020) e0233518.

[19] J.J. Abercrombie, K.P. Leung, H. Chai, R.P. Hicks, Spectral and Biological Evaluation of a Synthetic Antimicrobial Peptide Derived from 1-Aminocyclohexane Carboxylic Acid, Bioorg. Med. Chem. 23 (6) (2015) 1341–1347, https://doi.org/10.1016/J.BMC.2015.01.027.

[20] A.I. Benítez-Mateos, A. Schneider, E. Hegarty, B. Hauer, F. Paradisi, Spheroplasts Preparation Boosts the Catalytic Potential of a Squalene-Hopene Cyclase, Nature Commun. 13 (1) (2022) 1–9, https://doi.org/10.1038/s41467-022-34030-0.

[21] Y. Wei, A.A. Thyparambil, R.A. Latour, Protein Helical Structure Determination Using CD Spectroscopy for Solutions with Strong Background Absorbance from 190 to 230 Nm, Biochim. Biophys. Acta (BBA) - Proteins Proteomics 1844 (12) (2014) 2331–2337, https://doi.org/10.1016/J.BBAPAP.2014.10.001.

[22] T. Santos, G.F. Salgado, E.J. Cabrita, C. Cruz, G-Quadruplexes and Their Ligands: Biophysical Methods to Unravel G-Quadruplex/Ligand Interactions, Pharmaceuticals 14 (8) (2021) 769, https://doi.org/10.3390/PH14080769.

[23] A. Ghosh, E. Largy, V. Gabelica, DNA G-Quadruplexes for Native Mass Spectrometry in Potassium: A Database of Validated Structures in Electrospray-Compatible Conditions, Nucleic Acids Res 49 (4) (2021) 2333–2345, https://doi.org/10.1093/NAR/GKAB039.

[24] V.T. Angelova, T. Pencheva, N. Vassilev, E. K-Yovkova, R. Mihaylova, B. Petrov, V. Valcheva, Development of New Antimycobacterial Sulfonyl Hydrazones and 4-Methyl-1,2,3-Thiadiazole-Based Hydrazone Derivatives, Antibiotics 11 (5) (2022) 562, https://doi.org/10.3390/ANTIBIOTICS11050562.

[25] A. Rice, J. Wereszczynski, Probing the Disparate Effects of Arginine and Lysine Residues on Antimicrobial Peptide/Bilayer Association, Biochim. Biophys. Acta Biomembr. 1859 (10) (2017) 1941–1950, https://doi.org/10.1016/J.BBAMEM.2017.06.002.

[26] J.S. Bahnsen, H. Franzyk, A. Sandberg-Schaal, H.M. Nielsen, Antimicrobial and Cell-Penetrating Properties of Penetratin Analogs: Effect of Sequence and Secondary Structure, Biochim. Biophys. Acta Biomembr. 1828 (2) (2013) 223–232, https://doi.org/10.1016/J.BBAMEM.2012.10.010.

[27] L. Migliolo, M.R. Felício, M.H. Cardoso, O.N. Silva, M.A.E. Xavier, D.O. Nolasco, A. S. De Oliveira, I. Roca-Subira, J. Vila Estape, L.D. Teixeira, S.M. Freitas, A.J. Otero-Gonzalez, S. Gonçalves, N.C. Santos, O.L. Franco, Structural and Functional Evaluation of the Palindromic Alanine-Rich Antimicrobial Peptide Pa-MAP2, *Biochim. Biophys. Acta (BBA)* – Biomembr. 1858 (7) (2016) 1488–1498, https://doi.org/10.1016/J.BBAMEM.2016.04.003.

[28] H. Nikaido, Molecular Basis of Bacterial Outer Membrane Permeability Revisited, Microbiol. Mol. Biol. Rev. 67 (4) (2003) 593–656, https://doi.org/10.1128/mmbr.67.4.593-656.2003.

[29] H. Nikaido, M. Vaara, Molecular Basis of Bacterial Outer Membrane Permeability, Microbiol. Rev. 49 (1) (1985) 1–32, https://doi.org/10.1128/mmbr.49.1.1-32.1985.

[30] R. Shukla, F. Lavore, S. Maity, M.G.N. Derks, C.R. Jones, B.J.A. Vermeulen, A. Melcrová, M.A. Morris, L.M. Becker, X. Wang, R. Kumar, J. Medeiros-Silva, R.A. M. van Beekveld, A.M.J.J. Bonvin, J.H. Lorent, M. Lelli, J.S. Nowick, H. D. MacGillavry, A.J. Peoples, A.L. Spoering, L.L. Ling, D.E. Hughes, W.H. Roos, E. Breukink, K. Lewis, M. Weingarth, Teixobactin Kills Bacteria by a Two-Pronged Attack on the Cell Envelope, Nature 608 (7922) (2022) 390–396, https://doi.org/10.1038/s41586-022-05019-y.

[31] L.M. Yin, M.A. Edwards, J. Li, C.M. Yip, C.M. Deber, Roles of Hydrophobicity and Charge Distribution of Cationic Antimicrobial Peptides in Peptide-Membrane Interactions, J. Biol. Chem. 287 (10) (2012) 7738–7745, https://doi.org/10.1074/JBC.M111.303602.

[32] S. Manioglu, S.M. Modaresi, N. Ritzmann, J. Thoma, S.A. Overall, A. Harms, G. Upert, A. Luther, A.B. Barnes, D. Obrecht, D.J. Müller, S. Hiller, Antibiotic Polymyxin Arranges Lipopolysaccharide into Crystalline Structures to Solidify the Bacterial Membrane, Nature Commun. 13 (1) (2022) 1–12, https://doi.org/10.1038/s41467-022-33838-0.

[33] H. Gong, M.A. Sani, X. Hu, K. Fa, J.W. Hart, M. Liao, P. Hollowell, J. Carter, L. A. Clifton, M. Campana, P. Li, S.M. King, J.R.P. Webster, A. Maestro, S. Zhu, F. Separovic, T.A. Waigh, H. Xu, A.J. McBain, J.R. Lu, How Do Self-Assembling Antimicrobial Lipopeptides Kill Bacteria? ACS Appl. Mater. Interfaces 12 (50) (2020) 55675–55687, https://doi.org/10.1021/ACSAMI.0C17222.

[34] L.A. Clifton, F. Ciesielski, M.W.A. Skoda, N. Paracini, S.A. Holt, J.H. Lakey, The Effect of Lipopolysaccharide Core Oligosaccharide Size on the Electrostatic Binding of Antimicrobial Proteins to Models of the Gram Negative Bacterial Outer Membrane, Langmuir 32 (14) (2016) 3485–3494, https://doi.org/10.1021/ACS.LANGMUIR.6B00240.

[35] J. Flynn, A. Ryan, S.P. Hudson, Pre-Formulation and Delivery Strategies for the Development of Bacteriocins as next Generation Antibiotics, Eur. J. Pharm. Biopharm. 165 (2021) 149–163, https://doi.org/10.1016/J.EJPB.2021.05.015.

[36] E.H. Mood, L. Goltermann, C. Brolin, L.M. Cavaco, A.J. Nejad, N. Yavari, N. Frederiksen, H. Franzyk, P.E. Nielsen, Antibiotic Potentiation in Multidrug-Resistant Gram-Negative Pathogenic Bacteria by a Synthetic Peptidomimetic, ACS Infect. Dis. 7 (8) (2021) 2152–2163, https://doi.org/10.1021/ACSINFECDIS.1C00147.

[37] S. Bhattacharjya, P.N. Domadia, A. Bhunia, S. Malladi, S.A. David, High-Resolution Solution Structure of a Designed Peptide Bound to Lipopolysaccharide: Transferred Nuclear Overhauser Effects, Micelle Selectivity, and Anti-Endotoxic Activity, Biochemistry 46 (20) (2007) 5864–5874, https://doi.org/10.1021/BI6025159.

[38] L. Poirel, A. Jayol, P. Nordmanna, Polymyxins: Antibacterial Activity, Susceptibility Testing, and Resistance Mechanisms Encoded by Plasmids or Chromosomes, Clin. Microbiol. Rev. 30 (2) (2017) 557–596, https://doi.org/10.1128/CMR.00064-16.

[39] J.M. May, T.W. Owens, M.D. Mandler, B.W. Simpson, M.B. Lazarus, D.J. Sherman, R.M. Davis, S. Okuda, W. Massefski, N. Ruiz, D. Kahne, The Antibiotic Novobiocin Binds and Activates the ATPase That Powers Lipopolysaccharide Transport, J. Am. Chem. Soc. 139 (48) (2017) 17221–17224, https://doi.org/10.1021/jacs.7b07736.

[40] M.D. Mandler, V. Baidin, J. Lee, K.S. Pahil, T.W. Owens, D. Kahne, Novobiocin Enhances Polymyxin Activity by Stimulating Lipopolysaccharide Transport, J. Am. Chem. Soc. 140 (22) (2018) 6749–6753, https://doi.org/10.1021/JACS.8B02283.

[41] K. Bush, M.G.P. Page, What We May Expect from Novel Antibacterial Agents in the Pipeline with Respect to Resistance and Pharmacodynamic Principles,

J. Pharmacokinet. Pharmacodyn. 44 (2) (2017) 113–132, https://doi.org/10.1007/s10928-017-9506-4.
[42] A.S. Amiss, S.T. Henriques, N. Lawrence, Antimicrobial Peptides Provide Wider Coverage for Targeting Drug-Resistant Bacterial Pathogens, Pept. Sci. (2021), https://doi.org/10.1002/pep2.24246.
[43] M.F. Richter, P.J. Hergenrother, The Challenge of Converting Gram-Positive-Only Compounds into Broad-Spectrum Antibiotics, Ann. N Y Acad. Sci. 1435 (1) (2019) 18–38, https://doi.org/10.1111/nyas.13598.
[44] S. Herbert, P. Barry, R.P. Novick, Subinhibitory Clindamycin Differentially Inhibits Transcription of Exoprotein Genes in Staphylococcus Aureus, Infect. Immun. 69 (5) (2001) 2996–3003, https://doi.org/10.1128/IAI.69.5.2996-3003.2001.
[45] R. Gleckman, N. Blagg, D.W. Joubert, Trimethoprim: Mechanisms of Action, Antimicrobial Activity, Bacterial Resistance, Pharmacokinetics, Adverse Reactions, and Therapeutic Indications, Pharmacotherapy 1 (1) (1981) 14–19, https://doi.org/10.1002/J.1875-9114.1981.TB03548.X.
[46] A. Antonoplis, X. Zang, T. Wegner, P.A. Wender, L. Cegelski, Vancomycin-Arginine Conjugate Inhibits Growth of Carbapenem-Resistant E. Coli and Targets Cell-Wall Synthesis, ACS Chem. Biol. 14 (9) (2019) 2065–2070, https://doi.org/10.1021/acschembio.9b00565.
[47] A. Sabnis, K.L.H. Hagart, A. Klöckner, M. Becce, L.E. Evans, R.C.D. Furniss, D.A. I. Mavridou, R. Murphy, M.M. Stevens, J.C. Davies, G.J. Larrouy-Maumus, T. B. Clarke, A.M. Edwards, Colistin Kills Bacteria by Targeting Lipopolysaccharide in the Cytoplasmic Membrane, Elife (2021) 10, https://doi.org/10.7554/ELIFE.65836.
[48] C.K. Cote, I.I. Blanco, M. Hunter, J.L. Shoe, C.P. Klimko, R.G. Panchal, S.L. Welkos, Combinations of Early Generation Antibiotics and Antimicrobial Peptides Are Effective against a Broad Spectrum of Bacterial Biothreat Agents, Microb. Pathog. 142 (2020) 104050, https://doi.org/10.1016/J.MICPATH.2020.104050.
[49] C.F. Sousa, J.T.S. Coimbra, R. Richter, J.H. Morais-Cabral, M.J. Ramos, C.M. Lehr, P.A. Fernandes, P. Gameiro, Exploring the Permeation of Fluoroquinolone Metalloantibiotics across Outer Membrane Porins by Combining Molecular Dynamics Simulations and a Porin-Mimetic in Vitro Model, Biochim. Biophys. Acta Biomembr. 1864 (3) (2022) 183838, https://doi.org/10.1016/J.BBAMEM.2021.183838.
[50] U. Choi, C.R. Lee, Distinct Roles of Outer Membrane Porins in Antibiotic Resistance and Membrane Integrity in Escherichia Coli, Front. Microbiol. 10 (APR) (2019) 953, https://doi.org/10.3389/FMICB.2019.00953.
[51] H. Cetuk, A. Anishkin, A.J. Scott, S.B. Rempe, R.K. Ernst, S. Sukharev, Partitioning of Seven Different Classes of Antibiotics into LPS Monolayers Supports Three Different Permeation Mechanisms through the Outer Bacterial Membrane, Langmuir 37 (4) (2021) 1372–1385, https://doi.org/10.1021/acs.langmuir.0c02652.
[52] C. Thornsberry, P.J. Burton, Y.C. Yee, J.L. Watts, R.J. Yancey, The Activity of a Combination of Penicillin and Novobiocin against Bovine Mastitis Pathogens: Development of a Disk Diffusion Test, J Dairy Sci 80 (2) (1997) 413–421, https://doi.org/10.3168/JDS.S0022-0302(97)75952-6.

Supplementary Information for:

Arg-biodynamers as antibiotic potentiators through interacting with Gram-negative outer membrane lipopolysaccharides

Authors:

Mohamed A. M. Kamal [1 2], Justine Bassil [1 2], Brigitta Loretz [1], Anna K. H. Hirsch [1 2], Sangeun Lee [1 2], Claus-Michael Lehr [1 2*]*

1. Helmholtz Institute for Pharmaceutical Research Saarland (HIPS), Helmholtz Centre for Infection Research (HZI), Saarland University, 66123 Saarbrücken, Germany

2. Saarland University, Department of Pharmacy, 66123 Saarbrücken, Germany

Methods:

Molecular weight estimation for Arg-biodynamers via SDS PAGE

1mm thick 10% bioacrylamide gel was prepared and loaded with 10 µL sample volume + 2,5 µL gel loading dye after boiling the sample for 10 min to denature them. 5 µL of PageRuler ™ Prestained Protein Ladder was loaded in the next lane. The gel was run at 70V until the marker strats dviding and then the voltage was increased to 120V until complete separation took place. The gel was then stain-free visualized via UV and the ladder images were merged.

Bacteria permeabilization studies with Propidium Iodide (PI)

Treatment solutions (0.1% TritonX-100 or Arg-biodynamers or blank) were prepared in 1mL of Mueller Hinton Broth and then inoculated with a final count of 10^4 CFU/mL in 1.5 mL LoBind tubes. The tubes were incubated on a shaking heat plate at 37°C at 180 rpm for 24h. After 24h, 1.5 µL of 20 mM PI solution were added to make the PI final concentration 30 µM for 15 min. Afterwards, the tubes were centrifuged at 5000 g for 5 min to pellet the bacteria and subsequently washed twice with sterile PBS. The cells were then suspended in 300 µL PBS and lysed using Branson UltrasonicsTM S-250D probe ultrasonicator (Connecticut, USA) at 20% power for 10 seconds twice with rest time in between for cooling. Finally, the DNA-bound PI florescence was determined by taking 200 µL of the final solution into a 96-well plate and measured (ex.: 535 nm, em.: 617 nm using Spark® Cyto (Männedorf, Switzerland). Three replicates were performed. One-way ANOVA was performed to calculate the p values using GraphPad Prism 9.

Peptide and Arg-biodynamers backbones absorbance scans

100 µg/mL of Cys-TAT (CGRKKRRQRRR) and 100 µg/mL of Arg-biodynamers were dissolved in 50mM phosphate buffer pH 7. 100 µl of the solutions were then added to a quartz 96-well plate. An absorbance scan was conducted using Spark® Cyto (Männedorf, Switzerland).

Results:

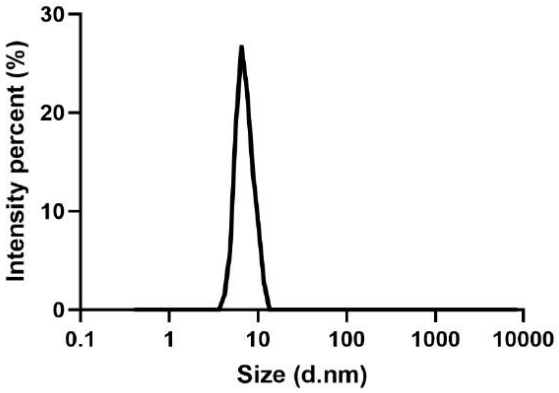

Figure S1: Example plot of the Size of Arg-Biodynamer using dynamic light scattering as a quality control example showing diameter of around 8 nm and PDI=0.22. The plot was averaged from 3 measurements.

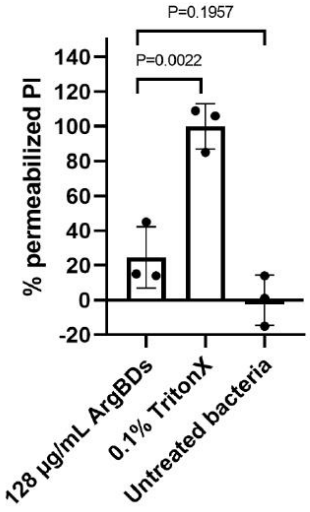

Figure S2: Amount of permeabilized PI by 128 µg/mL Arg-biodynamers into *E. coli* comparing to 0.1% TritonX as a positive control (100% permeabilization) and non-treated bacteria (0% Permeabilization). Three replicates were conducted. Datapoints represent the average and the error bars represent standard deviations. Arg-biodynamers; ArgBD

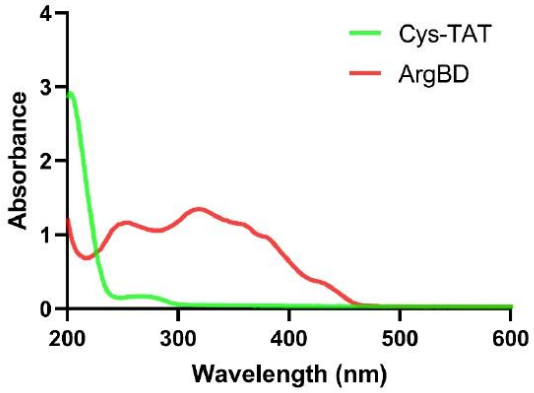

Figure S3: Absorbance scan showing the shift of the backbone absorbance from 202 nm (example peptide) to 254 nm (Arg-biodynamers). Arg-biodynamers; ArgBD

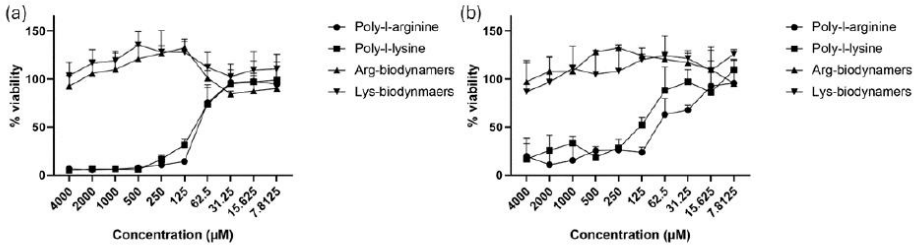

Figure S4: MTT assay for different treatments in (a) stimulated THP-1, and (b) RAW264.7 cells. Three replicates were conducted. Datapoints represent the average and the error bars represent the standard deviation.

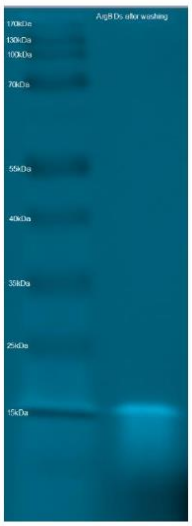

Figure S5: SDS PAGE for Arg-biodynamers (light blue) after washing showing the polymer size around 15kDa by comparison to a protein ladder (black). Arg-biodynamers; ArgBD

Strain	Colistin MIC (ng/mL)	Colistin MIC (+256 µg/mL ArgBD)	Fold improvement	LPS structure
E. coli Dh5α (Normal LPS)	500	125	4	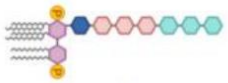
E. coli ClearColi (Mutated LPS)	31.25	1.95	16	
P. aeruginosa PA01 (Complex LPS)	1000	500	2	
P. aeruginosa PA14 (Complex LPS)	500	62.5	8	

Table S1: Treatment of *E. coli* with either wild LPS, or mutated LPS, PA01, and PA14 with colistin and colistin+Arg-biodynamers. Arg-biodynamers; ArgBD

Strain	ArgBD MIC (mg/mL)	Added LPS (μg/mL)	Bacterial growth medium	Fold activity change (x fold)
E. coli DH5α (normal LPS)	2	0	Meuller Hinton	
	4	5	Meuller Hinton	2
	4	20	Meuller Hinton	2
	8	50	Meuller Hinton	4
	0.032	0	M9	1/64
	0.032	0	RPMI + Glucose	1/64

Table S2: LPS as decoy and growth media effects on the antimicrobial effectiveness of Arg-biodynamers. Arg-biodynamers; ArgBD

Chemical synthesis of biodynamers:

General Devices, chemicals and analytical methods

Reagents and dry solvents as THF, DMF were purchased at the highest commercial quality and used without further purifications, unless otherwise stated. For all reactions, which were performed under inert gas conditions, schlenk flasks were dried in high vacuum and flooded with nitrogen before use. Corresponding reagents were injected using a septum or via argon counter flow. Thin layer chromatography (TLC) carried out on 0.25 mm *E. Merck* silica plates (60F-254), using shortwave UV light as the visualizing agent. The products were purified by flash chromatography on silica gel columns (Macherey-Nagel 60, 0.04−0.063 mm). High resolution mass (HRMS) was determined by LC−MS/MS using the Thermo Scientific Q Exactive Focus Orbitrap LC−MS/MS system. The purity of the final products was determined by Liquid chromatography-mass spectrometry (LC-MS), a Dionex UltiMate 3000 pump, autosampler, column compartment, detector, and ESI quadrupole MS from Thermo Fisher Scientific and are found to be >95%.

Proton (^{1}H) and carbon (^{13}C) nuclear magnetic resonance spectra were recorded on a *Bruker* Avance Neo 500 MHz spectrometer using deuterated solvents as an internal reference (Chloroform ($CDCl_3$): 7.26 ppm ^{1}H NMR, 77.2 ppm ^{13}C NMR; Dimethyl sulfoxide (DMSO–d_6): 2.50 ppm ^{1}H NMR, 39.5 ppm ^{13}C NMR). The chemical shifts were recorded in δ (ppm) and the coupling constants in Hertz (Hz). The following abbreviations were used to explain NMR peak multiplicities: s = singlet, d = doublet, t = triplet, q = quartet, p = pentet, m = multiplet, br = broad.

Synthetic Part

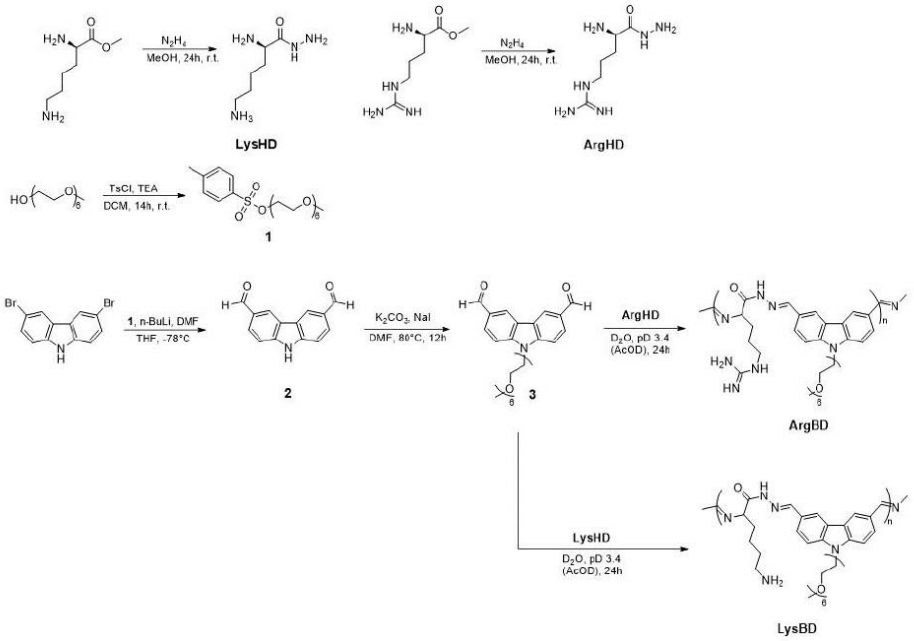

Figure S6: General scheme showing the synthesis of Arg-biodynamers and lysine biodynamers.

2,5,8,11,14,17-hexaoxanonadecan-19-yl 4-methylbenzenesulfonate (1)

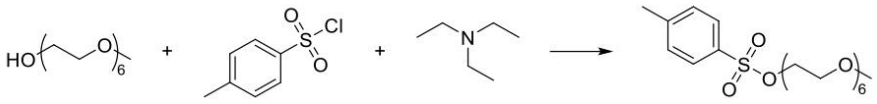

The synthesis of compound 1 was performed according to literature
A solution of hexaethyleneglycolmonomethylether (2.5 g, 8.44 mmol) and triethylamine (1.35 mL, 9.7 mmol) in dry CH_2Cl_2 (10 mL) was set stirring in an ice bath, and a solution of tosyl chloride (1.69 g, 8.86 mmol) in dry CH_2Cl_2 (20 mL) was added drop-wise over a period of 20 min. The ice bath was then removed, and the reaction was stirred at room temperature for 14 h. After this time, water (50 mL) was added and the reaction was quenched with 1M HCl (20 mL) solution. The resulting mixture was extracted with CH_2Cl_2 (100 mL). The organic phase was washed with brine (50 mL), dried over Na_2SO_4, filtered and concentrated to a yellow oil, which was subject to column chromatography (SiO_2, CH_2Cl_2: MeOH 95:5), yielding as a product (3 g, 79%) a colorless oil. All recorded spectra were similar with those reported in literature.

^{1}H NMR (500 MHz, $CDCl_3$; δ, ppm): 7.78 (d, J = 8.2 Hz, 2H), 7.33 (d, J = 8.4 Hz, 2H), 4.14 (t, J = 9.7 Hz, 2H), 3.68 – 3.53 (m, 22H), 3.36 (s, 3H), 2.43 (s, 3H).

^{13}C NMR (126 MHz, $CDCl_3$; δ, ppm): 144.89, 133.11, 129.92, 128.08, 72.03 - 68.77, 59.13, 21.74.

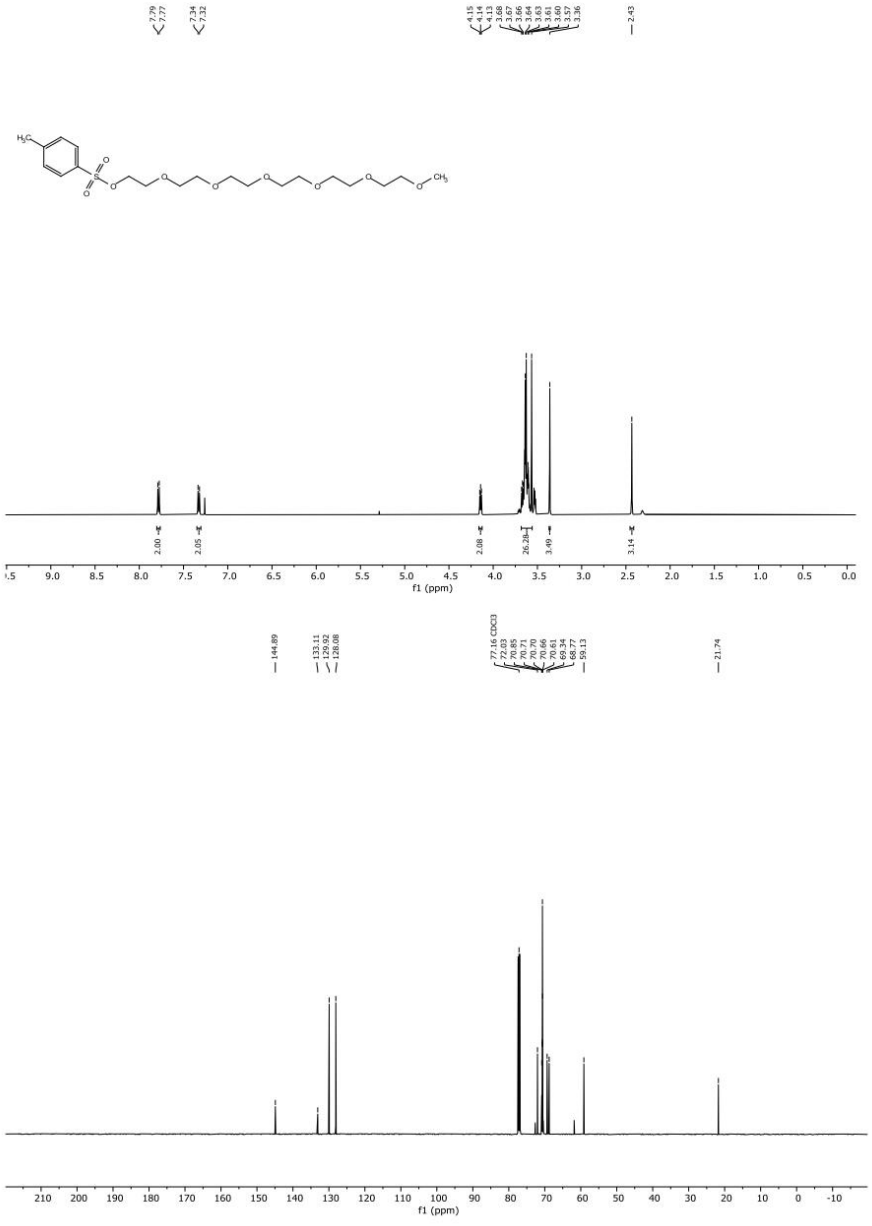

Figure S7: Proton NMR (top) and carbon NMR spectra of compound **(1)** in $CDCl_3$.

9H-carbazole-3,6-dicarbaldehyde (2)

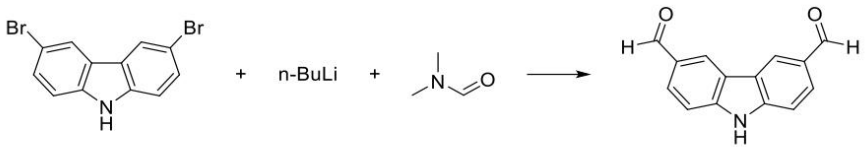

The general procedure for the synthesis of 2 was followed according to literature. 3,6-Dibromocarbazole (3 g, 9.29 mmol) was dissolved in anhydrous THF (60 mL) to give a pale-yellow solution, which was set stirring in a dry ice/acetone bath. An amount of 40 mL of BuLi solution (1.6 mol L^{-1} in hexane) was added over a period of 20 min, causing the reaction contents to darken in colour significantly. The cooling bath was removed for 1 h and then replaced. After 10 min, anhydrous DMF (7.5 mL, 9.7 mmol) was added over 10 min, immediately causing the precipitation of a yellow solid. The cooling bath was removed, and the reaction was stirred for 90 min at r.t. After this period, 1M HCl solution (50 mL) was added, and the reaction was suction filtered. The yellow solid was collected, and no further purification is needed. The filtrate was extracted with EtOAc (5 × 50 mL), and the combined organic phases were washed with brine (50 mL), dried over $MgSO_4$ and concentrated under vacuum to a yellow solid. The crude product, which exhibited deep blue fluorescence under 254 nm irradiation when spotted on a SiO_2 thin-layer chromatography plate, was purified by column chromatography (SiO2, CH_2Cl_2:MeOH (95:5)), yielding 1.5 g (75%) of a yellow solid. The spectral analysis matched those described in the literature (see below).

^{1}H NMR (500 MHz, $(CD_3)_2SO$): δ= 10.09 (s, 2H), 8.89 (s, 2H), 8.02 (d, *J* = 8.4 Hz, 2H), 7.73 (d, *J* = 8.4 Hz, 2H)

^{13}C NMR (500 MHz, $(CD_3)_2SO$)): δ= 191.52 (14,15), 143.74 (1,4), 128.71 (8,11), 126.71 (2,3), 124.28 (9,10), 122.20 (7,12), 111.73 (6,13).

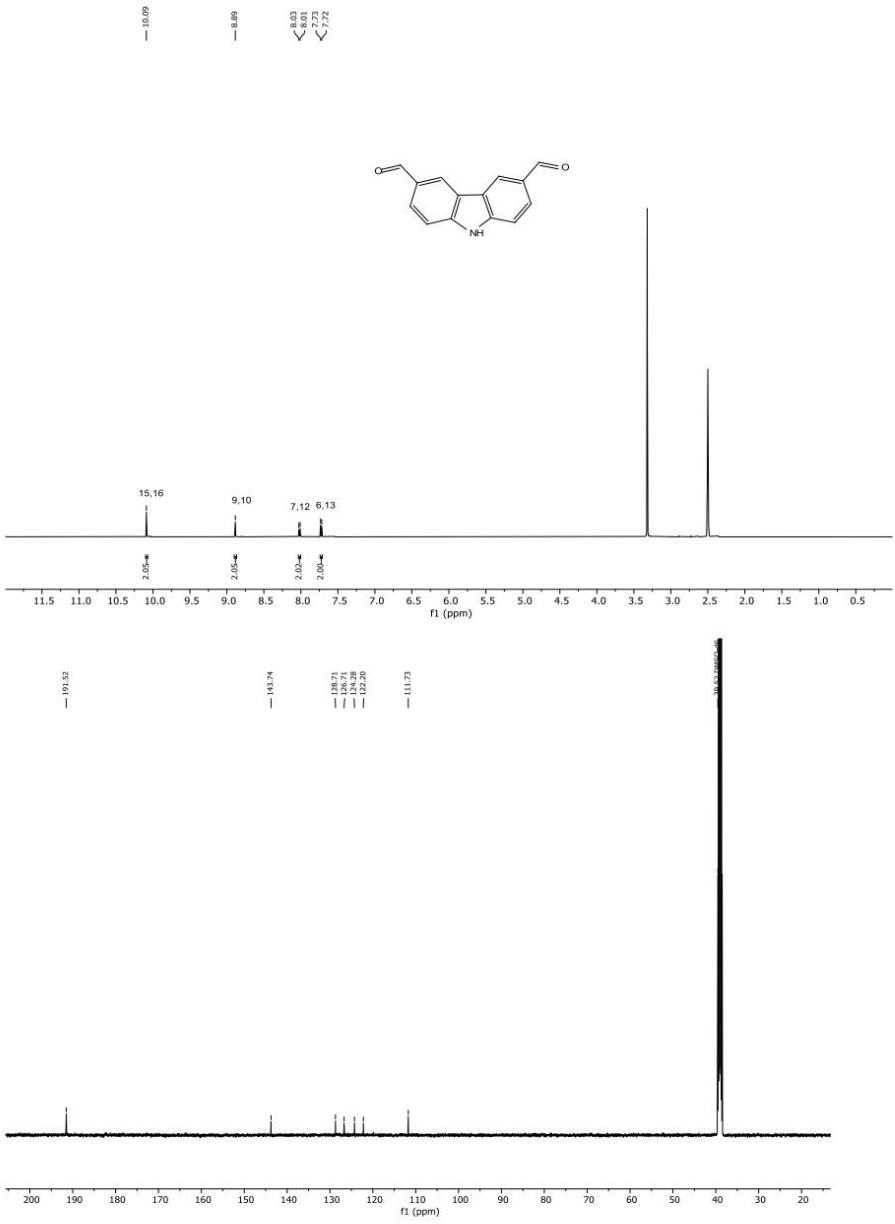

Figure S8: Proton NMR (top) and carbon NMR (bottom) spectra of compound **(2)** in $(CD_3)_2SO$.

9-(2,5,8,11,14,17-hexaoxanonadecan-19-yl)-9H-carbazole-3,6-dicarbaldehyde (3)

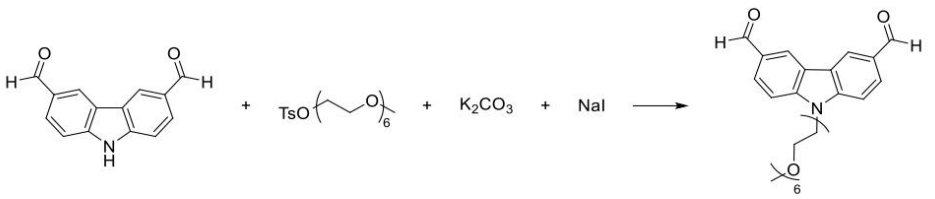

Compound 3 was prepared according to the specified literature.
To a solution of 9H-carbazole-3,6-dicarbaldehyde **(2)** (1 g, 4.48 mmol, 1 equiv.) and 2,5,8,11,14,17-hexaoxanonadecan-19-yl 4-methylbenzenesulfonate **(1)** (2 g, 4.48 mmol, 1 equiv.) in DMF (45 mL) were added K_2CO_3 (2 g, 14.56 mmol, 3.25 equiv.) and NaI (*ca* 10 mg, 0.01 equiv.). The reaction was stirred at 80◦C for 12 h. After cooling to cool to room temperature, water was added and the reaction mixture was extracted CH_2Cl_2 (100 mL) and was washed with brine (50 mL). The organic phase was dried over Na_2SO_4, and concentrated under vacuum. The product was isolated by flash Chromatography, on a reversed-phase silica column (Macherey-Nagel 60, 0.04-0.063 mm), using H_2O: ACN + 0.05% FA (gradient flow 5% to 100% ACN for 30 min) to give the product as a pale yellow oil (1.6 g, 71%) which occasionally solidified upon standing. ^{1}H NMR and ^{13}C NMR spectra are in agreement with those previously reported.

^{1}H NMR (500 MHz, $CDCl_3$): δ= 10.14 (s, 2H), 8.67 (s, 2H), 8.08 (d, J = 8.6 Hz, 2H), 7.64 (d, J = 8.6 Hz, 2H), 4.60 (t, J = 5.8 Hz, 2H), 3.95 (t, J = 5.8 Hz, 2H), 3.67–3.47 (m, 20H), 3.36 (s, 3H).

^{13}C NMR (126 MHz, $CDCl_3$): δ= 191.55, 145.16, 128.84, 127.82, 124.15, 123.25 110.31, 71.93, 71.01, 70.64-70.51, 69.35, 59.04, 44.10.

HRMS (ESI, m/z): calc for C27H35NNaO8: 524.2260; found: 524.2252

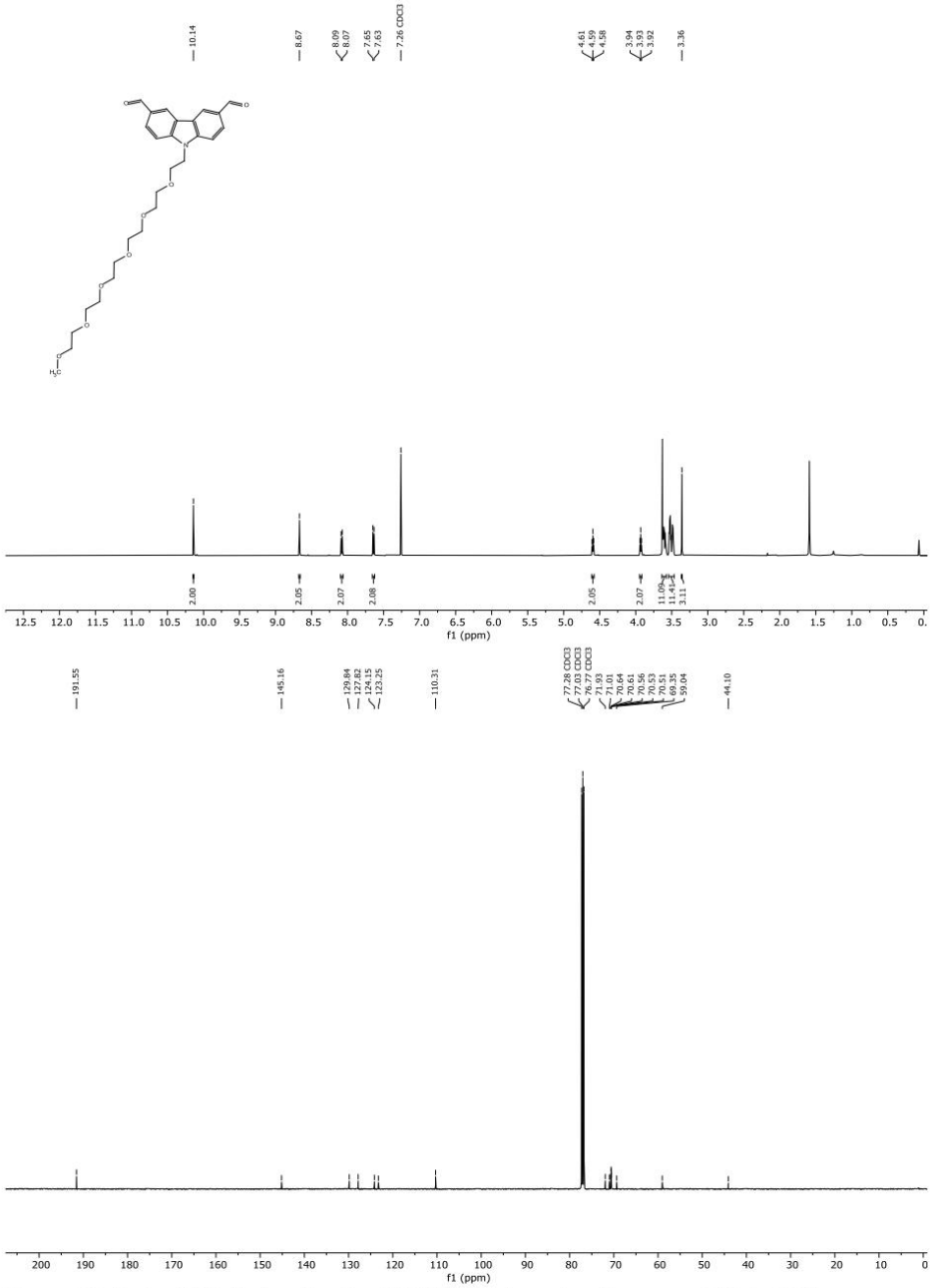

Figure S9: Proton NMR (top) and carbon NMR (bottom) spectra of compound **(3)** in $CDCl_3$.

Lysine Hydrazide

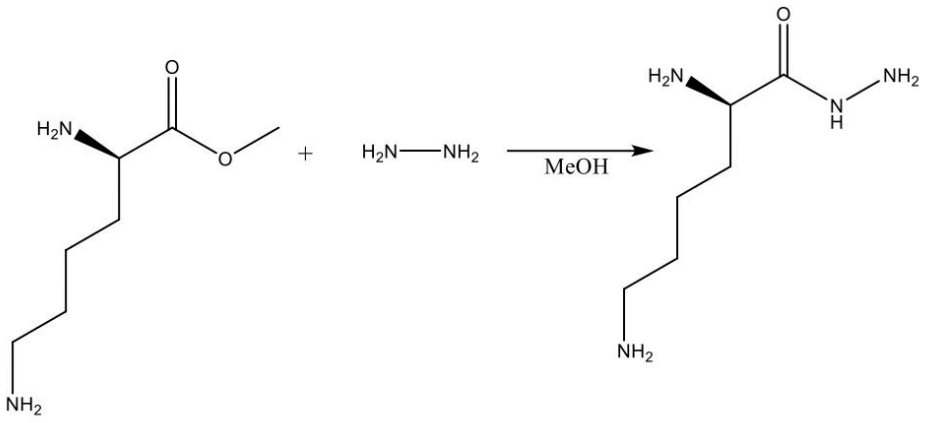

To a solution of methyl *D*-lysinate (100 mg, 624.15 µmol) in anhydrous MeOH (8 mL) was added hydrazine hydrate (2 mL, 8 folds) and the reaction was stirred at room temperature for 24 h. After the completion of the synthesis, MeOH was removed under vacuum (60°C, 20 mPa). Finally, 2 ml distilled water is added to the product and freeze dried overnight to remove excess hydrazine hydrate. 80 mg of product (80%) was obtained as a transparent oil. Care was taken to avoid exposure to moisture.

^{1}H NMR (500 MHz, (D_2O): δ= 3.41 (t, J = 6.6 Hz, 1H), 2.94 – 2.87 (m, 2H), 1.70- 1.60 (m, 4H), 1.36 – 1.21 (m, 2H).

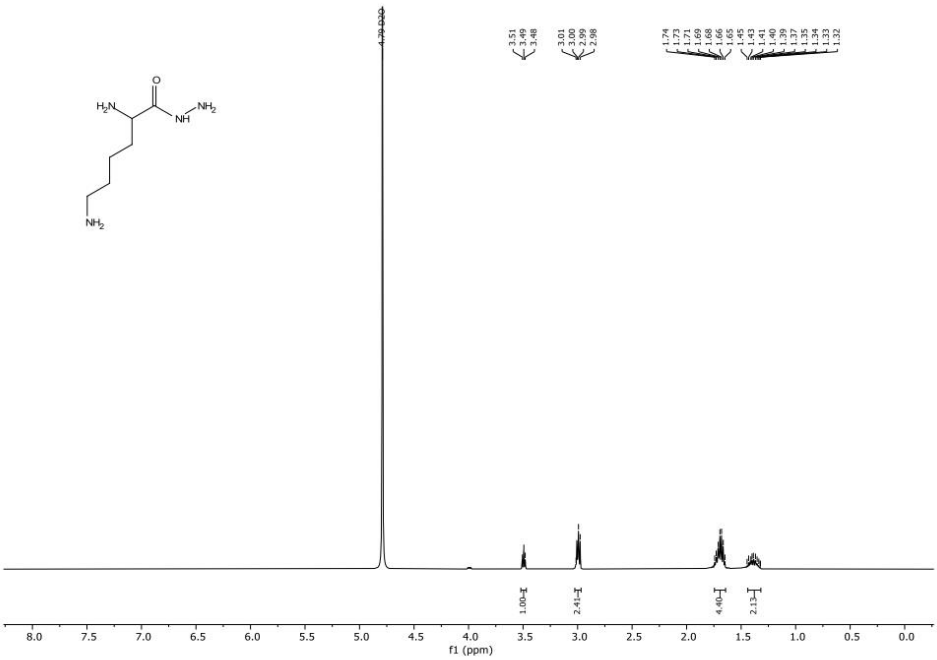

Figure S10: Proton NMR spectra of compound lysine Hydrazide in D_2O.

Arginine Hydrazide

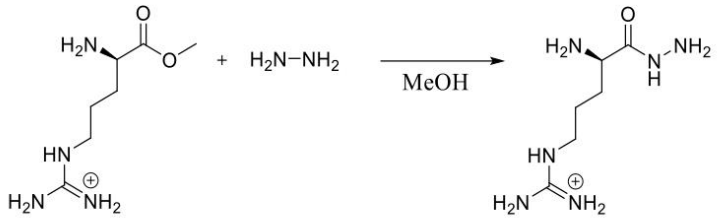

To a solution of methyl *D*-argininate (100 mg, 528.43 µmol) in anhydrous MeOH (8 mL) was added hydrazine hydrate (5 mL) and the reaction was stirred at room temperature for 24 h. After the completion of the synthesis, MeOH was removed under vacuum (60°C, 20 mPa). Finally, 2 ml distilled water is added to the product and freeze dried overnight to remove excess hydrazine hydrate. 80 mg of product (80%) was obtained as a transparent oil. Care was taken to avoid exposure to moisture.

^{1}H NMR (500 MHz, (D_2O): δ= 3.38 (t, J = 6.7 Hz, 1H), 3.20 (t, J = 6.7 Hz, 2H), 1.71 – 1.51 (m, 4H).

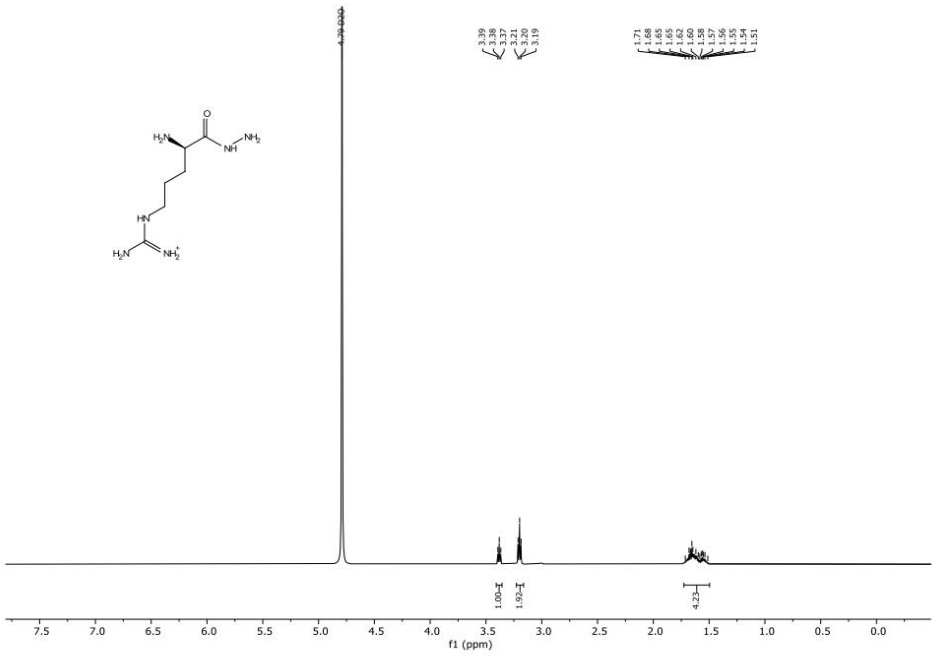

Figure S11: Proton NMR spectra of compound Arginine Hydrazide in D_2O.

Biodynamers spectra:

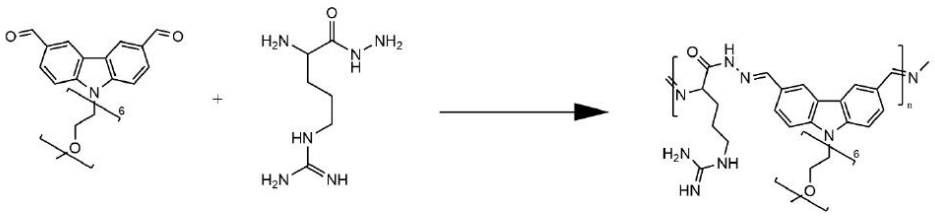

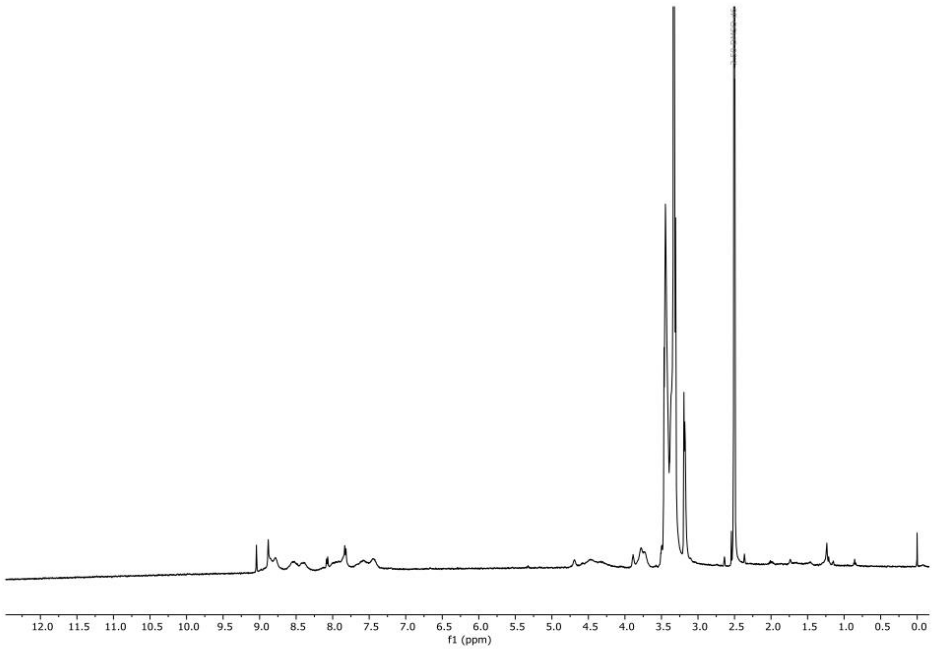

Figure S12: Proton NMR spectra of Arg-biodynamers.

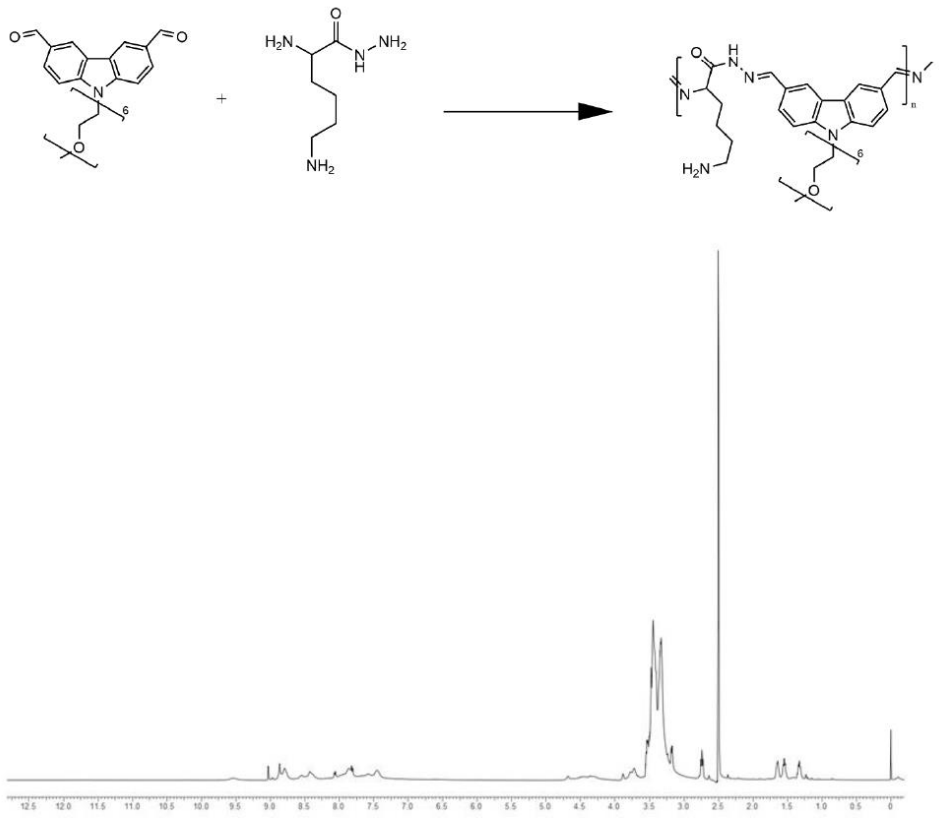

Figure S13: Proton NMR spectra of lysine biodynamers biodynamer.

9.3. Second Research Paper

"A Multivalent TAT-Arginine-Biodynamer Conjugate to Overcome the Bacterial Cell Envelope barrier by Bacteria-Specific Membrane Interactions"

Mohamed A. M. Kamal, Justine Bassil, Bart-Jan Niebuur, Tobias Kraus, Jennifer Herrmann, Marcus Koch, Anna K. H. Hirsch, Brigitta Loretz, Sangeun Lee, Claus-Michael Lehr

Manuscript to be submitted to Advanced Functional Materials journal

Contributions: M.A.M.K. conceived the project, designed, performed and interpreted all experiments (unless otherwise indicated), analyzed the data, and wrote the first draft of the manuscript. J.B. performed the chemical synthesis of the monomers of the polymer. B.J.N. and T.L. performed the SAXS experiments and interpreted the relevant data. J.H. performed MIC studies with *A. baumannii* and *S. aureus* strains. M.K. performed the TEM imaging. M.A.M.K, A.K.H.H., B.L., B.L., S.L., and C.M.L. helped interpret the results, secured funding, supervised the research, and provided critical revisions of the manuscript.

A Multivalent TAT–Arginine-Biodynamer Conjugate to Overcome the Bacterial Cell Envelope Barrier by Bacteria-Specific Membrane Interactions

Mohamed A. M. Kamal[1,2,3], Justine Bassil[1,2,3], Bart-Jan Niebuur[4], Tobias Kraus[4,5], Jennifer Herrmann[1,3,6], Marcus Koch[4], Anna K. H. Hirsch[1,2,3], Brigitta Loretz[1,3], Sangeun Lee[1,2,3 *], Claus-Michael Lehr[1,2,3 *]

1. Helmholtz Institute for Pharmaceutical Research Saarland (HIPS), Helmholtz Centre for Infection Research (HZI), Saarland University, 66123 Saarbrücken, Germany
2. Saarland University, Department of Pharmacy, 66123 Saarbrücken, Germany
3. PharmaScienceHub, Saarland University, Campus A2 3, 66123 Saarbrücken
4. Leibniz Institute for New Materials, Campus D2 2, 66123 Saarbrücken, Germany
5. Saarland University, Colloid and Interface Chemistry, 66123 Saarbrücken, Germany
6. German Center for Infection Research (DZIF), partner site Hannover - Braunschweig, 38124 Braunschweig, Germany

*Corresponding author

Emails: mohamedashrafmostafa.kamal@helmholtz-hips.de; justine.bassil@helmholtz-hips.de; bart-Jan.Niebuur@leibniz-inm.de; tobias.kraus@leibniz-inm.de; jennifer.herrmann@helmholtz-hips.de; marcus.koch@htwsaar.de; anna.hirsch@helmholtz-hips.de; brigitta.loretz@helmholtz-hips.de; sangeun.lee@uni-saarland.de; claus-michael.lehr@helmholtz-hips.de

Keywords: Cell-penetrating peptides; Antimicrobial peptides; antibiotics; antibacterial; macromolecules; biologics

Abstract:

Antimicrobial resistance is a global crisis driven by the scarce antibiotics pipeline of new antibiotics, especially due to the intrinsic resistance stemming from the membrane barrier, necessitating innovative materials for improved therapies. In this study, TAT–ArgBD, a conjugate of the cell-penetrating TAT peptide and arginine biodynamer (ArgBD), serves as multivalent macromolecular antibiotic and synergist. TAT–ArgBD rapidly kills 99.9% of *Pseudomonas aeruginosa* at 32 µg/mL within one hour, outperforming colistin, and shows minimum inhibitory concentrations (MICs) of 2–8 µg/mL against *Acinetobacter baumannii* and *Staphylococcus aureus*. More interestingly, it potentiates antibiotics such as novobiocin, chloramphenicol, and imipenem, leading to lowered MICs up to 256 folds. Notably, novobiocin, typically active only against Gram-positive bacteria, demonstrated potential to target Gram-negative bacteria when combined with TAT–ArgBD.

Mechanistic studies suggest TAT–ArgBD antimicrobial and synergistic actions stem from targeting POPG and cardiolipin, inducing bacterial membrane pore formation and adopting an α-helical structure with the bacterial lipids. With proven safety profile and a membranolytic index >64 against bacteria and low mammalian cell toxicity at effective bactericidal concentrations, TAT–ArgBD potential to enhance antibiotic

efficacy, as well as function as a stand-alone treatment, underscores their promise as a lead concept.

Introduction:

Antimicrobial resistance (AMR) has attracted more and more attention fueled by alarming predictions in the next decades, especially related to the emergence of multidrug-resistant (MDR) Enterobacterales, Carbapenem-resistant *Acinetobacter baumannii,* and Carbapenem-resistant *Pseudomonas aeruginosa*. [1], [2], [3] Several mechanisms contribute to the development of such MDR, but decreased antibiotic accumulation, either through reduced influx or increased efflux, is widely recognized as a universal resistance mechanism across various antibiotic classes.[4] Interestingly, membrane-acting antibiotics, such as polymyxins, does not have uptake into bacteria as a prerequisite for activity, but are a last resort in clinical guidelines due to resistance and safety concerns. [5], [6] Another factor which makes addressing the MDR difficult is that most novel antibiotics are derivatives of existing antibiotic structures, with limited efforts directed at developing antibiotics based on new chemical class. According to the World Health Organization (WHO), scarce antibiotic candidates with novel chemical structures are in clinical trials for systemic administration against Gram-negative bacteria, predominantly in phase I. Unfortunately, such candidates in a phase I clinical trial can have an expected success rate as low as just 7.9%. [7], [8] Therefore, employing synergistic agents permeabilizing bacterial membranes, like antimicrobial peptides or cell-penetrating peptides (CPPs), for poorly-accumulating antibiotics, thereby achieving a synergistic effect against resistant bacteria, is raised as one strategy.

HIV-1 TAT is a specific domain from Tat viral protein and is an established CPP which has been proven to bind strongly to POPG, a major component of the bacterial lipid membranes, with a K_d value of 7.5 µM (around 11 µg/mL) and as little as 4600 molecules to saturate the binding to one POPG liposome. The mechanism, by which TAT can interact and translocate through the lipid layers, is initiated by attraction to the phosphate groups via ionic interactions. Then the lipids and phosphate groups begin to thin, causing the attraction of the TAT towards the distal-side phosphate groups and the formation of a temporary water channel to translocate the TAT peptide to the other side of the lipid bilayer.[9], [10] As such mechanism is transient and the water channels formed collapse, free monomeric TAT is not expected to be antibacterial or cytotoxic. In contrast to free CPP, multivalent polymer–CPP conjugates, which were prepared by conjugating CPPs like TAT on a polymer backbone like dextran, form water channels simultaneously in addition to the backbone momentum. Multimeric TAT constructs were established before in literature and even reached clinical trials, which hints for potential applicability and safety for *in vivo* and human applications.[11]

Polymer-peptide conjugates can lead to some damage to membranes, especially bacterial membranes, synergistically enhancing the activity for poorly penetrating antibiotics, such as WD40, which was able to enhance clindamycin by 4096 folds.[12], [13], [14] Therefore, various types of polymers, both linear and branched, natural and synthetic, have been explored as backbones for polymer–CPP conjugates.[15], [16], [17] In this context, dynamic polymers may allow for flexibility and freedom to interact with the bacterial membrane, compared to rigid polymers as a backbone. Arginine–biodynamer (ArgBD) were recently studied for their dynamicity, biocompatibility, and physiochemical properties in literature, which make them suitable for biological applications. [18], [19], [20], [21] Furthermore, in a previous study, we proved that ArgBD alone significantly potentiated the efficacy of colistin against Gram-negative strains. ArgBD targets the LPS of Gram-negative bacteria and changes their secondary structure in the LPS microenvironment, especially at the interface with the lipid A component. The structural changes allowed for better accessibility into the bacterial cell envelope and could potentiate the effect of antibiotics, including colistin. Colistin acts similarly to a surfactant on the bacterial cell envelope on the lipid bilayer.[22]

In this study, we introduce a TAT–ArgBD conjugate to target both the LPS, and membrane lipids via ArgBD and HIV-1 TAT, respectively. This could offer greater specificity because bacteria happen to be the only species which simultaneously have both LPS, and lipids attached together in its cell envelope. By conjugating TAT and ArgBD, we anticipated an enhanced targeting of cell membranes through TAT's rapid membrane interaction from multivalency, along with the potentiating effect derived from ArgBD. Therefore, we compared the antibacterial effects of TAT–ArgBD, as well as its synergistic effects with conventional antibiotics on several bacteria strains.

Materials and methods:

Materials:

L929 (ATCC-CCL-1) cells were obtained from LGC standards (Molsheim, France). RAW264.7 cell line was obtained from ECACC (Salisburg, UK). *Staphylococcus aureus* Newman was provided by Prof. Marcus Bischoff from Saarland university hospital. *Escherichia coli* MG1655 (DSM18039), *A. baumannii* (DSM-30008), *P. aeruginosa* PA01 (DSMZ 22644), and *P. aeruginosa* PA14 (DSMZ 19882) were obtained from DSMZ (Braunschweig, Germany). RPMI 1640 medium, FCS, and Trypsin-EDTA were obtained from Thermofisher scientific (Waltham, USA). PrestoBlue™ Cell Viability Reagent was obtained from Sigma-Aldrich (St. Louis, USA). LDH Cytotoxicity Detection Kit (11644793001) was obtained from Roche (Penzberg, Germany). Mueller Hinton broth (MHB) was obtained from Scharlau microbiology (Barcelona, Spain). M9 Minimal salts 5x Powder was obtained from SERVA (Heidelberg, Germany). TritonX-100 (CAS: 9036–19-5) was obtained from Sigma Aldrich (St. Louis, USA). Free TAT peptide HpG(Homopropargylglycine)-GRKKRRQRRR was ordered from Genscript (Rijswijk, Netherlands). Paraformaldehyde methanol-free solution (16 %) was obtained from Thermofisher scientific (Waltham, USA). Glutaraldehyde 25% in H_2O was obtained from Sigma Aldrich (St. Louis, USA). Hexamethyldisilazane (CAS: 999-97-3) was obtained from Sigma Aldrich (St. Louis, USA) Novobiocin (CAS: 1476–53-5), Imipenem monohydrate (CAS: 74431-23-5), Chloramphenicol (CAS: 56-75-7), Colistimethate Sodium (CAS: 8068-28-8), Colistin Sulphate (CAS: 1264-72-8), Ciprofloxacin (CAS: 86393-32-0), Meropenem (CAS: 119478-56-7), Ceftazidime (CAS: 78439-06-2) were obtained from Cayman chemical (Michigan, USA), Molekula group (München, Germany), Sigma Aldrich (St. Louis, USA), Cayman chemical (Michigan, USA), AdipoGen Life Sciences (Fuellinsdorf, Switzerland), TCI chemicals (Eschborn, Germany), Sigma Aldrich (St. Louis, USA), LKT Labs (Minnesota, USA) respectively. Lipopolysaccharides from E. coli O111:B4 (L4391) was obtained from Sigma Aldrich (St. Louis, USA), 1,1′,2,2′-tetra-(9Z-octadecenoyl) cardiolipin (sodium salt) Cardiolipin, 1-hexadecanoyl-2-(9Z-octadecenoyl)-sn-glycero-3-phosphoethanolamine (POPE), 1-hexadecanoyl-2-(9Z-octadecenoyl)- sn-glycero-3-phospho-(1′-rac-glycerol) (sodium salt) (POPG) were obtained from Avanti Polar Lipids Inc. (Alabaster, AL, USA), Oxoid™ Sheep blood (SR0051B) was obtained from Thermofisher scientific (Waltham, USA).

Peptide quantification and conjugation rate calculation:

To quantify the TAT content/purity, free TAT or TAT–ArgBD were dissolved in Deuterium oxide with maleic acid as an internal standard, then ^{1}HNMR was measured on a Bruker AV500 (500 MHz) spectrometer. The following equation was applied to calculate the concentration of the TAT:

$$P_{\boldsymbol{sample}} = \frac{I_{sample} * N_{Ref} * M_{sample} * C_{Ref} * P_{Ref}}{I_{Ref} * N_{sample} * M_{Ref} * C_{sample}}$$

Where P, I, N, M, C stand for purity, integral, number of protons, molecular weight, and w/v concentration. The purity of the maleic acid and the TAT were assumed to be 100% as the purity of the maleic acid ≥99% and TAT–ArgBD was later washed to eliminate any unreacted impurities. The maleic acid proton signal at ppm 6.3 was used as the reference, while a methylene signal on the lysine residue at ppm 2.8 was used as the sample signal. The measured concentrations of TAT in free TAT sample and TAT–ArgBD were then adapted in all of the following experiments to ensure that no bias shall arise due to different quantification methods.

To calculate the conjugation rate, two methods were applied. First, TAT–ArgBD, which has X mg worth of TAT content (quantified via qNMR), was measured on a sensitive

balance (referred to as gravimetry method). The following equation was then applied to determine the conjugation rate:

$$Conjugation\ rate\ \left(\frac{mol}{mol}\right) = 100\% * \frac{Mass(X)_{TAT} * Mwt_{TAT-ArgBD\ repeating\ unit}}{Mwt_{TAT} * Weighed\ Mass_{TAT-ArgBD}}$$

The measurement was repeated twice using two batches and standard deviation was calculated accordingly.

As a secondary method (referred to as qNMR method), the ratio of the integrations of the methelene on Arginine (ppm 3.1) and Lysine (ppm 2.8) as the ArgBD backbone has indeed one arginine residue. The following equation was employed to determine the conjugation rate:

$$Conjugation\ rate\ \left(\frac{mol}{mol}\right) = 100\% * \frac{I_{Arg\ in\ TAT-ArgBD} - I_{Arg\ in\ ArgBD}}{I_{Arg\ in\ TAT}}$$

Where I is the integral. The integral of Lysine methelene was assumed to be equal to 4.0 in the software, hence, the integral of the arginine could be calculated. The $I_{Arg\ in\ ArgBD}$ was assumed to be 2.0 as every repeating unit in the backbone can only have exactly one arginine residue (not more, not less). This procedure was performed twice using the TopSpin 4.4, hence, the standard deviation could be calculated.

Conjugation rate using absorbance was calculated as well. The quantification of ArgBD and was based on four principals:

1. The quantification had to be based on a wavelength away from the newly formed aromatic triazole absorbance and closer to the amide bond absorbance (200 nm) to avoid interference.
2. The signal to background ratios of of TAT–ArgBD, TAT, and ArgBD were high and most acceptable in each of them at 216 nm, so this wavelength was selected for the analysis
3. Since TAT–ArgBD was washed extensively, the signal at 216 nm is supposed to come from ArgBD and TAT, so the following equations were concluded:

Eq. (1)

$$Absorbance\ at\ 216\ nm_{TAT-ArgBD} = a * Absorbance\ at\ 216\ nm_{TAT} + b * Absorbance\ at\ 216_{ArgBD}$$

Eq. (2)

$$a + b = 100\%$$

Where a and b variables are the % of the TAT and ArgBD in the TAT–ArgBD respectively.

4. Spectra of samples and blanks were measured using a quartz plates and 16 µg/mL were used which has Absorbance ≤1.5 to have linear quantification in the range 200–1000 nm

First, all spectra were normalized as the concentration of TAT–ArgBD was assumed to be unknown before this analysis by applying the following equation on every point of the spectrum:

Eq. (3)

$$Normalized\ absorbance_x = \frac{Absorbance_x - Blank\ Absorbance_x}{\sum(Absorbance_{200-1000\ nm} - Blank\ Absorbance_{200-1000\ nm})/_n}$$

Where x is the wavelength at which the absorbance of the samples was considered

n is the number of wavelengths between 200–1000 nm, which is equal to 801.

The 216 nm normalized absorbance from equation (3) was then used with equations (1) and (2) to solve for variables a and b. This procedure was done twice, and standard deviation was calculated.

To validate the conjugation calculation using absorbance, 17 µg/mL of ArgBD physically mixed with 32 µg/mL of TAT absorbance was measured and compared to 49 µg/mL mass concentration of TAT–ArgBD (32 µg/mL of TAT) and graphed to check if it is similar and to what degree.

Lipid-Conjugate dose-binding assay:

Different molar lipid or LPS concentrations were diluted in a quartz plate in a 10 mM phosphate buffer at pH 7.4. Then an equal volume of 250 µg/mL of TAT–ArgBD was added to the wells to obtain different molar ratios. The fluorescence was measured after 2h using the 301 nm excitation and 372 nm emission as well as 350 nm as excitation and 520 as emission. The fluorophores calibration was observed to be linear until 31.25 and 62.5 µg/mL, respectively. The lipids were weighed, dissolved in chloroform/methanol 3:1 solution, dried, suspended in 10 mM phosphate buffer, and sonicated for a few minutes. LPS (molecular weight was assumed to be 10 kDa) was directly suspended in 10 mM phosphate buffer and sonicated. The binding was determined by the following equation:

$$\%Quenching = 100\% * \frac{Fl_{sample} - Fl_{lipid\ background}}{Fl_{TAT-ArgBD} - Fl_{Buffer}}$$

For all biological assays, the activity per TAT content in TAT–ArgBD was reported.

Conjugate Time-kill against *P. aeruginosa*:

Different samples were diluted and prepared in M9 bacterial medium in a 96-well plate. An inoculum of around 5*10^5 CFU/mL as final concentration which was initially grown in Mueller Hinton broth but diluted in M9 was added to the treatment. The plates were placed in an incubator at 37 °C while shaking on an orbital shaker at 160 rpm. At the specific time point, samples were taken and diluted up to 10^8 in sterile PBS. 3 spots (10 µL each) per dilution were pipetted on an LB agar plate and left to dry before placing in a 30 °C overnight for counting on the next day. The detection limit was about 100 CFU/mL. After the colonies were counted, the original log CFU/mL concentration was calculated back. The detection limit was kept at 33 CFU/mL. The values were averaged, and the standard deviation was calculated.

Molecular weight determination via SLS:

The samples were prepared in 10 mM phosphate buffer pH 7.4 in 1 cm light path cuvette, and then inserted into a Zetasizer ZS Series (Malvern Instruments Limited, Malvern, UK) equipped with a HeNE laster (JDS uniphasr) at wavelength of 633 nm. The dn/dc was assumed to be 0.185 mL/g as the conjugate consisted largely of peptide

meoities and a refractive index of 1.33. The sample was measured multiple times with different concentrations to yield the Deybe plot and the molecular weight estimate.

Size determination via DLS:

The sample was diluted in 10 mM phosphate buffer pH 7.4 at 1 mg/mL concentration in a 1 cm path length cuvette. The particle size of the sample was measured via dynamic light scattering using Zetasizer ZS Series (Malvern Instruments Limited, Malvern, UK) observed from 173° backlight scattering in triplicates.

Secondary structure of the conjugate in different microenvironment:

The method was adapted from a previous publication with minor modifications.[22] 400 µL of 120 µg/mL worth of TAT were diluted in 10 mM phosphate buffer pH 7.4. POPE/POPG were mixed in 3:1 mol:mol ratio and prepared in the same manner as the dose-binding assay as mentioned above and finally diluted to 3.4 mM concentration. The samples were then loaded into 1 mm path length quartz cuvette and measured using a Jasco 1500 spectropolarimeter (Gross-Umstadt, Germany). The setting of the measurement was as follows: Temperature = 24 °C, Bandwidth= 1 nm, Number of accumulations = 16, Scanning speed = 20 nm/min. The measurements were smoothened according to the Savitzky-Golay algorithm.

Red Blood Cells (RBCs) hemolysis assay:

In two Protein Lobind® tubes, 100 µL of sheep whole blood was washed three times with 2 mL of PBS in a centrifuge at 1700g for 2 minutes. The pellet was resuspended carefully in 11 mL of PBS. A dilution series, 50 µL each, of different samples was prepared in Lobind® tubes. The positive control was 5% TritonX. The tubes were put in a shaking heat plate at 60 rpm at 37 °C for 60 min. The tubes were centrifuged for 5 min at 1700g and 20 µL were taken out carefully without touching the pellet, which was diluted with 50 µL of PBS in a flat-bottom 96-well plate. The amount of lysed RBCs was quantified via measuring absorbance at 414 nm. The following equation was applied:

$$\%Hemolysis = 100\% * \frac{Abs_{(sample\ with\ RBCs)} - Abs_{(sample\ without\ RBCs)}}{Abs_{(TritonX\ with\ RBCs)} - Abs_{(PBS\ with\ RBCs)}}$$

Minimum inhibitory concentration in different strains:

Due to the effects shown in Figure S1, Mueller–Hinton broth does interact with the TAT–ArgBD and quenches its fluorescence. This effect was previously described in literature for cationic macromolecules as the usual rich media, like Mueller Hinton broth, contain extracts from yeast or beef, which have so many undefined components which can bind to the macromolecules. [23], [24], [25], [26], [27] A bacterial growth medium with more and minimal defined components, hence, minimal bacterial media was used.

MIC testing was performed using the standard broth microdilution according to EUCAST guidelines (ISO20776-1:2019) with some modifications and using a concentration range of 0.03-64 µg/mL for all treatments.

The test medium was changed to either M9 or RPMI 1640 supplemented with 20 mM glucose (RPMIGluc). For both media, a higher inoculum was used to support sufficient growth over the 24 h observation period in the modified culture medium. This was 5-fold higher than recommended by EUCAST. For M9, a final OD_{600} in the well of 0.0025 was used. While for RPMIGluc, initial cell concentration was adjusted to McFarland

0.5 and for testing, the cell suspension was further diluted 1:40 in RPMIGluc to support an inoculum of approximately 2.5 x 10^6 CFU/mL.

Tobramycin quality controls in the minimal media of *P. aeruginosa* PA14, *P. aeruginosa* PA01, *E. coli, A. baumannii, S. aureus* Newman yielded MICs of 0.25, 0.25, 0.25, 0.5–0.1, 8–16 µg/mL, respectively.

Synergy of TAT–ArgBD with antibiotics:

A dilution series (left to right) of the antibiotic was prepared in along all rows of the 96 well plate at 4x the target final concentration (25 µL). TAT–ArgBD dilution series was prepared in separate tubes at 4x the target final concentration and 25 µL was added to each of the column (top to bottom) to form a checkerboard plate. The inoculation and incubation were conducted as in the MIC assay.

Fractional inhibitory concentration index (FICI) was calculated using the below equation:

$$FICI = \frac{MIC_{TAT-ArgBD\ in\ combination}}{MIC_{TAT-ArgBD\ alone}} + \frac{MIC_{antibiotic\ in\ combination}}{MIC_{antibiotic\ alone}}$$

Conjugate interactions with different media:

450 µg/mL of TAT–ArgBD was diluted in 100 µL of different media. The solutions were left for 2h to allow for interactions to take place. Fluorescence was measured using excitation 301 nm, emission 372 nm, and excitation 350 nm, emission 520 nm. The following calculation was performed to determine the signal coming from the TAT–ArgBD:

$$Signal = Flu_{sample\ in\ medium} - Flu_{medium\ only}$$

Viability and cytotoxicity assay on mammalian cells:

L929 (5,000 cells/well) and RAW 264.7 (8,000 cells/well) cells were seeded in a 96-well plate in RPMI 1640 supplemented with 10% FCS and incubated until cells reached confluency with fresh medium change every second day. Cells were washed once with PBS, and then the samples were added in RPMI 1640 without FCS and incubated at 37 °C with 5% CO_2. As the antimicrobial (efficacy) assays were performed in minimal media or RPMI 1640 with glucose (protein poor) as well, to have an unbiased selectivity index and comparison, the mammalian cells were also incubated in such medium. Dead control was 2% TritonX and the live control was cells incubated in RPMI 1640. After 24h, 50 µL of the cell supernatant was taken and put aside in another plate for the LDH assay. The cells were washed with PBS, then 10% PrestoBlue in PBS was added to the cells and incubated for a few hours, then fluorescence was measured at excitation of 535 nm and emission of 615 nm. The following equation was applied to measure viability:

$$\%viability = 100\% * \frac{Flu_{treated\ cells} - Flu_{dead\ control}}{Flu_{live\ control} - Flu_{dead\ control}}$$

The LDH was performed according to the manual of the kit. Afterwards, the absorbance was measured at 492 nm. The following equation was applied to calculate the cytotoxicity:

$$\%cytotoxicity = 100\% * \frac{Abs_{treated\ cells} - Abs_{live\ control}}{Abs_{dead\ control} - Abs_{live\ control}}$$

Bacteria morphological changes visualization:

P. aeruginosa PA14 was grown until reaching the log phase in M9 medium then was treated for 3h. Bacteria was then washed with PBS to remove the treatment and resuspended in PBS, which fixed with 2% paraformaldehyde and 2% glutaraldehyde overnight. Bacteria was then dehydrated with increasing increments of ethanol 30%, 40%, 50%, 60%, 70%, 80%, 90%, 100% for 15 min each on silicon wafers in a well plate. Finally, Hexamethyldisilazane was added and removed after 15 min, then left overnight under a hood to dry. On the next day, the samples were gold-sputtered using Quorum Q150R ES sputter-coater (Gala Instruments GmbH, Germany). The samples were then images with Zeiss SEM EVO HD15 (Zeiss, Germany).

Morphology and particle structure of TAT–ArgBD:

A 3 µL droplet of 10 mg/mL TAT–ArgBD in 10 mM phosphate buffer was deposited on a holey carbon film (S147-4, Plano, Germany) and blotted to a thin liquid film for two seconds. The sample was then plunged into liquid ethane (T = 108 K) using Gatan (Pleasonton, USA) CP3 cryo plunge system. The sample was afterwards transferred under liquid nitrogen to a cryo-TEM holder (Gatan 914) operating at T = 100 K. Finally, the sample was analyzed by a Cryogenic Trasnmission Electron Microscopy (cryo-TEM, JEM-2100 LaB6, JEOL, Akishima, Japan) at 200 kV and low-dose conditions.

Structural properties of TAT–ArgBD and TAT–ArgBD-treated vesicles:

Vesicles were prepared in the same way as done in the circular dichroism section with minor modifications. First, the lipids used weight ratio was changed to 25:68:7 POPG:POPE:MPEG-2000-DSPE. Secondly, the vesicles were extruded at least 15 times through a 100 nm filter using Avnati™ Extruder set (Alabaster, AL, USA).

Small Angle X-ray Scattering (SAXS) measurements were performed on a Xeuss 2.0 instrument (Xenocs SAS, Grenoble, France). A collimated beam from the K_α-line of a copper X-ray source with a wavelength of λ = 1.54 Å was focused on the sample with a spot size of 0.25 mm^2. 2D scattering images were recorded using a Pilatus 300K detector with pixel sizes of 0.172 x 0.172 mm^2 and a sample-to-detector distance of 1211 mm, calibrated using a silver behenate standard. The solutions were mounted into borosilicate capillaries and measured with an acquisition time of 600 s, and azimuthally averaged to obtain $I(q)$. Here, q is defined as $q = 4\pi \times \sin(\theta/2)/\lambda$ with θ being the scattering angle. All measurements were repeated 5 times. As no signs of sample aging were observed, all scattering patterns of each sample were averaged. Scattering by the buffer was measured separately and subsequently subtracted from the data.

The Beaucage function was used to determine the radius of gyration, R_g, of TAT–ArgBD dissolved in buffer.[28] The scattering patterns of bacteriomimetic vesicles and bacteriomimetic vesicles treated with TAT–ArgBD was modelled using the scattering profile of a series of Gaussian electron density distributions, implemented in the *X+* software.[29]

Results:

1. TAT–ArgBD synthesis and characterization

We designed TAT–ArgBD by conjugating the TAT at the terminus of the hexaethylene glycol chain (HEG), a side chain of the ArgBDs, to allow for flexibility of the peptide to interact (**Figure 1a**). To conjugate TAT on the ArgBDs, we choose copper-catalyzed azide-alkyne cycloaddition (CuAAC) click chemistry, as it is known to be efficient for macromolecules. To achieve this, the monomer of ArgBD, HEG-conjugated carbazole dialdehyde (HEG-CA), was prepared based on previously reported methods [22] and further modified to introduce azide groups (-N_3). The N_3-HEG-CA was synthesized starting from 3,7-dibromocarbazole via lithium-halogen exchange and formylation with DMF, yielding CA. This compound was then alkylated with the commercially available N_3 chain and, after purification, afforded N_3-HEG-CA. Arginine hydrazide, was synthesized by reacting *N*-methyl-D-arginine methyl ester with hydrazine hydrate in methanol for 24h. The chemical structures of each compound was characterized using ^{1}HNMR and ^{13}CNMR spectroscopy, as detailed in the supplementary information.

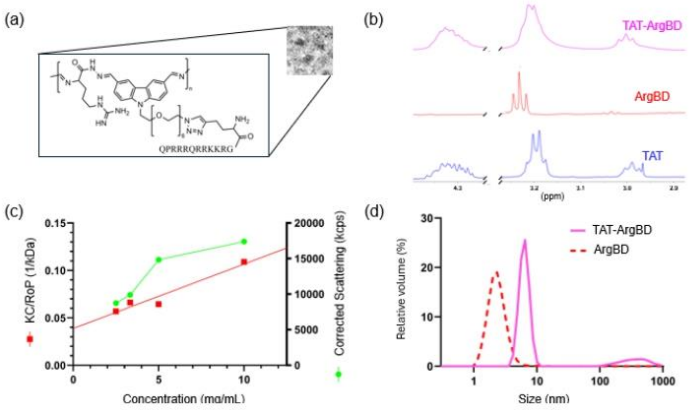

Figure 1: (a) Cryo-TEM snapshot and structure of TAT–ArgBD consisting of TAT peptide linked with a triazole linker to the ArgBD backbone. (b) HNMR spectra (ppm) showing (from left to right) peptide backbone, arginine δ methylene, lysine ε methylene after conjugating ArgBD to TAT. (c) Debye plot to determine the molecular weight by static light scattering (SLS) by measuring different concentrations of TAT–ArgBD yielding a molecular weight of 25.7 ± 4 kDa (KC/RoP y-intercept = 0.0389 ± 0.007 1/kDa, A2 second virial coefficient = 0.00339 ± 6.05e-4 mL·mol/g2, correlation coefficient (R2) = 0.94) (d) Volume particle size distribution as measured by dynamic light scattering (DLS) for TAT–ArgBD and ArgBD.

After synthesizing the monomers, we polymerized them yielding ArgBD-N_3 by using Schiff-base reactions between aldehydes and primary amines. The polymerization was performed at 1:1mol ratio of N_3-HEG-CA with arginine hydrazide in acidic aqueous solution for 24 h. Lastly, the alkyne-containing TAT was conjugated on the obtained ArgBD-N_3 using CuAAC to afford a triazole as a non-cleavable linker to get the structure shown in **Figure 1a**. Details of the synthesis and ^{1}HNMR spectra are provided in the Supplementary Information.

The crude reaction mixture was washed extensively using centrifugal filtration (3 kDa MWCO) to get rid of salts, catalysts, and unreacted free TAT and monomers of ArgBD. Using ^{1}HNMR, UV-Vis absorption and dynamic light scattering (DLS), we confirmed the presence of both TAT and ArgBD in the purified product. As seen in **Figure 1b** and **Figure S2**, we observed clear TAT ^{1}HNMR peaks from the purified product, as well as

typical UV-Vis absorption arising from carbazoles of ArgBD. We concluded the purified product includes both TAT and ArgBD with a molecular weight > 3 kDa, which evidence successful conjugation.

We then quantified the amount of TAT conjugated to ArgBD to determine the degree of TAT multivalency. Using quantitative NMR (qNMR), the conjugation rate was estimated to be 98 ± 0.64 mol/mol% or 67 ± 0.43 w/w% based on the arginine δ methylene and the lysine ε methylene ^{1}HNMR peaks shown in **Figure 1b**. For comparison, gravimetric analysis yielded a conjugation rate of 102 ± 5.85 mol/mol% or 69 ± 4.0 w/w%. Lastly, based on UV absorbance, which was validated to have an accuracy of 96% (Figure S3), the conjugation rate was found to be 96 ± 0.22 mol/mol% or 65 ± 0.15 w/w%. All three measurements confirm a conjugation rate of roughly 98 mol/mol%, which is not unprecedented for CuAAC reaction.[25], [26], [27] The high conjugation rate suggests a robust platform for creating multivalent constructs.

Static Light Scattering (SLS) was utilized to estimate the molecular weight of the TAT–ArgBD. The dn/dc of protein was used as the TAT–ArgBD consists mainly of peptides (TAT) and the ArgBD is peptide derivative composed of amino acids. SLS measurements indicated a molecular weight of 25.7 kDa, corresponding to around 12 repeating units of TAT–ArgBD per macromolecule, as shown in **Figure 1c**. On the other side, it is known that ArgBD can spontaneously fold into a nanorod, so the conjugate could have a folded structure as well.[18] Thus, the hydrodynamic diameter (D_H) of the nanostructure formed by the conjugate (TAT–ArgBD) as well as the backbone (ArgBD) were compared. The volume-based D_H of TAT–ArgBD and ArgBD were 6.5 and 2.3 nm, respectively (**Figure 1d**), which agrees with the cryo-TEM image at almost the resolution limit as shown in **Figure S4**.[18] R_g of the conjugate was measured to be 3.5 ± 0.2 nm using SAXS (**Figure S5**). The ratio between R_g (measured by SAXS) and R_h (measured by DLS) provides insights into the macromolecular geometry of the conjugate and equals 1.1 in the case of TAT–ArgBD. This value is typical for soluble polymers with an extended chain conformation (a value of 0.77 is expected for a homogeneous sphere). [30] Therefore, TAT–ArgBD is similarly expected to adopt an extended conformation.

2. Hemolysis and cytotoxicity towards mammalian cells

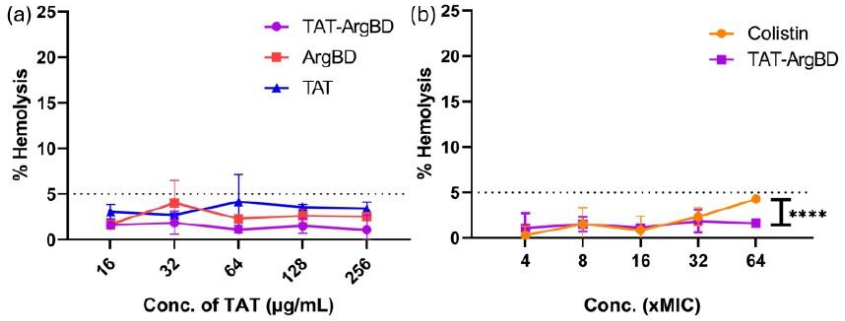

Figure 2: RBCs hemolysis assay for (a) TAT–ArgBD and the forming moieties of the conjugate. For TAT–ArgBD and TAT, the concentration of TAT was shown on the x-axis was used, while for Arg-BD sample the concentration of Arg-BD backbone found in the conjugate at the respective concentration was used. In (b), the hemolysis assay comparison for TAT–ArgBD and Colistin at the same fold MIC assuming that TAT–ArgBD and Colistin MICs are 2 µg/mL and 0.5 µg/mL with significance test (for 64-fold MIC data point) via one-way ANOVA, **** represent p value of <0.0001. 2–3 replicates were conducted.

As a core safety parameter, the % RBCs hemolysis by TAT-Arg was conducted (**Figure 2**). Multivalent peptide constructs often exhibit hemolytic activity, yet neither TAT–ArgBD nor its individual components induced significant hemolysis, even at concentrations well above the anticipated therapeutic levels (**Figure 2a**). As for **Figure 2b**, a head-to-head comparison of TAT–ArgBD and colistin was performed. At 64-fold MIC, TAT–ArgBD (256 µg/mL) was significantly superior to colistin (16 µg/mL) in terms of RBCs staying intact.

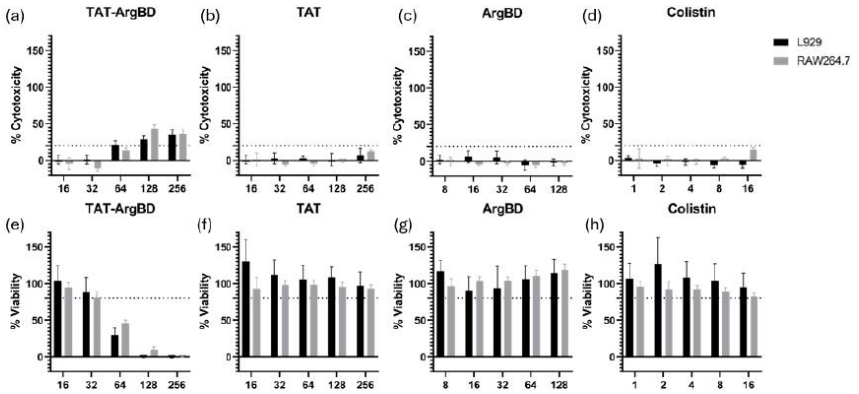

Figure 3: Cytotoxicity assessment by using lactate dehydrogenase (LDH) assay with L929 fibroblasts (black) and RAW264.7 macrophages (grey) with (a) TAT–ArgBD conjugate, (b) free TAT peptide, (c) ArgBD, and (d) Colistin. Viability assessment using PrestoBlue® was used as well with L929 fibroblasts (black) and RAW264.7 macrophages (grey) to assess the metabolic activity in the presence of (e) TAT–ArgBD, (f) free TAT peptide, (g) ArgBD, and (h) Colistin. The dead control (assumed to be 100% cytotoxicity and 0% viability) was 2% TritonX in medium while the live control (assumed to be 0% cytotoxicity and 100% vaibility) was treated with just medium. The dotted line representing significant toxicity threshold was plotted at 20% cytotoxicity (LDH) and 80% viability (PrestoBlue®). For all sub-figures, n=7-9, N=3. The mean was plotted, and error bars represent standard deviation.

To assess the safety of the conjugate towards mammalian cells, L929 mouse fibroblasts were exposed at various concentrations for 24h. 16 µg/mL of colistin and 256 µg/mL of TAT–ArgBD were chosen as the highest tested concentrations, which was later observed to be 64-fold MIC for both compounds. In terms of membrane damage (LDH release, **Figure 3a–d** in black), TAT–ArgBD at concentrations ≤ 64 µg/mL (≤16-fold MIC) have no significant membrane damage toxicity (>20%) was observed. As shown in **Figure 3e–h**, no reduced metabolic activity (PrestoBlue® assay) was observed except for ≥ 64 µg/mL of TAT–ArgBD.[31], [32]

TAT–ArgBD cytotoxicity was further evaluated in RAW264.7 macrophages, representing immune cells, to ensure its safety across multiple cell types. In fibroblasts, TAT–ArgBD showed no significant cytotoxicity at any concentration tested (Figure 3). Colistin induced mild membrane damage and reduced viability only at 16 µg/mL (**Figure 3d, 3h**).

3. Antimicrobial activity

Having established the safety aspects for the TAT–ArgBD, its antimicrobial activity was investigated to evaluate its potential use as a stand-alone agent. The antimicrobial activity of ArgBD and TAT were also assessed to determine if they have any notable antimicrobial activity before they are conjugated. A MIC assay was conducted against a panel of Gram-negative (*P. aeruginosa*, *E. coli, A. baumannii*) and Gram-positive (*S. aureus*) strains. As shown in Table 1, the TAT–ArgBD showed good antimicrobial activity against all strains except for *E. coli,* while TAT and ArgBD, were not active. It could also be noted that the multimeric nature caused TAT–ArgBD to have improved antimicrobial activity of ≥32 folds in *P. aeruginosa* compared to free TAT.[14]

Table 1: Minimum inhibitory concentration (MIC, µg/mL) of TAT–ArgBD, ArgBD, and TAT in different strains. n=2–3

	TAT–ArgBD	ArgBD	TAT
P. aeruginosa (PA14)	4	>64	>64
P. aeruginosa (PAO1)	4	>64	>64
E. coli MG1655	16	>64	>64
A. baumannii DSM 300008	2–8	>64	>64
S. aureus Newman	2	64–>64	64–>64

*Different media were used for different organisms as detailed in the methods section.

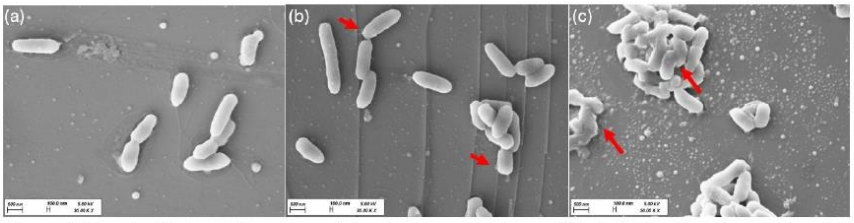

Figure 4: Scanning Electron Microscopy of *Pseudomonas aeruginosa* PA14 bacteria after exposure for 2h to different treatments, which are (a) no treatment, (b) 4 µg/mL of TAT–ArgBD, (c) 16 µg/mL of TAT–ArgBD. Red arrows point to intracellular components leaking from the membrane

4.Mechanism of action

To elucidate the mechanism by which TAT–ArgBD exhibits antimicrobial activity, we investigated its interactions with the bacterial cell envelope using lipid-binding assay, SEM imaging, circular dichroism, and SAXS. We investigated the origin of the observed activity of TAT–ArgBD. Given that 1) TAT is known to target lipid bilayer [33], 2) TAT–ArgBD is a macromolecule which overcomes difficult penetrating bacterial membranes [34], [35] and 3) ArgBD has previously been shown to enhance antibiotic activity by interacting with LPS on the bacterial envelope [22], we hypothesized that TAT–ArgBD also exerts its antibacterial effects by targeting the bacterial envelope. Thus, we visualized the effect of TAT–ArgBD on the cell membrane using SEM. PA14 bacteria were incubated for 2h with different concentrations (0, 4, 16 µg/mL) of TAT–ArgBD. PA14 bacteria clearly shows holes likely caused by an inhibiting but not lethal concentration of TAT–ArgBD (4 µg/mL) hitting the bacterial cell envelope at a certain point causing the leakage of the intracellular components of the bacteria (**Figure 4b**). Treatment with a higher likely lethal concentration of TAT–ArgBD (16 µg/mL) resulted in the formation of larger pores in the bacterial cell membrane, as depicted in **Figure 4c**. This membrane disruption was accompanied by extensive damage, leading to bacterial cross-linking and the aggregation of cells into larger clumps. These observations support the hypothesis that TAT–ArgBD exerts its antibacterial effects through its action on the bacterial cell membrane.

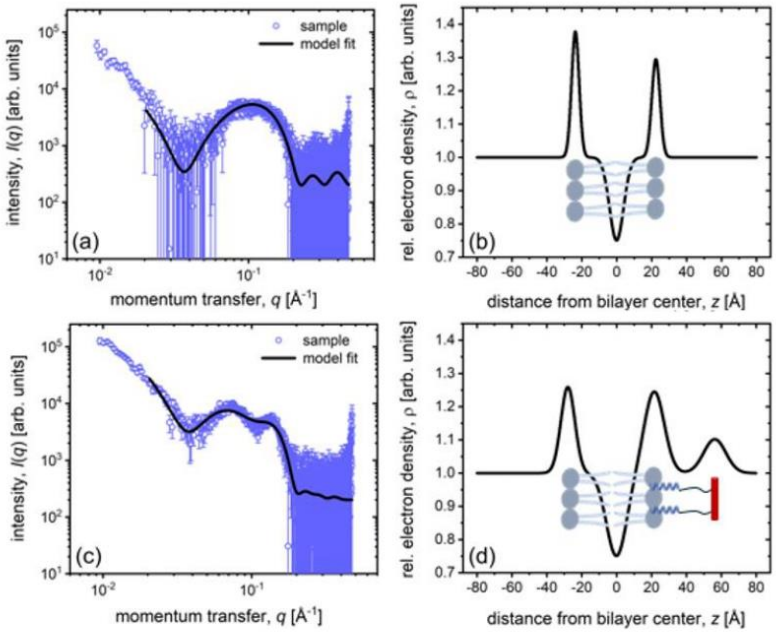

Figure 5: Results from small angle X-ray scattering on bacteriomimetic vesicles and bacteriomimetic vesicles treated with TAT-ArgBD. (a) SAXS pattern of bacteriomimetic vesicles (blue data) and model fit using a multilayer model consisting of three Gaussian electron density profiles (black line). (b) The resulting electron density profiles without any treatment, in relation to distance from the bilayer center, z, with sketched lipids forming a lipid bilayer (c) SAXS pattern of bacteriomimetic vesicles treated with TAT-ArgBD (blue data) and model fit using a multilayer model consisting of four Gaussian electron density profiles (black line). (d)The resulting electron density profiles of vesicles treated with TAT-ArgBD in dependence on distance from the bilayer center, z, with sketched conjugate with varying position partially embedding into the lipid bilayer.

Figure 5 shows the SAXS patterns of bacteriomimetic vesicles and bacteriomimetic vesicles treated with TAT–ArgBD. The SAXS pattern of the vesicles **(Figure 5a)** shows forward scattering below q = 0.02 Å^{-1}, which is due to scattering by the entire vesicles and a broad peak centered around q = 0.1 Å^{-1}, resulting from scattering at the bilayers. A multilayer model with three Gaussian electron density profiles to describe the lipid headgroups in the inner layer, the methyl chains within the bilayers and the lipid headgroups in the outer layer, respectively, was used to model the scattering pattern. The data at small q-values (below 0.02 Å^{-1}) were excluded from the fit because the curvature of the bilayers as a result of the finite size of the vesicles was not included in the model. **Figure 5b** presents the electron density profile of the bilayer in relation to distance from the bilayer center, z, resulting from the fit, normalized to that of the buffer. The distance between the maxima of the two outer peaks, representing the lipid head-groups in the inner and outer layer, respectively, describes the thickness of the bilayer, and amounts to 45 Å. The asymmetry of the profile is presumably due to density differences between the inner and outer parts of the bilayer, because of its curvature, like previously published SAXS measurements on vesicle systems.[36]

Similar to the SAXS pattern of vesicles, the one of bacteriomimetic vesicles treated with TAT–ArgBD (**Figure 5c**) shows forward scattering below q = 0.02 Å^{-1}. However, the appearance of a double peak around q = 0.1 Å^{-1} indicates a strong change in the bilayer structure. A combination of four Gaussian electron density profiles is used to model the scattering curve. While the model reproduces the double peak, it should be noted that there are differences between the shape of the peaks of the SAXS pattern and those predicted by the model. Therefore, only a qualitative description of the results is possible. The resulting electron density profile, shown in **Figure 5d**, gives insights into the bilayer structure. Several observations can be made. Firstly, a broadening of the Gaussians describing the lipid headgroups (around z = -25 Å and z = 25 Å, respectively) and methyl chains in the interior of the bilayers (at z = 0) indicate a more heterogeneous structure as compared to bacteriomimetic vesicles in the absence of TAT–ArgBD. Secondly, the enhanced electron density around z = 60 Å indicates that the center of mass of the conjugate is located very close to the bilayers-solvent interface outside the bilayer, representing the normal distribution of conjugates closer to and further from the center of the layer. Both observations hint towards the embedding of the conjugate into the outer part of the bilayer, leading to the effects seen *in bacterio*, as elaborated by the sketch in **Figure 5d**.This hypothesis is furthermore supported by the increased symmetry of the Gaussians describing the lipid headgroups: The presence of the conjugate increases the electron density on the outer part of the vesicle, reversing the lowered density due to the curvature of the vesicles to become almost equal.

To further understand the mechanism, we studied how TAT–ArgBD interacts with lipids

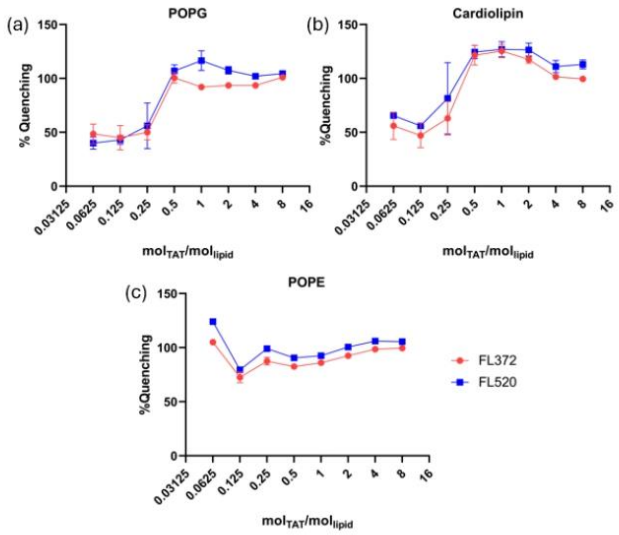

Figure 6: Dose-response curve of fluorescence quenching of TAT–ArgBD following two fluorophores (excitation 301 nm, and 372 nm with emission of 350, and 520 nm, respectively) with (a) POPG, (b) Cardiolipin, and (c) POPE.

by analyzing its intrinsic fluorescence properties. A strong interaction was hypothesized to result in fluorescence quenching as TAT–ArgBD binds to lipid vesicles. We plotted this quenching effect against the molar ratio of TAT–ArgBD to the lipids POPE, cardiolipin, and POPG (**Figure 6**). These lipids were selected as key representatives of bacterial membranes, given that the bacterial cell envelope is

largely composed of phospholipids, namely POPE, cardiolipin, and POPG, which are particularly abundant and play critical roles in maintaining the structure and function of Gram-negative and Gram-positive bacterial membranes, making them an appropriate focus for this study.[37]

As for the anionic POPG, the IC_{50} values of the fluorescence quenching with POPG could be calculated as 0.287 mol/mol ± 0.013 (emission at 372 nm) and 0.267 mol/mol ± 0.016 (emission at 520 nm) (**Figure 6a**). Meanwhile for cardiolipin, the values were also similar, in specific, the IC_{50} values were 0.267 mol/mol ± 0.003 (emission at 372 nm) and 0.25 mol/mol ± 0.019 (emission at 520 nm) (**Figure 6b**). The zwitterionic POPE was tested with no observed binding with TAT–ArgBD up to the highest tested ratio (**Figure 6c**). While the binding with the LPS could not be assessed as LPS could not be solubilized at the molar ratio due to its very high molecular weight. This agrees with the fact that both interacted lipids are anions and close in chemical structure, hence can attract cationic molecules [39]. To visualize this interaction on a molecular level, it can be estimated that one TAT moiety binds approximately four lipid molecules at the IC_{50}. While this estimation does not allow for definitive conclusions, it suggests that the activity does not follow a conventional 1:1 binding modality, as seen in enzyme-substrate interactions. Instead, it points toward a more complex mechanism, likely influenced by the conformation of the lipid-TAT–ArgBD complex within bacterial membranes.

To investigate the secondary structure of TAT–ArgBD depending on the peptide bond

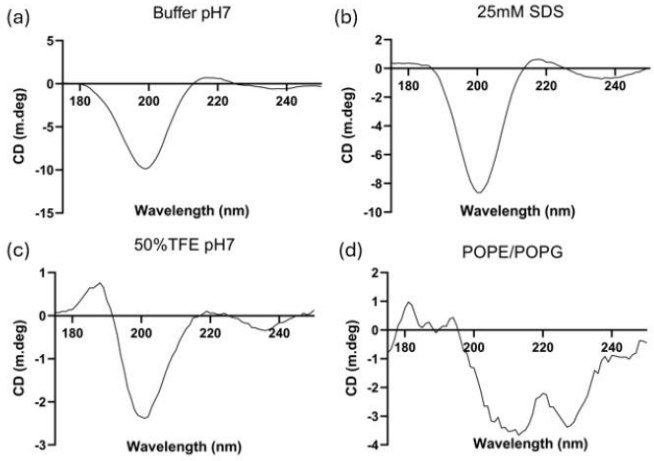

Figure 7: Circular dichroism spectra of TAT–ArgBD in (a) phosphate buffer, (b) SDS, (c) 50% TFE, (d) POPE/POPG vesicles.

polarization of light, circular dichroism (CD) was performed. In buffer and the absence of any lipids, TAT–ArgBD exhibited a predominant random coil structure, characterized by a negative peak near 200 nm, while having a very slight triple helix character signified by a ratio between the $-\theta_{200}/\theta_{220}$ of 16.23 which is much less triple helix character than collagen for instance (**Figure 7a**).[38] In the presence of SDS, which mimics vesicular structures, no difference was noted from the in-buffer spectrum (**Figure 7b**). Similarly, in a hydrophobic lipid mimicking environment (50% Trifluoroethanol), no significant differences were noted (**Figure 7c**), indicating that TAT–ArgBD has no tendency for a certain secondary structure in lipid membranes in

general. In vesicle made of a mixture of POPE and POPG, TAT–ArgBD displayed a pronounced α-helical structure, evidenced by district negative bands near 208 nm and 222 nm (**Figure 7d**). These findings demonstrate that TAT–ArgBD does not adopt an organized secondary structure in buffer, lipid-like, or hydrophobic environment. However, its significant transition to a α-helical conformation in the presence of POPE/POPG vesicles hints towards selective targeting of bacterial membranes.[35][36]

6. Bacteria killing kinetics

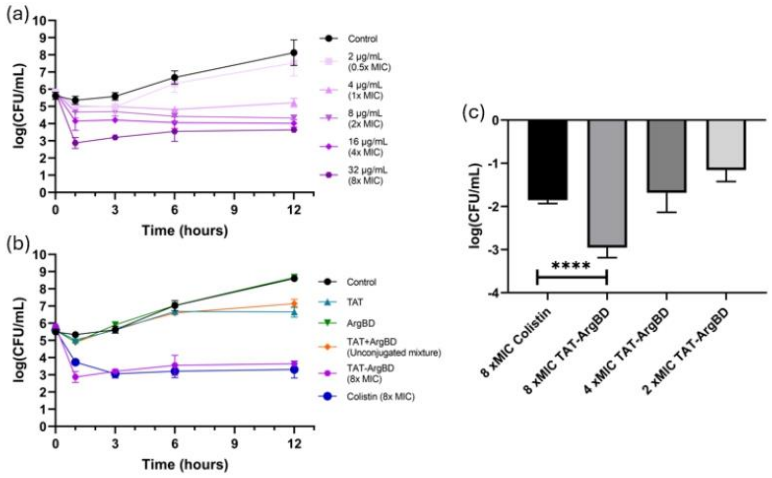

Figure 8: Time-kill assay for Pseudomonas aeruginosa PA14 for (a) different concentrations of TAT–ArgBD in the range of (0.5-8 -fold MIC), and (b) 32 µg/mL of TAT–ArgBD (8-fold MIC) conjugates compared to its single chemical components (32 µg/mL TAT and 16 µg/mL ArgBD) having the equivalent amount and their unconjugated physical mixture as well as comparison with 2 µg/mL of Colistin (8-fold MIC). (c) Head-to-head comparison of the decrease of the PA14 count after just 1h of treatment. **** represents $p < 0.0001$ on one-way ANOVA.

Having established that TAT–ArgBD interacts with the bacterial cell envelope, we next evaluated the antimicrobial efficacy over time. A time-kill assay was conducted using CFU counting to determine the speed and extent of bacterial clearance. As shown in **Figure 8a**, 8 µg/mL of TAT–ArgBD caused 1-log decrease of PA14 bacteria withing an hour, while higher doses (32 µg/mL) achieved even 3-log (99.9%) bacterial killing within the same time period. The maximum killing speed occurred within the first hour, and gradually shifted to a steady state after 6h, probably due to the absorption of partially degraded TAT–ArgBD onto the bacterial membrane.

In **Figure 8b**, TAT–ArgBD was compared to its chemical components (ArgBD and TAT) without covalent bonding, it is noted that each single component possesses no effect at all against PA14 neither is their physical mixture. However, a mild growth inhibition was noticed in the case of free TAT, hence, TAT is considered here as the active moiety of the TAT–ArgBD conjugate. The concentrations of TAT and ArgBD were calculated based on the conjugation rates, corresponding to their respective masses in 32 µg/mL conjugated TAT in TAT–ArgBD. Additionally, 2 µg/mL of colistin (8-fold MIC) was compared to 32 µg/mL of TAT–ArgBD (8-fold MIC) in terms of the killing kinetics, as

colistin is an established antibiotic with a membrane-targeting mechanism of action. [37] As a result, TAT−ArgBD showed a 6-fold greater killing efficiency against PA14 compared to colistin within the first hour. (**Figure 8b and 8c**). However, killing kinetic of TAT–ArgBD and colistin were comparable after 3h. TAT–ArgBD demonstrated a concentration-dependent rapid elimination of PA14 bacteria within minutes of exposure. Its superior killing kinetics in the first hour compared to colistin, emphasizes the potential as a fast-acting and potent antimicrobial against *P. aeruginosa*.

7.Synergy

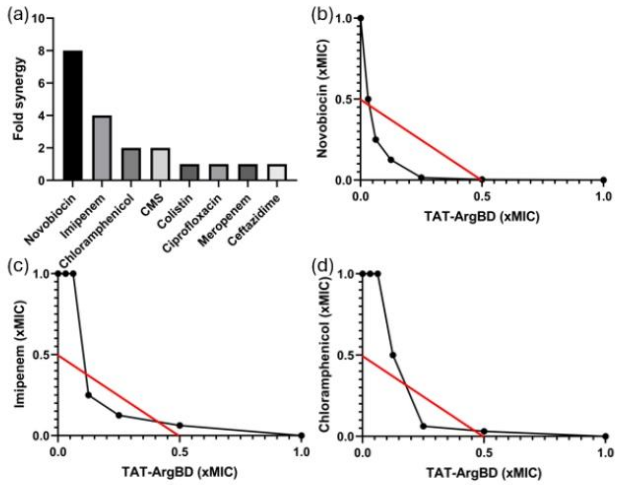

Figure 6: (a) Synergy in *Pseudomonas aeruginosa* PA 14 depicted by fold MIC reduction when various antibiotics are combined with 0.5 µg/mL (0.125-fold MIC) of TAT–ArgBD. Checkerboard assays for TAT–ArgBD in combination with (b) Novobiocin, (c) Imipenem, and (d) Chloramphenicol. Lower left of the red line represents FICI of $\leq$ 0.5 (significant synergy). MICs of TAT−ArgBD, Novobiocin, Imipenem, Chloramphenicol, Colistimethate Sodium (CMS), Colisitn, Ciprofloxacin, Meropenem, Ceftazidime were 4, 256, 0.5, 32, 0.5, 0.25, 0.25, 0.125, 2 µg/mL.

Given the rapid bactericidal activity of TAT–ArgBD, we evaluated its ability to enhance the efficacy of existing antibiotics against PA14 bacteria. As a screening assay, MIC reduction assay was conducted for several antibiotics, ceftazidime, chloramphenicol, colistimethate sodium (CMS), colistin, ciprofloxacin, imipenem, meropenem, and novobiocin, combined with just 0.5 µg/mL of TAT–ArgBD corresponding to a sublethal concentration (0.125-fold MIC). Synergistic effects were observed with 4 antibiotics, novobiocin, chloramphenicol, CMS, and imipenem, as shown in **Figure 9a**. Since CMS is a prodrug and its active form, colistin, showed no promising synergy, both were excluded from follow-up studies. Subsequently, follow-up bacterial inhibition checkerboard assay against *P. aeruginosa* PA14 was performed for the three synergistic antibiotics. As shown in **Figure 9b**, TAT–ArgBD showed strong synergy with novobiocin, with a fractional inhibitory concentration index (FICI) of 0.25 and a maximum MIC reduction of 256 folds. Similar synergies were observed with imipenem, yielding a FICI of 0.375 and a maximum MIC reduction of 16-folds (**Figure 9c**), while with chloramphenicol resulting in a FICI of 0.312 and a maximum MIC reduction of 32-folds (**Figure 9d**). It is particularly noteworthy, as summarized in **Table 2**, that antibiotics are typically active only against Gram-positive bacteria and inactive against

P. aeruginosa synergized and became highly active against Gram-negative *P. aeruginosa*.

Table 2 A summary of the MIC in PA14, the fold reduction in MIC of antibiotics synergized by TAT–ArgBD (2 μg/mL), and their known target-specific activities

	MIC (μg/mL)		Fold MIC reduction	FICI	Activity against PA	Spectrum	Target
	w/o TAT–ArgBD	+ TAT–ArgBD					
Novobiocin	256	1	256	0.25	No	G+	DNA gyrase [39]
Imipenem	0.5	0.031	16	0.375	Yes (except CRPA)	Broad	Penicillin-binding proteins [40]
Chloramphenicol	32	1	32	0.312	No	Broad	70S ribosome [41]

Discussion:

Drug conjugation strategies, including antimicrobial peptide conjugation, have attracted attention as an efficient approach for enhancing its efficacy. RWK peptide conjugated to a methoxy core using a triazole linker improve the potency of the free RWK peptide against A. *baumannii* from >100 μM to 7.5 μM (>13.3 folds).[42] Glucose-cored glycocluster through a PEG and a triazole linkers(13aG/GalEG$_3$) could improve the antimicrobial efficacy for a multivalency of 4 compared to the monomeric form was improved 23–24 folds.[43]

TAT–ArgBD falls into the category of amphiphilic compounds, which has a length of 12–16 repeating units for optimal antimicrobial activity—a criterion met by the material design of TAT–ArgBD.[44] By conjugating the TAT peptide onto ArgBD with a multivalency of approximately 12, TAT–ArgBD achieved more than a 16-fold improvement compared to free TAT in terms of antimicrobial activity against *P. aeruginosa, S. aureus,* and *A. baumannii*. By conjugating TAT on the ArgBD with a multivalency of around 12, TAT–ArgBD improved TAT peptide by >16 folds against *P. aeruginosa, S. aureus, A. baumannii.* In contrast, a recent study explored multivalent antimicrobial peptides by conjugating WLBU2 peptide onto a dextran backbone, which improved WLBU2's efficacy by more than fourfold. However, TAT conjugated to dextran showed no significant antimicrobial activity.[14] We speculate that the unique structure and characteristics of ArgBD enabled the TAT–ArgBD to interact with bacterial membranes due to the greater structural adaptability and significantly enhancing the potency of multivalent TAT. The flexible hexaethylene glycol spacer facilitates thermodynamically favorable structures of TAT like α-helix.[45] Additionally, the intrinsic ability of ArgBD to interact with the LPS layer further amplifies this activity.

We compared the potency of TAT–ArgBD with colistin as an approved antibiotic due its membrane activity, close to the TAT–ArgBD proposed mechanism. While colistin is an established antibiotic, its clinical use is limited due to renal toxicity and poor pharmacokinetics.[46] For example, a clinical study showed that colistin can cause acute kidney injury at concentrations as low as 2.2 μg/mL, which is above its breakpoint for *P. aeruginosa*. Hence, it is unlikely that colistin treats an infected patient without causing serious side effects.[47]

The design and size of TAT–ArgBD offer significant advantages, as its size of over 4.5 nm prevents it from being filtered through the glomeruli, allowing it to function as a long-circulating antimicrobial. This potentially maximizes the AUC/MIC ratio and hence has better safety profile in potential human applications.[48], [49] Additionally, TAT-decorated nanostructures were observed to have a superior tissue penetration ability, so it has higher chances of reaching the site of infection.[50] However, the PK/PD profile of TAT–ArgBD needs further investigation to confirm these expected advantages.

Conjugating peptides to backbone to yield a multivalent construct often led to increased hemolysis of RBCs.[12] Although TAT–ArgBD is an amphiphilic cationic polymer, TAT–ArgBD was shown to be exceptionally safe with a membranolytic index (Hemolytic concentration/MIC) of >64 relative to similar materials, even in the absence of corona-forming serum proteins.[42], [43], [51], [52] This safety parameter becomes especially relevant in the case of IV systemic applications.[53] Interestingly, while isolated RBCs showed no lysis even above suspected therapeutic concentrations, mammalian cells were more susceptible to metabolic inhibition. For instance, 128 μg/mL (32-fold MIC) of TAT–ArgBD reduced metabolic activity, suggesting mitochondrial inhibition. At the same concentration, cells were mostly still intact and had some low LDH release. This phenomenon is hypothesized to be due to the TAT–ArgBD interactions with cardiolipin, which is a shared lipid between bacterial

membranes and mitochondria.[31], [32] The increased susceptibility of macrophages relative to fibroblasts suggests that endocytosis can be contributing to the uptake of TAT–ArgBD into cells, thus greater susceptibility, as macrophages have higher potential for endocytosis than fibroblasts.[54] In summary, TAT–ArgBD has a LDH CC_{50} of > 256 µg/mL, which yields a selectivity index (CC_{50}/MIC) of >64. To put this into perspective, colistin has a LDH CC_{50} of 25 µg/mL (50-fold MIC) with kidney cells, thus this highlights the potential for developing TAT–ArgBD further for *in vivo* experiments.[55]

Beyond the safety profile, TAT–ArgBD demonstrates potent bactericidal activity. As per the CLSI guidelines, minimum bactericidal concentration (MBC) is defined as the 3-log decrease (≥ 99.9%) of the inoculum in the time-kill assay.[56] TAT–ArgBD could meet this criterion at a concentration of 32 µg/mL, therefore, the 1-hour MBC can be determined as 32 µg/mL, which happens to not induce toxicity in all our safety studies, which is a key determinant to consider for further development into human use.[57] To put this into perspective, a study had pooled 187 time-kill assays, where colistin scored as the best of the antibiotics in terms of fewer persister bacteria surviving the antibiotic after treatment among 54 antibiotics, while TAT–ArgBD was shown to be superior to colistin in the first hour [58]. At longer incubations, this superiority is compromised, probably explained by the biodegradable nature of TAT–ArgBD as it depends on its multivalency as well as the TAT moieties which are susceptible to cleavage by bacteria proteases, such as LasB. Additionally, TAT–ArgBD exhibited potent activity against all tested strains except for *E. coli*. This fact hints towards potential microbiome-sparing properties to maintain a healthy microbiome in the human body. However, there is a need for future studies to confirm this.[59]

In addition to the stand-alone antimicrobial activity, TAT–ArgBD could demonstrate strong potential as an adjuvant, converting Gram-positive or narrow-spectrum antibiotics into broad-spectrum antibiotics against *P. aeruginosa* for instance. In a study by Krishnamoorthy *et al*, it was shown that *P. aeruginosa* with hyperporation could reduce the MIC of novobiocin, chloramphenicol, ciprofloxacin, and meropenem by 32-, 8-, 4-, and 4-folds, respectively.[60] Notably, this ranking of MIC reductions is the exact same as achieved by combining them with TAT–ArgBD, suggesting that pore formation is the mechanism of action of TAT–ArgBD by which TAT–ArgBD at higher concentration can act as a stand-alone antibacterial.[61] To put this into clinical perspective, novobiocin has a breakpoint of 4 µg/mL against bovine mastitis pathogens and we could achieve 1 µg/mL, which shows that novobiocin is likely to be safe and effective at this concentration.[62] Additionally, the EUCAST susceptibility breakpoint for chloramphenicol is 2 µg/mL for most pathogens, hence 1 µg/mL has the potential to be applicable to use as combined here in humans against *P. aeruginosa* infections.[63] Normally, imipenem is active against PA14, however, it could be even improved here even more so that only as little as 0.031 µg/mL can inhibit bacterial growth, which can become then relevant in carbapenem-resistant strains.

This mechanism of action was further explored by a variety of techniques where pore-formation was shown with a non-lethal concentration of TAT–ArgBD. While these pores are probably caused by strong binding of TAT–ArgBD to POPG and cardiolipin as shown by binding assays, leading to the formation of a more organized complex structure of TAT–ArgBD with the bacterial cell envelope, likely to be an α-helical structure. Furthermore, SAXS suggests that the conjugate is partially embedded into the outer part of the vesicles.

Conclusions:

TAT–ArgBD is introduced as a novel multivalent antimicrobial conjugate which addresses critical gaps in combating bacterial infections. The resulting construct demonstrated potent antibacterial activity against both Gram-negative (*P. aeruginosa* and *A. baumannii*) as well as Gram-positive (*S. aureus*) bacteria, by improving the activity of free TAT by tens of folds (MICs as low as 2 μg/mL) and a rapid onset of action (1-hour MBC of 32 μg/mL). Additionally, TAT–ArgBD showed synergy with antibiotics like novobiocin, chloramphenicol, and imipenem, enhancing their efficacy against Gram-negative bacteria and expanding (in case of novobiocin) spectrum of activity from Gram-positive to encompass Gram-negative pathogens. Mechanistic studies showed that TAT–ArgBD operates through bacterial membrane pore formation and ordering the structure of TAT–ArgBD to α-helical structure by embedding into POPG and cardiolipin lipids of the bacterial cell envelope.

Besides the potential use if TAT–ArgBD as a single-agent anti-infective and as synergistically acting agent in combination therapy, its lower antibacterial activity against *E. coli* compared to exclusively pathogenic bacteria also hints towards putatively microbiome-sparing properties. Our results suggest that dynamically bio-responsive polymers, like biodynamers, functionalized with multiple membrane-active peptides, enable unique molecular interactions with bacterial membranes in addition to the intrinsic ability of ArgBD to interact with the LPS layer. This may distinguish them from other polymeric constructs, such as dendrimers, PLGA-, or dextran-based backbones. Biodynamer-constructs obviously bear potential to develop highly potent and safe antibacterial therapeutics, especially against MDR infections by some clinically relevant pathogens. Future research should adapt and optimize this platform for other peptides as well as explore the utility of it for local or systemic applications in complex *in vitro* models or *in vivo*.

References:

[1] WHO, "WHO bacterial priority pathogens list, 2024," *Bacterial pathogens of public health importance to guide research, development and strategies to prevent and control antimicrobial resistance*, p. 72, 2024, Accessed: Jul. 29, 2024. [Online]. Available: https://www.who.int/publications/i/item/9789240093461

[2] E. Tacconelli *et al.*, "Discovery, research, and development of new antibiotics: the WHO priority list of antibiotic-resistant bacteria and tuberculosis," *Lancet Infect Dis*, vol. 18, no. 3, pp. 318–327, Mar. 2018, doi: 10.1016/S1473-3099(17)30753-3.

[3] A. Bali, M. A. M. Kamal, G. Mulla, B. Loretz, and C. M. Lehr, "Functional Materials to Overcome Bacterial Barriers and Models to Advance Their Development," *Adv Funct Mater*, vol. 33, no. 45, p. 2304370, Nov. 2023, doi: 10.1002/ADFM.202304370.

[4] R. F. Langendonk, D. R. Neill, and J. L. Fothergill, "The Building Blocks of Antimicrobial Resistance in Pseudomonas aeruginosa: Implications for Current Resistance-Breaking Therapies," *Front Cell Infect Microbiol*, vol. 11, p. 665759, Apr. 2021, doi: 10.3389/FCIMB.2021.665759.

[5] M. E. Falagas and S. K. Kasiakou, "Toxicity of polymyxins: a systematic review of the evidence from old and recent studies," *Crit Care*, vol. 10, no. 1, p. R27, Feb. 2006, doi: 10.1186/CC3995.

[6] M. Borowiak, J. Fischer, J. A. Hammerl, R. S. Hendriksen, I. Szabo, and B. Malorny, "Identification of a novel transposon-associated phosphoethanolamine transferase gene, mcr-5, conferring colistin resistance in d-tartrate fermenting Salmonella enterica subsp. enterica serovar Paratyphi B," *Journal of Antimicrobial Chemotherapy*, vol. 72, no. 12, pp. 3317–3324, Dec. 2017, doi: 10.1093/JAC/DKX327.

[7] E. Kim, J. Yang, S. Park, and K. Shin, "Factors Affecting Success of New Drug Clinical Trials," *Ther Innov Regul Sci*, vol. 57, no. 4, pp. 737–750, Jul. 2023, doi: 10.1007/S43441-023-00509-1.

[8] "Antibacterial products in clinical development for priority pathogens." Accessed: Dec. 01, 2024. [Online]. Available: https://www.who.int/observatories/global-observatory-on-health-research-and-development/monitoring/antibacterial-products-in-clinical-development-for-priority-pathogens

[9] H. D. Herce and A. E. Garcia, "Molecular dynamics simulations suggest a mechanism for translocation of the HIV-1 TAT peptide across lipid membranes," *Proc Natl Acad Sci U S A*, vol. 104, no. 52, pp. 20805–20810, Dec. 2007, doi: 10.1073/PNAS.0706574105.

[10] F. Her Choong and B. Keat Yap, "Cell-Penetrating Peptides: Correlation between Peptide-Lipid Interaction and Penetration Efficiency," *ChemPhysChem*, vol. 22, no. 5, pp. 493–498, Mar. 2021, doi: 10.1002/CPHC.202000873.

[11] J. Reeman, L. M. Ittner, K. A. Vallis, and O. Tietz, "Strength in numbers: cell penetrating peptide clusters to build next-generation therapeutics," *Trends Chem*, vol. 6, no. 11, pp. 669–683, Nov. 2024, doi: 10.1016/J.TRECHM.2024.09.003/ASSET/56B0B991-1212-4D0E-97D7-93C0C4512123/MAIN.ASSETS/GR4.JPG.

[12] S. P. Liu, L. Zhou, R. Lakshminarayanan, and R. W. Beuerman, "Multivalent antimicrobial peptides as therapeutics: Design principles and structural diversities,"

Int J Pept Res Ther, vol. 16, no. 3, pp. 199–213, Sep. 2010, doi: 10.1007/S10989-010-9230-Z.

[13] J. P. Tam, Y. A. Lu, and J. L. Yang, "Antimicrobial dendrimeric peptides," *Eur J Biochem*, vol. 269, no. 3, pp. 923–932, Feb. 2002, doi: 10.1046/J.0014-2956.2001.02728.X.

[14] L. W. Chan *et al.*, "Selective Permeabilization of Gram-Negative Bacterial Membranes Using Multivalent Peptide Constructs for Antibiotic Sensitization," *ACS Infect Dis*, vol. 7, no. 4, pp. 721–732, Apr. 2021, doi: 10.1021/acsinfecdis.0c00805.

[15] Y. Lin *et al.*, "Design and Self-Assembly of Peptide-Copolymer Conjugates into Nanoparticle Hydrogel for Wound Healing in Diabetes," *Int J Nanomedicine*, vol. 19, pp. 2487–2506, Mar. 2024, doi: 10.2147/IJN.S452915.

[16] S. Li *et al.*, "Structure, stability, and mechanism of dextran–CPP–Ca2+ conjugates: A novel high-efficiency calcium ion delivery system," *Food Chem*, vol. 408, p. 135190, May 2023, doi: 10.1016/J.FOODCHEM.2022.135190.

[17] B. Lebleu *et al.*, "Cell penetrating peptide conjugates of steric block oligonucleotides," *Adv Drug Deliv Rev*, vol. 60, no. 4–5, pp. 517–529, Mar. 2008, doi: 10.1016/J.ADDR.2007.09.002.

[18] S. Lee *et al.*, "Proteoid biodynamers for safe mRNA transfection via pH-responsive nanorods enabling 1 endosomal escape Introductory paragraph 20," *Journal of Controlled Release*, vol. 353, pp. 915–929, Jan. 2023, doi: 10.1016/J.JCONREL.2022.12.018.

[19] Y. Liu, J. M. Lehn, and A. K. H. Hirsch, "Molecular Biodynamers: Dynamic Covalent Analogues of Biopolymers," *Acc Chem Res*, vol. 50, no. 2, pp. 376–386, Feb. 2017, doi: 10.1021/acs.accounts.6b00594.

[20] S. Lee *et al.*, "PH-Dependent morphology and optical properties of lysine-derived molecular biodynamers," *Mater Chem Front*, vol. 4, no. 3, pp. 905–909, Mar. 2020, doi: 10.1039/c9qm00651f.

[21] Y. Liu, M. C. A. Stuart, E. Buhler, J. M. Lehn, and A. K. H. Hirsch, "Proteoid Dynamers with Tunable Properties," *Adv Funct Mater*, vol. 26, no. 34, pp. 6297–6305, Sep. 2016, doi: 10.1002/ADFM.201601612.

[22] M. A. M. Kamal, J. Bassil, B. Loretz, A. K. H. Hirsch, S. Lee, and C. M. Lehr, "Arg-biodynamers as antibiotic potentiators through interacting with Gram-negative outer membrane lipopolysaccharides," *European Journal of Pharmaceutics and Biopharmaceutics*, vol. 200, p. 114336, Jul. 2024, doi: 10.1016/J.EJPB.2024.114336.

[23] J. F. Kreisberg *et al.*, "Growth inhibition of pathogenic bacteria by sulfonylurea herbicides," *Antimicrob Agents Chemother*, vol. 57, no. 3, pp. 1513–1517, Mar. 2013, doi: 10.1128/AAC.02327-12.

[24] J. M. Schuurmans, A. S. Nuri Hayali, B. B. Koenders, and B. H. ter Kuile, "Variations in MIC value caused by differences in experimental protocol," *J Microbiol Methods*, vol. 79, no. 1, pp. 44–47, Oct. 2009, doi: 10.1016/J.MIMET.2009.07.017.

[25] S. Štumpf, G. Hostnik, M. Primožič, M. Leitgeb, J. P. Salminen, and U. Bren, "The Effect of Growth Medium Strength on Minimum Inhibitory Concentrations of Tannins and Tannin Extracts against E. coli," *Molecules 2020, Vol. 25, Page 2947*, vol. 25, no. 12, p. 2947, Jun. 2020, doi: 10.3390/MOLECULES25122947.

[26] D. Hörömpöli *et al.*, "The antibiotic negamycin crosses the bacterial cytoplasmic membrane by multiple routes," *Antimicrob Agents Chemother*, vol. 65, no. 4, Apr. 2021, doi: 10.1128/AAC.00986-20.

[27] D. K. Mercer *et al.*, "Antimicrobial Susceptibility Testing of Antimicrobial Peptides to Better Predict Efficacy," *Front Cell Infect Microbiol*, vol. 10, p. 540826, Jul. 2020, doi: 10.3389/FCIMB.2020.00326/BIBTEX.

[28] B. Hammouda, "Analysis of the Beaucage model," *urn:issn:0021-8898*, vol. 43, no. 6, pp. 1474–1478, Oct. 2010, doi: 10.1107/S0021889810033856.

[29] T. Ben-Nun, A. Ginsburg, P. Székely, and U. Raviv, "X+: A comprehensive computationally accelerated structure analysis tool for solution X-ray scattering from supramolecular self-assemblies," *J Appl Crystallogr*, vol. 43, no. 6, pp. 1522–1531, Dec. 2010, doi: 10.1107/S0021889810032772/AJ5158SUP2.PDF.

[30] B. M. Tande, N. J. Wagner, M. E. Mackay, C. J. Hawker, and M. Jeong, "Viscosimetric, hydrodynamic, and conformational properties of dendrimers and dendrons," *Macromolecules*, vol. 34, no. 24, pp. 8580–8585, Nov. 2001, doi: 10.1021/MA011265G/ASSET/MA011265G.FP.PNG_V03.

[31] S. E. Horvath and G. Daum, "Lipids of mitochondria," *Prog Lipid Res*, vol. 52, no. 4, pp. 590–614, Oct. 2013, doi: 10.1016/J.PLIPRES.2013.07.002.

[32] K. Boguszewska, M. Szewczuk, J. Kazmierczak-Baranska, and B. T. Karwowski, "The Similarities between Human Mitochondria and Bacteria in the Context of Structure, Genome, and Base Excision Repair System," *Molecules 2020, Vol. 25, Page 2857*, vol. 25, no. 12, p. 2857, Jun. 2020, doi: 10.3390/MOLECULES25122857.

[33] Y. Rao, S. J. J. Kwok, J. Lombardi, N. J. Turro, and K. B. Eisenthal, "Label-free probe of HIV-1 TAT peptide binding to mimetic membranes," *Proc Natl Acad Sci U S A*, vol. 111, no. 35, pp. 12684–12688, Sep. 2014, doi: 10.1073/PNAS.1411817111.

[34] H. Nikaido, "Molecular Basis of Bacterial Outer Membrane Permeability Revisited," *Microbiology and Molecular Biology Reviews*, vol. 67, no. 4, pp. 593–656, 2003, doi: 10.1128/mmbr.67.4.593-656.2003.

[35] H. Nikaido and M. Vaara, "Molecular basis of bacterial outer membrane permeability," *Microbiol Rev*, vol. 49, no. 1, pp. 1–32, 1985, doi: 10.1128/mmbr.49.1.1-32.1985.

[36] T. W. Hsu *et al.*, "Revealing cholesterol effects on PEGylated HSPC liposomes using AF4-MALS and simultaneous small- and wide-angle X-ray scattering," *J Appl Crystallogr*, vol. 56, no. 4, pp. 988–993, Jul. 2023, doi: 10.1107/S1600576723005393/TJ5034SUP1.PDF.

[37] E. Krok, M. Stephan, R. Dimova, and L. Piatkowski, "Tunable biomimetic bacterial membranes from binary and ternary lipid mixtures and their application in antimicrobial testing," *Biochimica et Biophysica Acta (BBA) - Biomembranes*, vol. 1865, no. 7, p. 184194, Oct. 2023, doi: 10.1016/J.BBAMEM.2023.184194.

[38] R. Usha and T. Ramasami, "The effects of urea and n-propanol on collagen denaturation: using DSC, circular dicroism and viscosity," *Thermochim Acta*, vol. 409, no. 2, pp. 201–206, Jan. 2004, doi: 10.1016/S0040-6031(03)00335-6.

[39] M. D. Mandler, V. Baidin, J. Lee, K. S. Pahil, T. W. Owens, and D. Kahne, “Novobiocin Enhances Polymyxin Activity by Stimulating Lipopolysaccharide Transport,” *J Am Chem Soc*, vol. 140, no. 22, pp. 6749–6753, Jun. 2018, doi: 10.1021/JACS.8B02283.

[40] Y. Yang, N. Bhachech, and K. Bush, “Biochemical comparison of imipenem, meropenem and biapenem: permeability, binding to penicillin-binding proteins, and stability to hydrolysis by β-lactamases,” *Journal of Antimicrobial Chemotherapy*, vol. 35, no. 1, pp. 75–84, Jan. 1995, doi: 10.1093/JAC/35.1.75.

[41] M. S. Svetlov *et al.*, “High-resolution crystal structures of ribosome-bound chloramphenicol and erythromycin provide the ultimate basis for their competition,” *RNA*, vol. 25, no. 5, pp. 600–606, May 2019, doi: 10.1261/RNA.069260.118.

[42] B. C. Hoffknecht, D. J. Worm, S. Bobersky, P. Prochnow, J. E. Bandow, and N. Metzler-Nolte, “Influence of the Multivalency of Ultrashort Arg-Trp-Based Antimicrobial Peptides (AMP) on Their Antibacterial Activity,” *ChemMedChem*, vol. 10, no. 9, pp. 1564–1569, Sep. 2015, doi: 10.1002/CMDC.201500220.

[43] S. Cecioni, J. P. Praly, S. E. Matthews, M. Wimmerová, A. Imberty, and S. Vidal, “Rational Design and Synthesis of Optimized Glycoclusters for Multivalent Lectin–Carbohydrate Interactions: Influence of the Linker Arm,” *Chemistry – A European Journal*, vol. 18, no. 20, pp. 6250–6263, May 2012, doi: 10.1002/CHEM.201200010.

[44] J. Klousnitzer, W. Xiang, V. M. Polynice, and B. Deslouches, “Comparative Properties of Helical and Linear Amphipathicity of Peptides Composed of Arginine, Tryptophan, and Valine,” *Antibiotics*, vol. 13, no. 10, p. 954, Oct. 2024, doi: 10.3390/ANTIBIOTICS13100954/S1.

[45] A. K. H. H. Hirsch, E. Buhler, and J. M. Lehn, “Biodynamers: Self-organization-driven formation of doubly dynamic proteoids,” *J Am Chem Soc*, vol. 134, no. 9, pp. 4177–4183, Mar. 2012, doi: 10.1021/ja2099134.

[46] R. L. Nation and J. Li, “Colistin in the 21st century,” *Curr Opin Infect Dis*, vol. 22, no. 6, pp. 535–543, Dec. 2009, doi: 10.1097/QCO.0B013E328332E672.

[47] L. Sorlí *et al.*, “Trough colistin plasma level is an independent risk factor for nephrotoxicity: A prospective observational cohort study,” *BMC Infect Dis*, vol. 13, no. 1, pp. 1–9, Aug. 2013, doi: 10.1186/1471-2334-13-380.

[48] M. P. Bohrer, C. Baylis, H. D. Humes, R. J. Glassock, C. R. Robertson, and B. M. Brenner, “Permselectivity of the Glomerular Capillary Wall: FACILITATED FILTRATION OF CIRCULATING POLYCATIONS,” *J Clin Invest*, vol. 61, no. 1, pp. 72–78, Jan. 1978, doi: 10.1172/JCI108927.

[49] S. N. Tammam, H. M. E. Azzazy, and A. Lamprecht, “Biodegradable Particulate Carrier Formulation and Tuning for Targeted Drug Delivery,” *J Biomed Nanotechnol*, vol. 11, no. 4, pp. 555–577, Apr. 2015, doi: 10.1166/JBN.2015.2017.

[50] Z. Li *et al.*, “A Multifunctional Nanosystem Based on Bacterial Cell-Penetrating Photosensitizer for Fighting Periodontitis Via Combining Photodynamic and Antibiotic Therapies,” *ACS Biomater Sci Eng*, 2021, doi: 10.1021/acsbiomaterials.0c01638.

[51] B. C. Hoffknecht, H. B. Albada, M. Sturm, P. Prochnow, J. E. Bandow, and N. Metzler-Nolte, “Synthesis and antibacterial activity of trivalent ultrashort Arg-Trp-based antimicrobial peptides (AMPs),” *Medchemcomm*, vol. 6, no. 2, pp. 372–376, 2015, doi: 10.1039/c4md00327f.

[52] M. M. Konai, B. Bhattacharjee, S. Ghosh, and J. Haldar, “Recent Progress in Polymer Research to Tackle Infections and Antimicrobial Resistance,” *Biomacromolecules*, vol. 19, no. 6, pp. 1888–1917, Jun. 2018, doi: 10.1021/ACS.BIOMAC.8B00458.

[53] N. Ilić *et al.*, “Selective antimicrobial activity and mode of action of adepantins, glycine-rich peptide antibiotics based on anuran antimicrobial peptide sequences,” *Biochimica et Biophysica Acta (BBA) - Biomembranes*, vol. 1828, no. 3, pp. 1004–1012, Mar. 2013, doi: 10.1016/J.BBAMEM.2012.11.017.

[54] H. Takahama, F. Sasaki, and T. Kinoshita, “Structural and endocytotic differences of fibroblasts and macrophages in the tail fin of amphibian larvae during metamorphosis,” *Arch Histol Cytol*, vol. 55, no. 4, pp. 437–448, 1992, doi: 10.1679/AOHC.55.437.

[55] A. Gallardo-Godoy *et al.*, “Activity and Predicted Nephrotoxicity of Synthetic Antibiotics Based on Polymyxin B,” *J Med Chem*, vol. 59, no. 3, pp. 1068–1077, Feb. 2016, doi: 10.1021/ACS.JMEDCHEM.5B01593/SUPPL_FILE/JM5B01593_SI_002.CSV.

[56] “M26 AE Bactericidal Activity of Antimicrobial Agents.” Accessed: Aug. 18, 2024. [Online]. Available: https://clsi.org/standards/products/microbiology/documents/m26/

[57] W. Couet *et al.*, “Pharmacokinetics of Colistin and Colistimethate Sodium After a Single 80-mg Intravenous Dose of CMS in Young Healthy Volunteers,” *Clin Pharmacol Ther*, vol. 89, no. 6, pp. 875–879, Jun. 2011, doi: 10.1038/CLPT.2011.48.

[58] J. E. Salcedo-Sora and D. B. Kell, “A Quantitative Survey of Bacterial Persistence in the Presence of Antibiotics: Towards Antipersister Antimicrobial Discovery,” *Antibiotics 2020, Vol. 9, Page 508*, vol. 9, no. 8, p. 508, Aug. 2020, doi: 10.3390/ANTIBIOTICS9080508.

[59] G. Reid, J. Howard, and B. S. Gan, “Can bacterial interference prevent infection?,” *Trends Microbiol*, vol. 9, no. 9, pp. 424–428, Sep. 2001, doi: 10.1016/S0966-842X(01)02132-1.

[60] G. Krishnamoorthy, I. V. Leus, J. W. Weeks, D. Wolloscheck, V. V. Rybenkov, and H. I. Zgurskaya, “Synergy between active efflux and outer membrane diffusion defines rules of antibiotic permeation into gram-negative bacteria,” *mBio*, vol. 8, no. 5, Sep. 2017, doi: 10.1128/MBIO.01172-17.

[61] X. Zhang *et al.*, “Copper Clusters: An Effective Antibacterial for Eradicating Multidrug-Resistant Bacterial Infection In Vitro and In Vivo,” *Adv Funct Mater*, vol. 31, no. 14, p. 2008720, Apr. 2021, doi: 10.1002/ADFM.202008720.

[62] “eucast: Clinical breakpoints and dosing of antibiotics.” Accessed: Oct. 08, 2024. [Online]. Available: https://www.eucast.org/clinical_breakpoints

[63] C. Thornsberry, P. J. Burton, Y. C. Yee, J. L. Watts, and R. J. Yancey, “The Activity of a Combination of Penicillin and Novobiocin Against Bovine Mastitis Pathogens: Development of a Disk Diffusion Test,” *J Dairy Sci*, vol. 80, p. 413, 1997, doi: 10.3168/jds.S0022-0302(97)75952-6.

Acknowledgements:

The authors would like to thank, Pascal Paul for help with SEM imageing, Petra König for help with cell culture, Dr. Sari Rasheed, Dr. Annette Boese, Alexandra Amann, Viktoria George for help with antimicrobial assays. Dr. Jia-Jhen Kang (NSRRC) is acknowledged for valuable discussions on the interpretation of the SAXS data.

Conflict of Interest:

All authors declare no conflict of interest.

ToC:

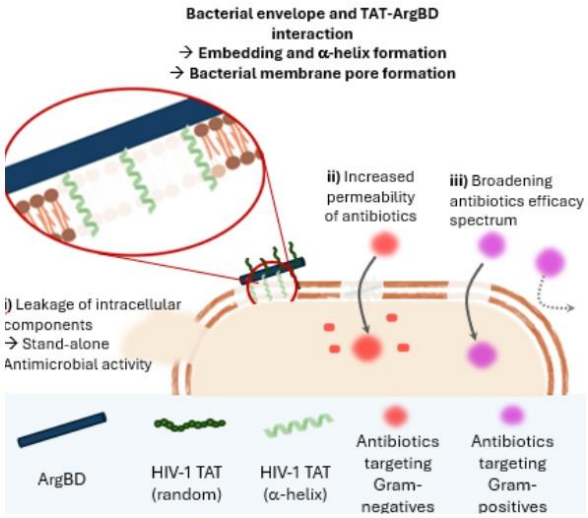

A conjugate of the TAT cell-penetrating peptide with ArgBD dynamic polymer resulting in TAT–ArgBD construct which is a novel antibacterial with a good safety profile as well as an excellent potentiator for antibiotics. These effects are driven by the multivalent nature of the conjugate, as well as the peptide affinity to membrane lipids via α-helical structures.

Supplementary Information

A Multivalent TAT–Arginine-Biodynamer Conjugate to Overcome the Bacterial Cell Envelope Barrier by Bacteria-Specific Membrane Interactions

Mohamed A. M. Kamal[1,2,3], Justine Bassil[1,2,3], Bart-Jan Niebuur[4], Tobias Kraus[4,5], Jennifer Herrmann[1,3,6], Marcus Koch[4], Anna K. H. Hirsch[1,2,3], Brigitta Loretz[1,3], Sangeun Lee[1,2,3*], Claus-Michael Lehr[1,2,3*]

1. Helmholtz Institute for Pharmaceutical Research Saarland (HIPS), Helmholtz Centre for Infection Research (HZI), Saarland University, 66123 Saarbrücken, Germany
2. Saarland University, Department of Pharmacy, 66123 Saarbrücken, Germany
3. PharmaScienceHub, Saarland Universtiy, Campus A2 3, 66123 Saarbrücken
4. Leibniz Institute for New Materials, Campus D2 2, 66123 Saarbrücken, Germany
5. Saarland University, Colloid and Interface Chemistry, 66123 Saarbrücken, Germany
6. German Center for Infection Research (DZIF), partner site Hannover - Braunschweig, 38124 Braunschweig, Germany

*Corresponding author

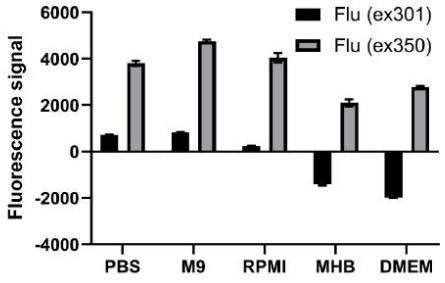

Figure S1: Fluorescence signal of TAT-ArgBD after incubation in different media after subtracting the background of the medium alone.

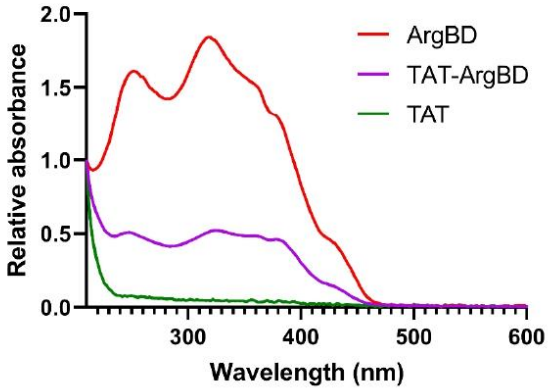

Figure S2: Absorbance scans for TAT-ArgBD conjugate, ArgBD polymer, and TAT peptide, normalized to absorbance at 210 nm.

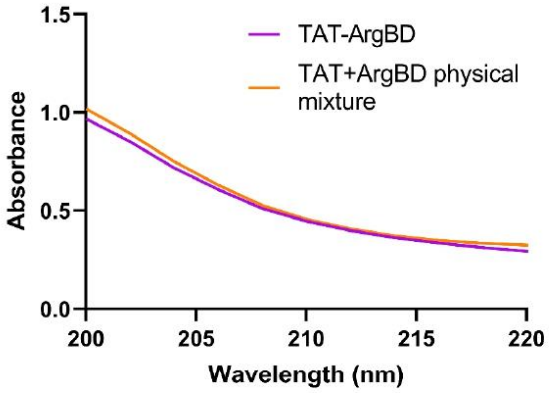

Figure S3: Absorbance scan for 100% TAT-ArgBD conjugate compared to 65% TAT peptide mixed with 35% ArgBD polymer as a validation for the conjugation rate calculation.

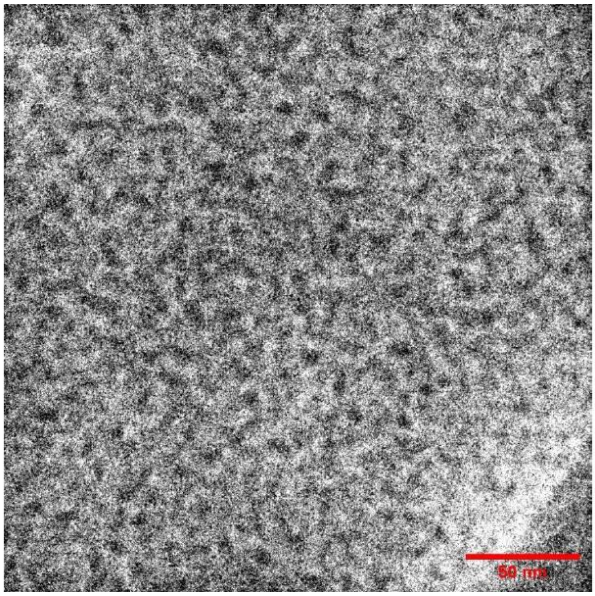

Figure S4: Cryo-TEM showing TAT-ArgBD particles of less than 10 nm.

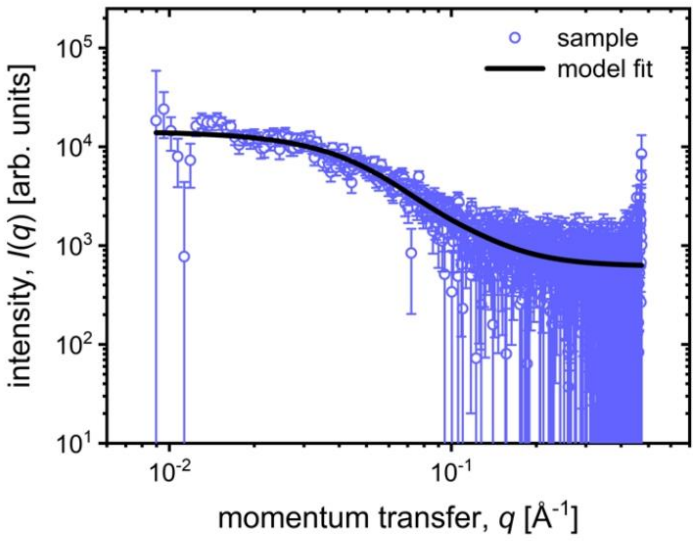

Figure S5: SAXS pattern of TAT-ArgBD in phosphate buffer. A weak shoulder at ~0.05 Å is visible, which shows the presence of uncorrelated particles in the nanometer size range. Fitting the SAXS pattern using a Beaucage function yields R_g = 3.5 ± 0.2 nm.[1] The black line is a model fit, as described in the main manuscript.

Experimental Chemistry Part:

General Devices, chemicals and analytical methods

Reagents and dry solvents as THF, DMF were purchased at the highest commercial quality and used without further purifications, unless otherwise stated. For all reactions, which were performed under inert gas conditions, schlenk flasks were dried in high vacuum and flooded with nitrogen before use. Corresponding reagents were injected using a septum or via argon counter flow. Thin layer chromatography (TLC) carried out on 0.25 mm *E. Merck* silica plates (60F-254), using shortwave UV light as the visualizing agent. The products were purified by flash chromatography on silica gel columns (Macherey-Nagel 60, 0.04−0.063 mm). High resolution mass (HRMS) was determined by LC−MS/MS using the Thermo Scientific Q Exactive Focus Orbitrap LC−MS/MS system. The purity of the final products was determined by Liquid chromatography-mass spectrometry (LC-MS), a Dionex UltiMate 3000 pump, autosampler, column compartment, detector, and ESI quadrupole MS from Thermo Fisher Scientific and are found to be >95%.

Proton (^{1}H) and carbon (^{13}C) nuclear magnetic resonance spectra were recorded on a *Bruker* Avance Neo 500 MHz spectrometer using deuterated solvents as an internal reference (Chloroform ($CDCl_3$): 7.26 ppm ^{1}H NMR, 77.2 ppm ^{13}C NMR; Dimethyl sulfoxide (DMSO–d_6): 2.50 ppm ^{1}H NMR, 39.5 ppm ^{13}C NMR). The chemical shifts were recorded in δ (ppm) and the coupling constants in Hertz (Hz). The following abbreviations were used to explain NMR peak multiplicities: s = singlet, d = doublet, t = triplet, q = quartet, p = pentet, m = multiplet, br = broad.

Synthetic Part

9H-carbazole-3,6-dicarbaldehyde (1)

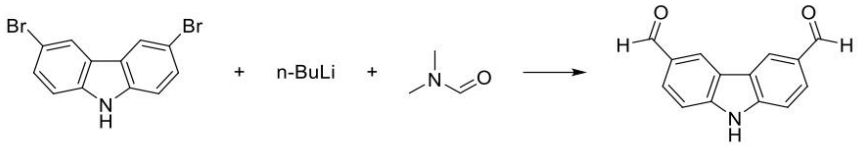

The general procedure for the synthesis of 2 was followed according to literature.[2] 3,6-Dibromocarbazole (3 g, 9.29 mmol) was dissolved in anhydrous THF (60 mL) to give a pale-yellow solution, which was set stirring in a dry ice/acetone bath. An amount of 40 mL of BuLi solution (1.6 mol L^{-1} in hexane) was added over a period of 20 min, causing the reaction contents to darken in colour significantly. The cooling bath was removed for 1 h and then replaced. After 10 min, anhydrous DMF (7.5 mL, 9.7 mmol) was added over 10 min, immediately causing the precipitation of a yellow solid. The cooling bath was

removed, and the reaction was stirred for 90 min at r.t. After this period, 1M HCl solution (50 mL) was added, and the reaction was suction filtered. The yellow solid was collected, and no further purification is needed. The filtrate was extracted with EtOAc (5 × 50 mL), and the combined organic phases were washed with brine (50 mL), dried over $MgSO_4$ and concentrated under vacuum to a yellow solid. The crude product, which exhibited deep blue fluorescence under 254 nm irradiation when spotted on a SiO_2 thin-layer chromatography plate, was purified by column chromatography (SiO2, CH_2Cl_2:MeOH (95:5)), yielding 1.5 g (75%) of a yellow solid. The spectral analysis matched those described in the literature (see below).

^{1}H NMR (500 MHz, $(CD_3)_2SO$): δ= 10.09 (s, 2H), 8.89 (s, 2H), 8.02 (d, *J* = 8.4 Hz, 2H), 7.73 (d, *J* = 8.4 Hz, 2H)

^{13}C NMR (500 MHz, $(CD_3)_2SO$)): δ= 191.52 (14,15), 143.74 (1,4), 128.71 (8,11), 126.71 (2,3), 124.28 (9,10), 122.20 (7,12), 111.73 (6,13).

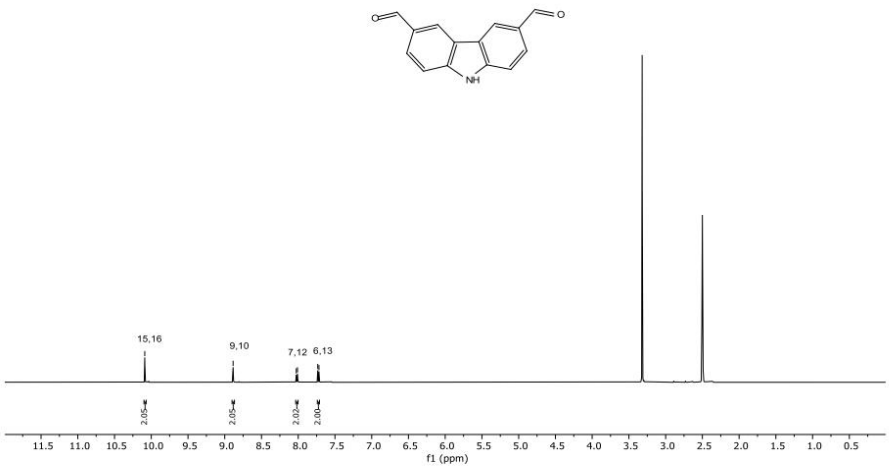

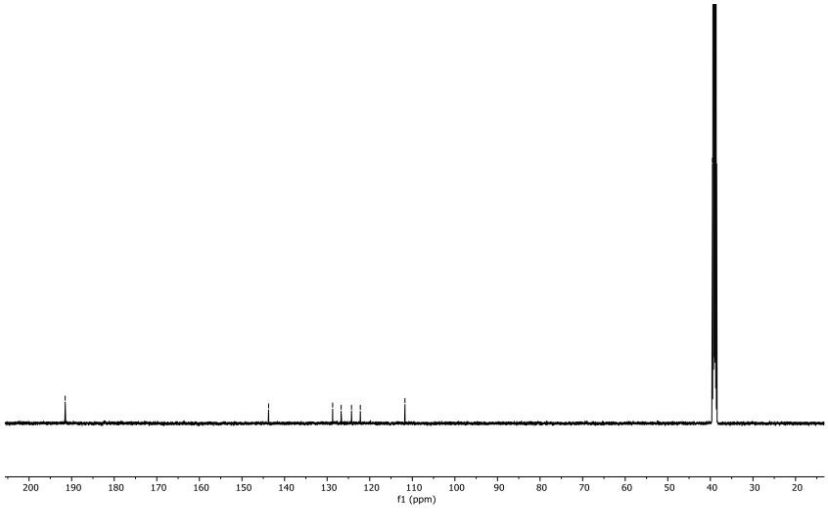

Figure S6: Proton NMR (top) and carbon NMR (bottom) spectra of compound **(1)** in $(CD_3)_2SO$.

9-(20-azido-3,6,9,12,15,18-hexaoxaicosyl)-9H-carbazole-3,6-dicarbaldehyde (2)

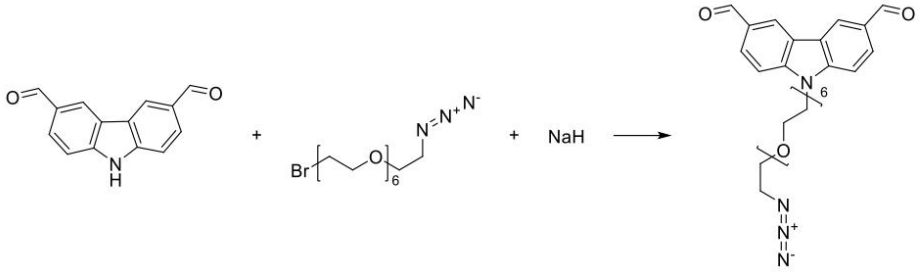

The general procedure for the synthesis of 4 was modified according to literature.[2] Under nitrogen atmosphere, NaH (17.92 mg, 447.97 µmol) was added to a solution of 9*H* -carbazole-3,6-dicarbaldehyde (100 mg, 447.97 µmol) in dry DMF (7 mL) and was stirred at r.t. for 15 min. Then, the bromo-azide chain (185.59 mg, 447.97µmol) was added, and reaction mixture was stirred overnight at r.t. Afterwards, water was added and the mixture was extracted with EtOAc. The combined organic layers were dried over $MgSO_4$, and concentrated under reduced pressure. The crude product was purified via high-performance liquid chromatography (conditions = Gradient flow “10ml/min” (ACN+0.05%FA: H2O+0.05%FA) = 5%ACN → 100% in 60 min) affording 93 mg (37%) of the desired product as a yellow oil.

^{1}H NMR (500 MHz, ($CDCl_3$): δ= 10.13 (s, 2H), 8.65 (s, 2H), 8.07 (d, *J* = 8.5 Hz, 2H), 7.63 (d, *J* = 8.5 Hz, 2H), 4.58 (t, *J* = 5.5 Hz, 2H), 3.92 (t, *J* = 5.5 Hz, 2H), 3.66 – 3.57 (m, 16H), 3.36 (t, *J* = 5.1 Hz, 2H). **^{13}C NMR** (500 MHz, (CDCl3)): δ= 191.89 (14,15), 145.50 (1,4), 130.18 (8,11), 128.17 (7,12), 124.47 (9,10), 123.59 (2,3), 110.67 (6,13), 70.93 (chain), 51.05 (20), 44.45 (40).

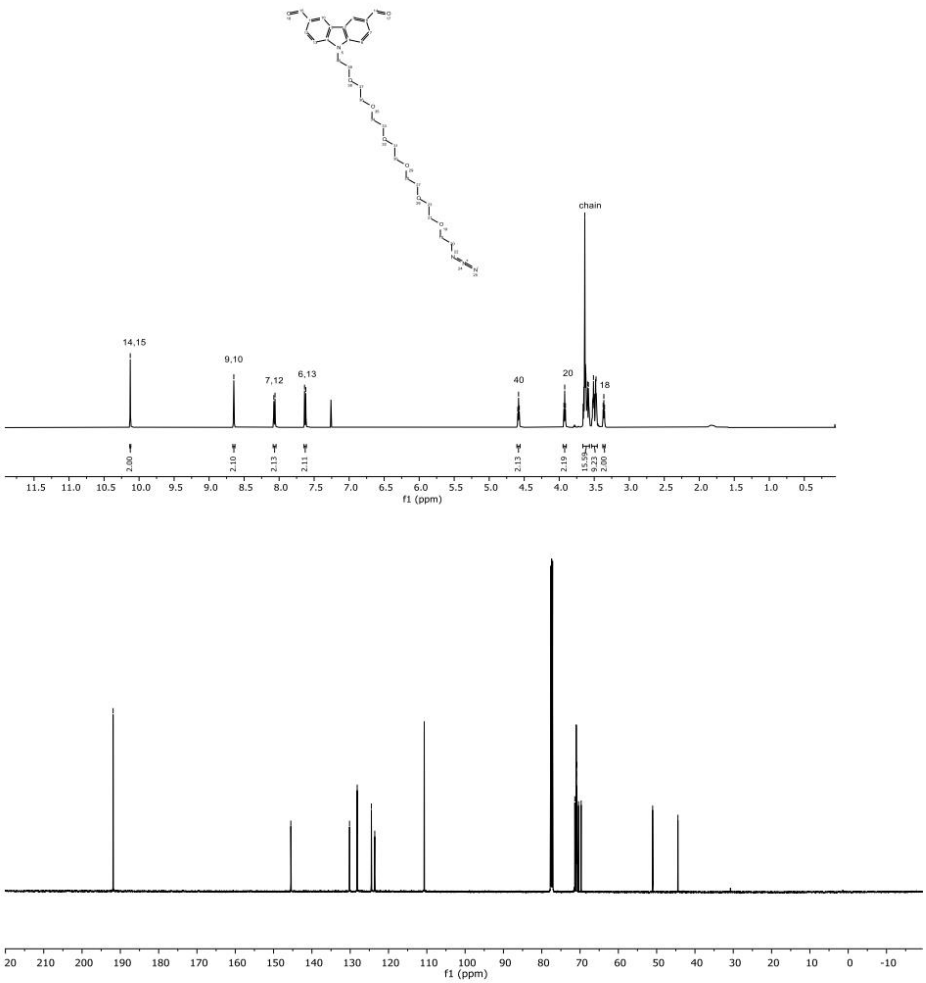

Figure S7: Proton NMR (top) and carbon NMR (bottom) spectra of compound 2 in $CDCl_3$.

Arginine Hydrazide (3)

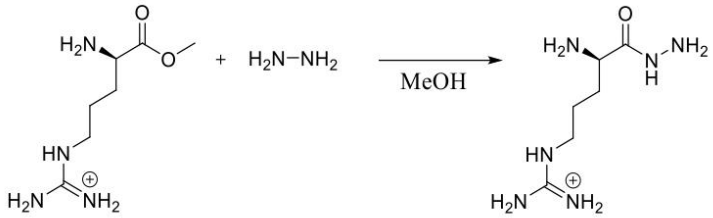

To a solution of methyl *D*-argininate (100 mg, 528.43 µmol) in anhydrous MeOH (8 mL) was added hydrazine hydrate (5 mL) and the reaction was stirred at room temperature for 24 h. After the completion of the synthesis, MeOH was removed under vacuum (60°C , 20 mPa). Finally, 2 ml distilled water is added to the product and freeze dried overnight to remove excess hydrazine hydrate. 80 mg of product (80%) was obtained as a transparent oil. Care was taken to avoid exposure to moisture.

^{1}H NMR (500 MHz, (D_2O): δ= 3.38 (t, J = 6.7 Hz, 1H), 3.20 (t, J = 6.7 Hz, 2H), 1.71 – 1.51 (m, 4H).

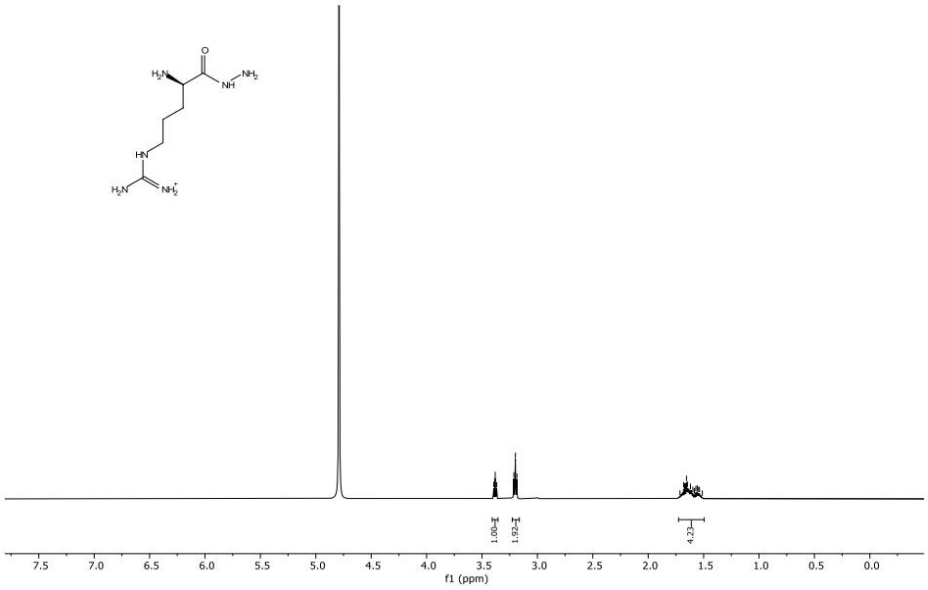

Figure S8: Proton NMR spectra of compound Arginine Hydrazide in D_2O.

Biodynamers synthesis:

The synthesis of ArgBD was conducted as previously described in a previous publication. [2]

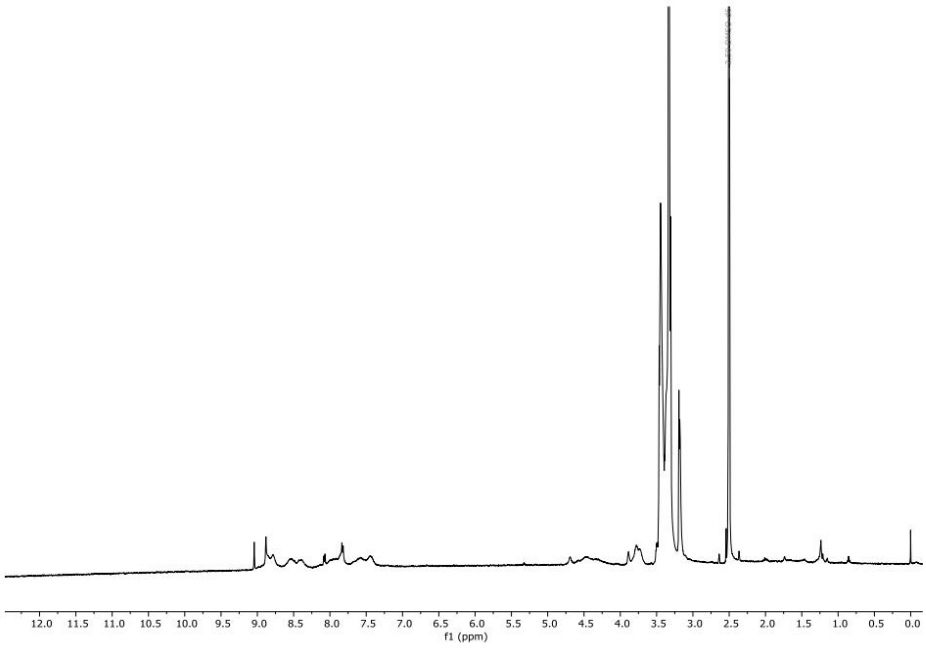

Figure S9: Proton NMR spectra of ArgBD biodynamer.

TAT-ArgBD

The ArgBD with azide terminus was synthesized following the previous reported protocol with slight modifications.[2] ArgBD with azide terminus was synthesized by mixing 10 µmol of compound **5** with 10 µmol of arginine hydrazide in 1 mL deuterium oxide acidified with deuterated acetic acid at pD 3.4. The mixture was kept for 24 hours at room temperature with occasional mixing and sonication. Upon completion, a reddish transparent solution was observed.

sodium ascorbate (10 equiv.) , $CuSO_4$ (6.7 equiv.) , and BTTAA (2-(4-((bis((1-(tert-butyl)-1H-1,2,3-triazol-4-yl)methyl)amino)methyl)-1H-1,2,3-triazol-1-yl)acetic acid) (13.4 equiv.) were added as catalysts. Afterwards, 1.2 equivalent of HIV-1 TAT peptide with Homopropargylglycine terminus was dissolved in 7 mL tert-butanol with 1 mL 10x PBS and added to the reaction mixture of the ArgBD with azide terminus. The reaction was left for another 24 hours with stirring at r.t. After the reaction completion, the crude mixture was washed extensively through Pall 3kDa MWCO with MilliQ water five times. Upon freeze drying, a yellowish powder was acquired and aliquoted for further use.

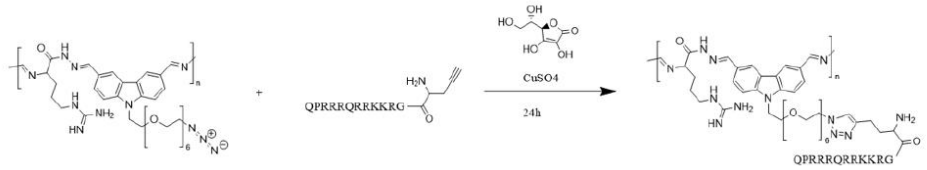

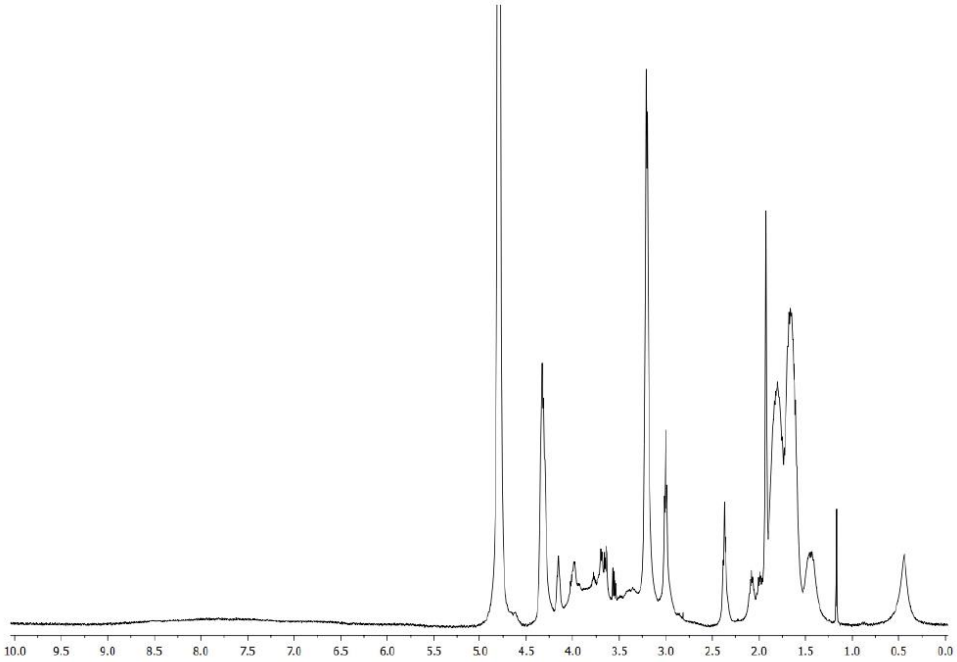

Figure S10: Proton NMR spectrum of TAT-ArgBD in D_2O.

Due to the quenching of the aromatic protons and in order to prove the formation the triazole ring in the CuAAC reaction. A non-polymerized version of the TAT-ArgBD was synthesized and without the carbazole moiety to avoid interference of the aromatic protons. The reaction was conducted in the exact same way as TAT-ArgBD and purified on a preparative HPLC column.

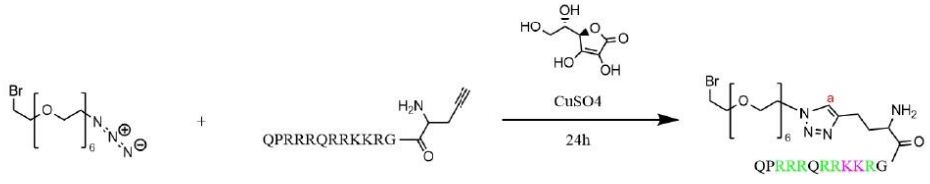

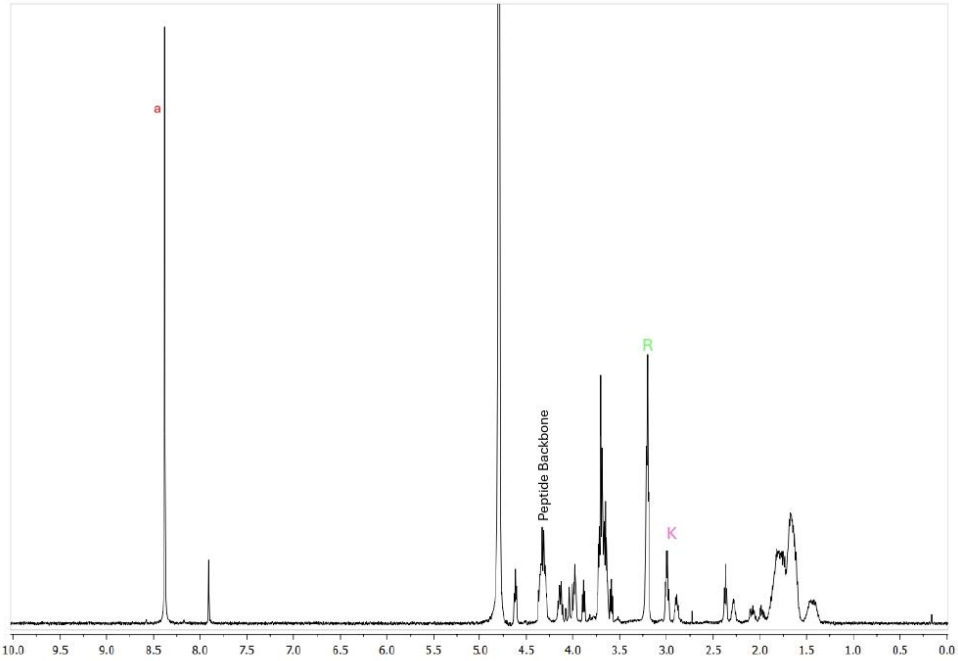

Figure S11: Proton NMR spectrum of TAT-ArgBD in D_2O.

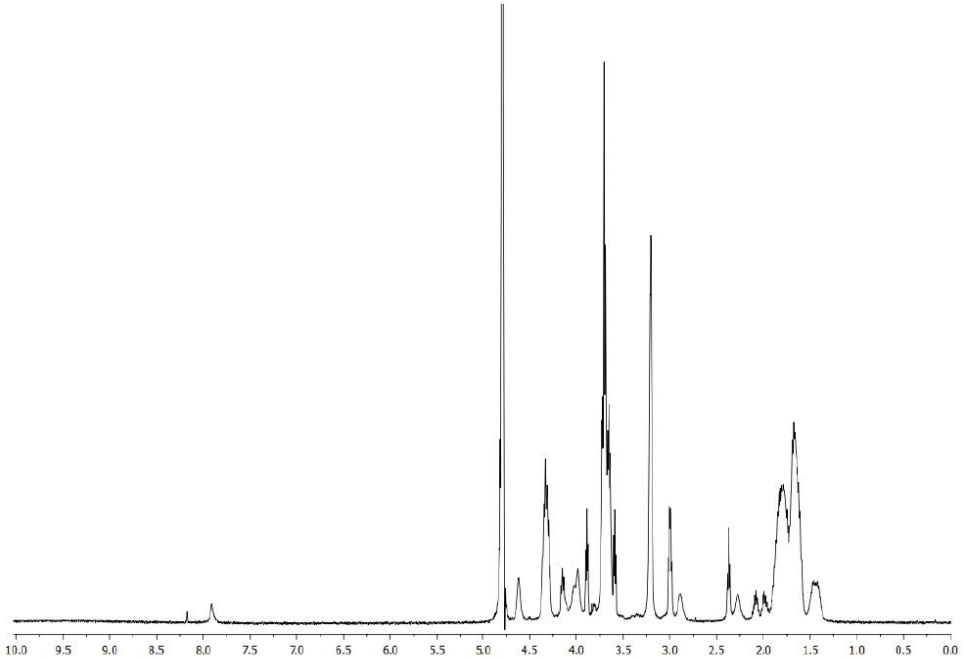

Figure S12: Proton NMR spectrum of HpG-TAT in D_2O.

References:

[1] B. Hammouda, Analysis of the Beaucage model, J Appl Crystallogr 43 (2010) 1474–1478. https://doi.org/10.1107/S0021889810033856.

[2] M.A.M. Kamal, J. Bassil, B. Loretz, A.K.H. Hirsch, S. Lee, C.M. Lehr, Arg-biodynamers as antibiotic potentiators through interacting with Gram-negative outer membrane lipopolysaccharides, European Journal of Pharmaceutics and Biopharmaceutics 200 (2024) 114336. https://doi.org/10.1016/J.EJPB.2024.114336.